



**University of Ferrara
Physics Department**

Doctoral Thesis

**Flat Facetted PV concentrator systems and
dichroic evolution**

TUTOR:
Prof. Giuliano Martinelli

CANDIDATE:
Andrea Antonini

XVIII Cycle (2005)

Summary of nomenclature

N_A, N_D	acceptor and donor densities respectively
τ_e, τ_h	electron & hole minority carrier lifetimes respectively
L_e, L_h	electron & hole minority carrier diffusion lengths respectively
μ_e, μ_h	electron & hole mobilities respectively ($\text{cm}^2/\text{V}\cdot\text{sec}$)
D_e, D_h	electron & hole diffusivities respectively (cm^2/sec)
n_e, n_h	the electron & hole concentrations respectively
n_{e0}, n_{h0}	electron & hole concentrations in thermal equilibrium
n_i	intrinsic carrier concentration
n_{ep0}	electron concentration in p-type silicon at equilibrium
n_{hn0}	hole concentration in n-type silicon at equilibrium
n_{ep}, n_{en}	electron concentration in p-type and n-type silicon respectively
n_{hn}, n_{hp}	hole concentration in n-type and p-type silicon respectively
n_c, n_v	effective density of states in the conduction and valance bands respectively
μ	Fermi level
E_{CB}, E_{VB}	energy of the band edge of the conduction and valance bands respectively
q	electron charge (1.6×10^{-19} coulombs)
m_e	electron mass (9.11×10^{-31} kg)
k	Boltzman's constant (1.38×10^{-23} J/K)
c	speed of light (3.0×10^8 m/s)
h	Planck's constant (6.625×10^{-34} J-sec)
T	absolute temperature (K)
kT/q	thermal voltage (≈ 26 mV at 300 K)
ρ	resistivity ($\Omega\text{-cm}$)
σ	conductivity ($\Omega\text{-cm}$) ⁻¹
E_g	bandgap
J, J_0	current density and reverse saturation current density respectively (A/cm^2)
V	voltage
FF	fill factor
V_{oc}	open circuit voltage (V)
I_{sc}, J_{sc}	short circuit current (A) and current density (A/cm^2) respectively

Summary

Introduction	7
CHAPTER 1 PHYSICS OF SEMICONDUCTORS FOR PV	11
1.1 Semiconductors for PV applications	11
1.2 Electrons-holes generation – photoelectric properties	14
1.3 Recombination processes	20
CHAPTER 2 SOLAR CELLS	30
2.1 Qualitative description	30
2.2 Idealized solar cell	32
2.3 Real solar cells	43
2.4 Strings of solar cells	52
CHAPTER 3 SOLAR CONCENTRATION	54
3.1 Silicon solar cells performances under concentrated illumination	54
3.2 Non-silicon semiconductor solar cells under concentration	58
3.3 Solar concentrators	60
3.4 Efficiency of PV concentrators	68
CHAPTER 4 - FLAT FACETTED SOLAR CONCENTRATOR DISHES: GLOBAL AND DICHROIC REFLECTIVE APPROACHES	71
4.1 Flat faceted profiles for PV concentrator dishes	71
4.2 Dense array PV panel and cooling	81
4.3 Dichroic approach	86
CHAPTER 5 FABRICATION OF SILICON SOLAR CELLS FOR CONCENTRATION	95
5.1 General description and state of art	95
5.2 Silicon solar cell for concentration - 1	96
5.3 Silicon solar cell for concentration – 2	106
5.4 Silicon solar cell for concentration – 3	112

CHAPTER 6 RESULTS	116
6.1 PV cells measurements under concentrated light flux	116
6.2 Single cell measurement results under concentration	120
6.3 Si PV panel under concentration	127
6.4 Si cells for concentration fabricated at the SSL of the University of Ferrara	129
Conclusion and Future Developments	142
Bibliography	144
Acknowledgments	152

Introduction

The energy harvesting is one of the main problems of the current and future world society. It's a complex issue for its connection among political, environmental and technological aspects.

The civilization of our world has hugely grown up in the last two centuries, mainly for the introduction of the fossil fuels; these are energetic resources given us by the nature after billion years of chemical processes. However, they have four main problems: they are finite and not distributed all over the world, produce pollution and greenhouse effect. Another, different, very powerful resource is the nuclear fuel; paradoxically, one of it's problem is that it's too powerful. This fact make it a very dangerous choice as energy source in our world, for it's potentialities in army applications. There are other important topics which make this fuel not suitable for our current society like the radioactive waste problems, the danger of terroristic attack, failures in nuclear centrals and the not global diffusion of the uranium mines, which could create political frictions [1].

The world needs other power sources, cleaner and more diffuses, in order to give at all the countries the conditions of development. The more immediate source responding at all these requirements is the solar energy. It's one of the more distributed energy source, it's clean and it's enough for the humanity requires. Indeed, the current world energy demand is about 140×10^6 GWh for year; considering that in the Sahara desert the annual solar energy striking a m^2 is about 2900KWh, the surface required for the production of the world energy demand, with a conversion energy efficiency in electrical current of 10%, is about 500000 Km^2 ; it's the 6% of the total area of the Sahara desert. Considering the globe, the world power demand is about 1/10000 of the power from the Sun to the Earth. Appears evident that the solar energy could be a very interesting resource.

Extrapolating the collected data of the energy market it's possible to deduce the evolution of energy sources, at least in the near future; figure 1 shows their past and forecasted future, while figure 2 sketch data on the oil extractions. These are two examples illustrating the potentiality of the renewable energies.

Another very important issue is the CO_2 emission from the fossil fuels combustion. The effects of the introduction of greenhouse gases in the atmosphere are documented and forecasted by scientists all over the world; the produced changes in climate could have

heavy consequences, with the increasing of the intensity of the meteorological events. At the current state of knowledge appear to be very desirable to move toward ecological power sources. To give an estimation of the amount of CO₂ inputted in the air, the coal combusted to deliver the equivalent of the solar energy on a 1m² during an year (considering an average value of sun irradiation) produces 1Tons of CO₂ (400 Kg for natural Gas).

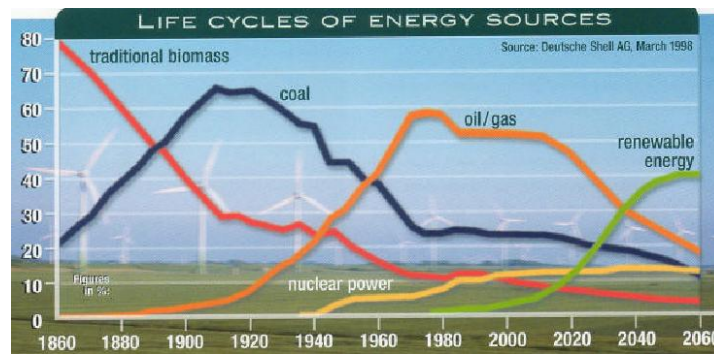


Figure 1- Past evolution and the forecasting of the energy source utilization.

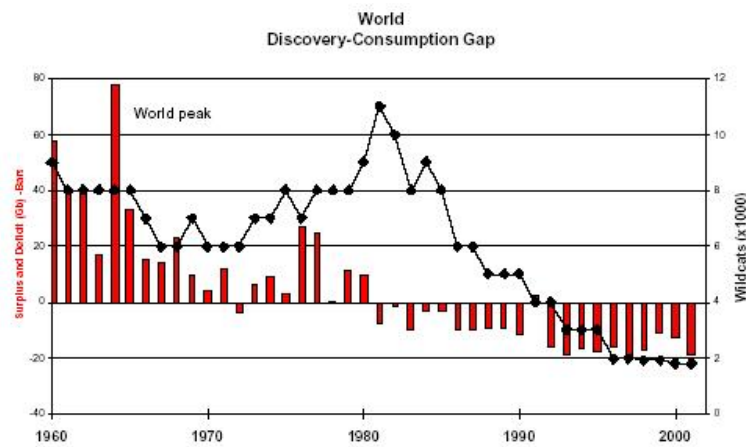


Figure 2 - The red bars represent the divergence between the energy of the discovered fossil fuel fields and of the energy consumption during the years and the black line indicates the exploration well drillings numbers.

The problem for the solar energy is find the way to convert the light efficiently in term of costs and energy pay back time. The big advantage of its wide diffusion is, from another point of view, a problem, because the amount of power on unit of area is quite low for the human requirements (1KW/m², as average), considering the present way to convert it in useful forms.

The radiation could be collected in order to get a solar thermal furnace, or converted directly into electricity by photovoltaic solar panels. Both these two approach have advantages and disadvantages. One important point for photovoltaic is its capability to be not centralized; it's possible to produce energy without a big central power, but grid connecting a lot of small PV systems.

The market of photovoltaic has, however, some challenging topics, which lead to the very high cost of the PV power (about 7-8 €/W). In particular, the most critical issues are the limitation on the production of PV materials, their quite long energy pay back time (in the order of 3 years for c-Si) [2] and the intrinsic high cost for the base PV material. At the current state of art, the PV industry is dominated by the silicon solar cell technology; to overcome the mentioned problems related to this industry, the PV world is researching new solutions, following different routes; one way is the developing of new materials with PV properties of very low cost (thin film cells), even with lower efficiency compared to the current silicon modules. Another way is the reduction of the amount of expensive material normally used in PV applications, without decrease the produced power; this approach is pursued in the concentrated photovoltaic. In the concentrated PV, large surfaces of low cost material with particular optical properties (lens or mirrors) are used to collect the solar radiation and to concentrate it on a small area of PV cells; the reduction in the amount of PV material required is equal at the concentration factor [3]. This way allows us to overcome the problems related on the PV materials, but other new difficulties are present.

A number of different concentrated PV system solutions have been proposed worldwide. The attention of the PV world on this approach is rapidly grown up in the last years; this mainly because the capability of the industry working in all the fields needed at the concentrated PV systems appears now to be ready. A concentrated PV system is indeed composed by many technological aspects belonging at different fields, like optics, electronic and mechanical engineering, besides, obviously, photovoltaic science and technology; the good level of maturation of each of the required parts is necessary to achieve the goal of a competitive cost for the concentrated photovoltaic energy.

The concentration gives some particular advantages, compared to the traditional, flat plate photovoltaic; apart from the already mentioned reduction of costs by the cut of the more expansive component of a PV panel, the PV cells, the concentration allows us to utilize very high efficiency devices and permits to work under particular conditions; dedicated cells are able to improve their conversion efficiency with the increasing of

illumination. Moreover, new classes of solar light concentrators can be designed in order to utmost capitalize the energy from the Sun. One example is here presented, producing a spatial spectral splitting of the incident light using a dichroic approach.

CHAPTER 1 PHYSICS OF SEMICONDUCTORS FOR PV

1.1 Semiconductors for PV applications

Semiconductors are materials characterized by a resistivity in the order of $10^{-2} < \rho < 10^9$ Ohm-cm. In an energy diagram, they have an energy gap without allowed energy states; a material is classified semiconductor if this gap is in the range of 0.2-2.5 eV [4]. Although the PV material are semiconductors, not every semiconductor are useful for PV applications; one important feature is the value of the energy gap, i.e. the energy to ionise an electron. This energy has to be not so higher to correspond at the energy of the UV radiation, nor so low to be a small fraction of the radiation energy in the most photon populated part of the solar spectrum.

In photovoltaic devices the light with enough energy releases the electrons of the semiconductor from their chemical bounds; this effect moves the electrons on higher energy levels respect to the original locations, jumping an energy step of the order of the energy converted. The time of boundless for the photo-excited electrons before recombination has to be high enough to allow the charges to reach an internal and localized electrical field; this driving force, acting on the charges in a restricted region inside the device, creates the conditions for the electric current.

In the following description the behaviour of crystalline solar cells is mainly treated, with particular regard to the silicon solar cells. In these cases the energy band diagram has two allowed bands, the valence band (VB) and the conduction band (CB), separated from the forbidden energy gap which has a value characteristic of every semiconductor.

In semiconductors two electronic species, electrons and holes, contribute at the electric current; the electrons move in CB while the holes in VB; the global conductance of the material depends on the distinct characteristics of them, following the (1.1):

$$\sigma = qn_e\mu_e + qn_h\mu_h \quad 1-1$$

Consequently, the conductivity of semiconductors is directly dependent on the concentration of carriers in the different bands. In the classical regime for electrons and

holes, which is satisfied when the Fermi-Dirac distribution function for the electrons and holes (1.2-1.3) are under the conditions (1.4), the particles can be treated like elements of a classical gas, described with the Boltzmann statistic (1.5).

$$f_e(\mathcal{E}) = \frac{1}{e^{(\mathcal{E}-\mu)/kT} + 1} \quad 1-2$$

$$f_h(\mathcal{E}) = 1 - f_e(\mathcal{E}) \quad 1-3$$

$$f_e \ll 1 \quad \mathbf{a} \quad 1-4$$

$$f_h \ll 1 \quad \mathbf{b}$$

$$f(\mathcal{E}) \cong e^{-(\mathcal{E}-\mu)/kT} \quad 1-5$$

Intrinsic semiconductors suit these conditions because the Fermi level μ is located in the middle of the E_g [4].

It is possible to increase the conductivity of a semiconductor doping the material with particular atoms. The introduction of these foreign elements releases the bounds of some electrons and creates new levels in the otherwise forbidden energy band. The utilization of some elements as impurities allows us to create energy levels close to the edges of the conduction band and to the valence band, as shown in fig(1-1).

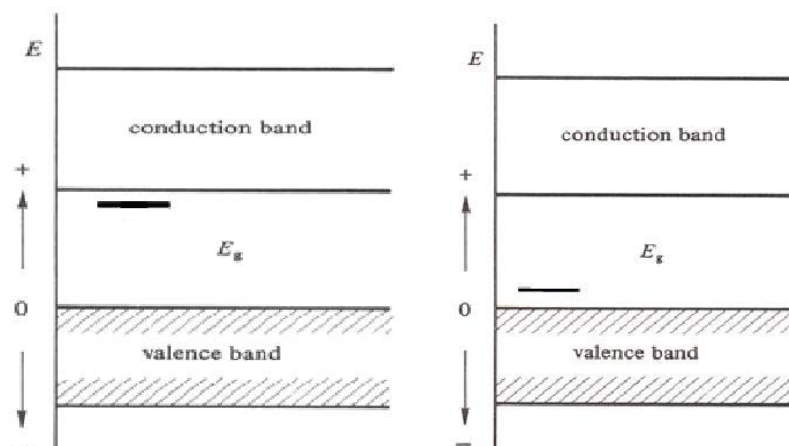


Figure 1-1-Energy band diagram in the real space of a semiconductor with a donor (a) and an acceptor(b) level

The impurities of interest for the doping of semiconductors are the elements which can create electron energy levels closed to the CB and the VB. These species, respectively the donors and the acceptors, have the characteristic of make weak bound for the correspondent majority carriers, i.e. electrons or holes; this fact permits to boost the quantity of the two kind of carriers in the semiconductor. The dependence of the resistivity of silicon as function of the doping level of boron and phosphorous is depicted in fig(1-2).

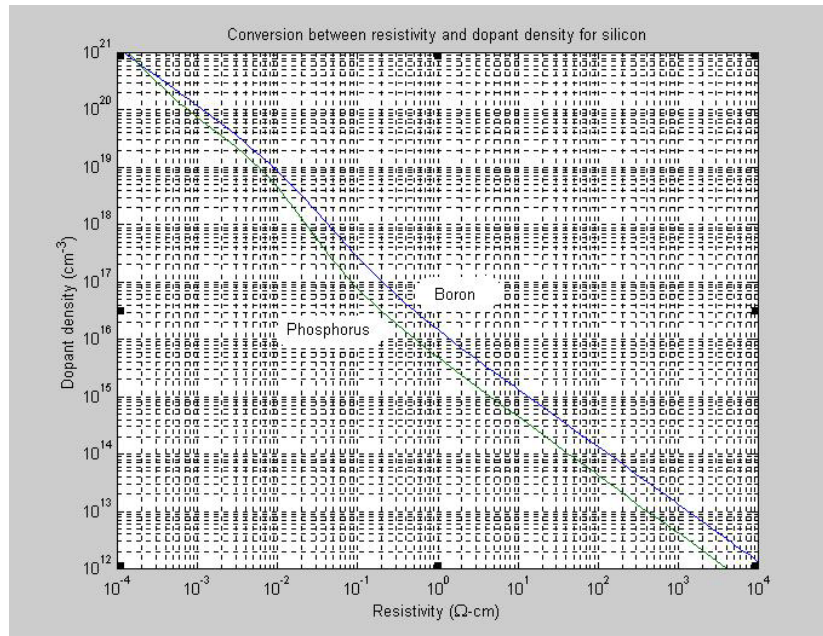


Figure 1-2- Doping concentration vs. resistivity for silicon; the characteristics for phosphorus and boron impurities are represented.

An important effect of the doping is the consequent shift of the Fermi level μ ; it's the electron's chemical potential and it's related with the concentration of free electrons n_e and holes n_h as in (1.6)

$$\mu = E_c - kT \ln\left(\frac{n_c}{n_e}\right) = E_v + kT \ln\left(\frac{n_v}{n_h}\right) \quad 1-6$$

In fig.(1-3) is sketched the band energy diagram in the real space of a *n-type* semiconductor.

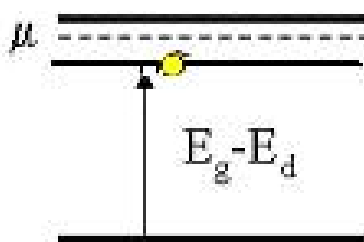


Figure 1-3 – Fermi level qualitative representation for an n-type semiconductor

1.2 Electrons-holes generation – photoelectric properties

The more interesting photovoltaic materials have a value of the energy gap not much lower than the energy corresponding the Wien wavelength for the Sun solar spectrum (520 nm) because it corresponds to the most powerful part of it; in Table 1.1 there are the E_g values for some of these materials at 300K. The silicon, with its band gap of 1.12eV, is the most used photovoltaic material, in the current PV technology. The fraction of power of the solar spectrum radiations converted by an high efficiency silicon solar cell is depicted in fig. (1-4); the absorbed energy flux is given from all the area of the solar spectrum with wavelength lower then the silicon absorption threshold, i.e. about 1100nm. The considered solar spectrum is the AM 1.5, i.e. the solar light flux with a certain air mass absorbing part of the solar radiation; it's the standard spectrum for terrestrial PV applications [5]; the flux is rounded, for convenience, at 1kWm^{-2} (one sun).

	<i>Germanium</i>	<i>Silicon</i>	<i>GaAs</i>	<i>InGaP</i>
Energy Gap (eV)	0.66	1.12	1.424	1.9

Table 1-1

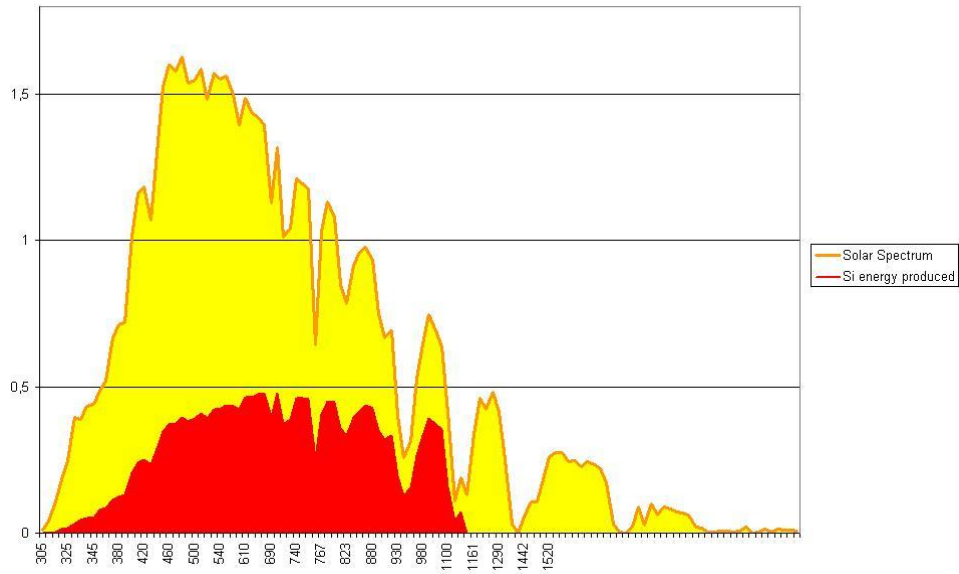


Figure 1-4 – The red area represents the power portion of the solar spectrum (yellow and red area) electrically converted from an high efficiency solar cell (SunPower HECO 252)

The silicon has an indirect band gap; as shown in fig.(1-5a) the lower edge of the CB in the momentum space has a k-value that doesn't correspond at that of the upper edge of the VB, as it happen in direct band gap semiconductors, as, for example, GaAs, in fig.(1-5b); both total momentum and total energy must be conserved in the level transitions; so, an up-transition with ionization energy equal at the band gap in an indirect gap semiconductor can happen only if the momentum is conserved through absorption of phonons. A photon carries an high energy but very low momentum, compared with the momentum of phonons, while a phonon has low energy compared to the energy gap, but not negligible momentum, as estimate in (1.7-1.8) considering a photon energy of 1eV. For these reasons the conservation rules for momentum and energy in the electron transitions in a indirect semiconductor can be approximated with (1.9-1.10).

$$k_{\text{photon}} = \frac{p}{\hbar} = \frac{E/c}{\hbar} \approx \frac{1 \text{ eV} (1.60 \times 10^{-19} \text{ J/eV})}{(3.00 \times 10^8 \text{ m/s})(1.05 \times 10^{-34} \text{ Js})} \approx 5 \times 10^6 \text{ m}^{-1} \quad 1-7$$

$$k_{\text{photon}} \ll k_{\text{max}} \approx \frac{2\pi}{a} \approx \frac{2\pi}{3.00 \times 10^{-10} \text{ m}} \approx 2 \times 10^{10} \text{ m}^{-1} \quad 1-8$$

$$\bar{k}_i + \bar{q} = \bar{k}_f \quad 1-9$$

$$E_i + h\nu = E_f$$

1-10

Where \bar{q} represents the phonon momentum, while \bar{k}_i and \bar{k}_f are the initial and final momentum of the electron for the transition.

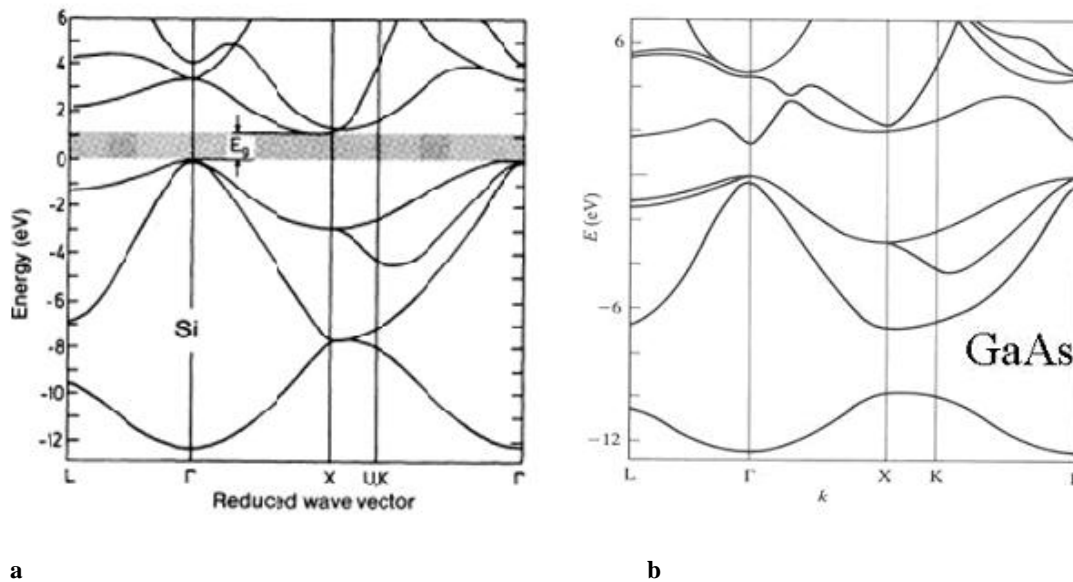


Figure 1-5 – Band diagram in the momentum space of silicon (a) and gallium arsenide (b).

The indirect bandgap leads to a particular absorption function for the silicon, with an absorbing coefficient $\alpha(\lambda)$ dependent on the temperature, as shown in fig.(1-6) for two different temperatures; for the spectral energy fraction lower than the ionization energy required for any k-direct transition from the VB to the CB, a phonon with a defined momentum is needed. The higher is the temperature, the higher is the phonon population and consequently the probability to find the necessary momentum.

For semiconductors, the light absorbed has an exponential behaviour for each wavelength, so the global light absorption function is given by (1.11), where I_0 represents the incident light not reflected at the front surface.

$$I_{abs}(x) = \int_0^{\lambda_{max}} I_0(\lambda) [1 - e^{-\alpha(\lambda)x}] d\lambda$$

1-11

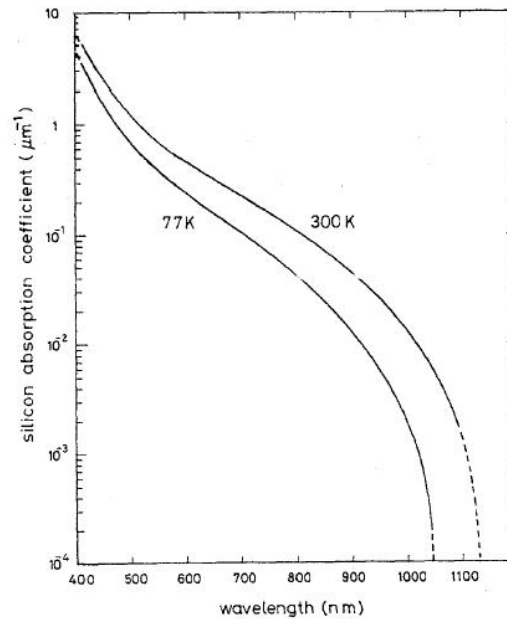


Figure 1-6 – Silicon absorption coefficient vs. wavelength of the radiation at two different temperatures

The indirect band gap of silicon also leads to very high minority carrier lifetimes (commonly it can vary from less than $1\mu\text{s}$ up to more than 1ms), compared with the direct band gap semiconductors (order of nanoseconds), because of the selection rules in the de-excitation. While the light absorption can happen even without the phonon contribution, i.e. with direct absorption, for the radiation with energy enough to promote electrons at energy levels higher than the bottom of the CB, the radiative recombination is far less probable; this because the electrons in the CB thermalize very fast, moving toward the bottom of the band in times of the order of $\sim 10^{-12}\text{s}$ [6]; for this electrons descent through energy levels there aren't significant impediments because the allowed energy states in the band are approximately a continuum, so the required global momentum to moves in the k-space toward the bottom of the CB (for electrons) can be delivered by a number of different momentum combinations. The excess electron energy is released as phonons. The electron-hole recombination can be due to different processes, not only the radiative one, which, indeed, plays a marginal role in the indirect semiconductors; however, the time required for the recombination, which is the process bringing the material at the complete thermal equilibrium, is many order of magnitude higher than the thermalization of the carriers in each band. The fast thermalization of the electrons in the CB and of the holes in the VB gives orbital occupancy distributions of electrons and holes very closed at the equilibrium Fermi-Dirac distribution in each band separately; this fact leads to the definition of the *quasi-Fermi levels* for the two bands (μ_c and μ_v for the CB and VB,

respectively), in conditions of quasi thermal equilibrium; in both the case μ represents the electron chemical potential. The distributions of the carriers in this conditions are (1.12a-1.12b):

$$f_c(\varepsilon) = \frac{1}{e^{(\varepsilon - \mu_c)/kT} + 1} \quad \mathbf{a} \quad \mathbf{1-12}$$

$$f_v(\varepsilon) = \frac{1}{e^{(\varepsilon - \mu_v)/kT} + 1} \quad \mathbf{b}$$

If the quasi-Fermi levels are not constant throughout the crystal, the ionized charges, both majority carriers due to the doping and the minority carriers generated by external source (light, for example), contributes at the electric current. In particular the current density of electrons and holes, respectively in the the CB and VB, are given by (1.13a-1.13b):

$$\vec{J}_e = \tilde{\mu}_e n_e \vec{\nabla} \mu_c \quad \mathbf{a} \quad \mathbf{1-13}$$

$$\vec{J}_h = \tilde{\mu}_h n_h \vec{\nabla} \mu_v \quad \mathbf{b}$$

If the carrier concentrations are in the extrinsic but nondegenerate range (1.14a 1.14b) the quasi-Fermi level for the CB and VB are given by (1.15a –1.15b) following the (1.6).

$$n_i \ll n_e \ll n_c \quad \mathbf{a} \quad \mathbf{1-14}$$

$$n_i \ll n_h \ll n_v \quad \mathbf{b}$$

$$\mu_c = E_c - kT \ln\left(\frac{n_c}{n_e}\right) \quad \mathbf{a} \quad \mathbf{1-15}$$

$$\mu_v = E_v + kT \ln\left(\frac{n_v}{n_h}\right) \quad \mathbf{b}$$

The currents in the two bands are given by (1.16a-1.16b); there are two different physical contributions: one due to the effect of an electrical field created by the gradient of the band edges (drift), and another produced by concentration gradients of the carriers (diffusion).

$$\vec{J}_e = e\tilde{\mu}_e n_e \vec{E} + eD_e \vec{\nabla} n_e \quad \mathbf{a}$$

1-16

$$\vec{J}_h = e\tilde{\mu}_h n_h \vec{E} - eD_h \vec{\nabla} n_h \quad \mathbf{b}$$

The diffusion coefficients D_i for the two different species accounts the motion interactions with the lattice for particles moved by thermal agitation; these coefficients are related to the mobility, which represents the effect of interaction, like a sort of viscosity, between the carriers and the lattice for a motion driven by an electric field.

In condition of low injection, the drift current for the minority carriers can be considered negligible, because of it's very low compared to the drift current produced by the majority carriers, depending directly on the particle concentrations; diversely, the diffusion current depends on the concentration gradient, so the minority carriers contribution can be relevant compared to the one of the majorities. Out of the low injection conditions, both the species participate at the current with both the drift and diffusion components. In high injection the hole and electron concentrations will be approximately equal.

A very important issue for the semiconductor electronic devices, and in particular for the solar cells, is that, in low injection conditions, minority carriers flow predominantly by diffusion in quasi-neutral regions [7], where the quasi-neutral conditions are (1.17a-1.17b) for n and p semiconductors, with the condition of the respective doping concentration approximately constant throughout the regions.

$$p - n + N_d \approx 0 \quad \mathbf{a}$$

1-17

$$n - p + N_a \approx 0 \quad \mathbf{b}$$

Both the n and p zones in a silicon solar cell, except done for the depletion region, can be considered as quasi-neutral; the diffusion behaviour is then dominant for the carriers collection.

While the silicon solar cells behaviour is based on diffusion of minority carriers, thin film cells, as well as compound semiconductor solar cell structures, have electric field assisted transport for the carriers. Indeed, direct semiconductors have lifetimes of minority carriers too short for an efficient charges collection by diffusive transport process. Epitaxially grown solar

cell, for example, are often designed with a doping or band gap gradients to build up an electric field through the active device regions. Amorphous silicon thin film (a-Si) cells, having a very low minority carriers lifetime, are *pin* structures so the charges are collected from the intrinsic layer by drift current.

The number of electron-holes generated by the AM 1.5 solar light in silicon can be calculated by (1.18), if the AM 1.5 spectrum and the E_g of the material are known; in the best condition, the reflectance of the material in the range of interest can be considered negligible, so all the radiation of energy higher than E_g is converted in hole-electron pairs.

$$N_{e-h} = \int \frac{I_{abs}(x)}{h * c} dx \quad 1-18$$

The minority ionized charges, has already mentioned, will recombine in order to achieve the thermal equilibrium; if the external injection source doesn't stop its effect but assumes a steady behaviour, the particles in the material achieve quasi-equilibrium, or steady state, condition. The minority carriers lifetime is the fundamental parameter which describes the rate of recombinations; it is the result of many different processes as described in the next paragraph.

1.3 Recombination processes

The principal processes governing the electrons-holes recombination in silicon can be summarized in the following three [8]:

- 1) recombination through deep-level impurities (or *Shockley-Read-Hall* or multiphonon), characterized by τ_{SRH}
- 2) radiative recombination, characterized by τ_{rad}
- 3) Auger recombination, characterized by τ_{Auger}

SRH

In indirect semiconductors under low and medium injection conditions the dominant process is the first one [9]; to calculate it, some parameters of each kind of impurities in the lattice are necessary: the density of the recombination levels (N_T), the capture cross sections (σ_n and σ_p) for electrons and holes respectively, and the energy levels inside the energy gap (E_T). The more detrimental among the impurities, because of their capture cross sections, are some metallic ions[10,11,12], but even molecules composed by non-metallic atoms (i.e. B_xO_x , for Boron doped bulk in silicon)[13, 14] contribute significantly at the reduction of the minority carriers lifetime. The worst impurities are those with E_T near the midgap, because the capture cross section is usually the higher. Every present specie has to be evaluated and the superposition of their effects gives the bulk minority SRH lifetime; for each impurity, characterized with particular parameters, the SRH lifetime is given by (1.19)

$$\tau_{SRH} = \frac{\tau_h(n_{e0} + n_{e1} + \Delta n_e) + \tau_e(n_{h0} + n_{h1} + \Delta n_h)}{n_{h0} + n_{e0} + \Delta n_e} \quad 1-19$$

With n_{ei} and n_{hi} given by (1.20a-1.20b), τ_e and τ_h by (1.21a-1.21b) while Δn_e and Δn_h are the excess carriers densities, equals when trapping effect can be neglected. In (1-21) v_{te} and v_{th} are the average thermal velocity of electrons and holes for electrons and holes respectively.

$$\begin{aligned} n_{e1} &= n_i e^{(E_T - E_i)/kT} & \mathbf{a} \\ n_{h1} &= n_i e^{-(E_T - E_i)/kT} & \mathbf{b} \end{aligned} \quad 1-20$$

$$\begin{aligned} \tau_e &= \frac{1}{\sigma_e v_{te} N_T} & \mathbf{a} \\ \tau_h &= \frac{1}{\sigma_h v_{th} N_T} & \mathbf{b} \end{aligned} \quad 1-21$$

Trapping happens when impurity levels in the semiconductor forbidden gap capture electrons (holes) and emit back the particles in the CB (VB) after a short blocking time; as long as the charges are trapped, $\Delta n_e \neq \Delta n_h$. Trapping is of major concern in wide semiconductor band. When trapping is an issue, lifetime measurements can be carry out

with a background illumination for saturate these trap centres. A sketch of the trapping compared with SRH recombination is depicted in fig (1-7) [8]

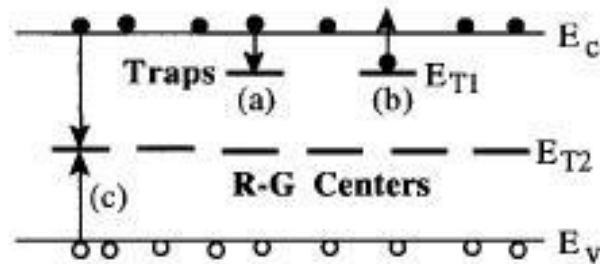


Figure 1-7 – Graphical representations of electrons trapping (a), emission back to the CB from the trap (b), and recombination through a deep level

The energy liberated during this recombination process is dissipated by lattice vibrations, so it's also called multiphonon process.

The SRH recombination effect is the dominant also at the surfaces; in these regions there's a plenty of states lying in the forbidden gap, because of the severe lattice symmetry broken, as depicted in fig.(1-8).

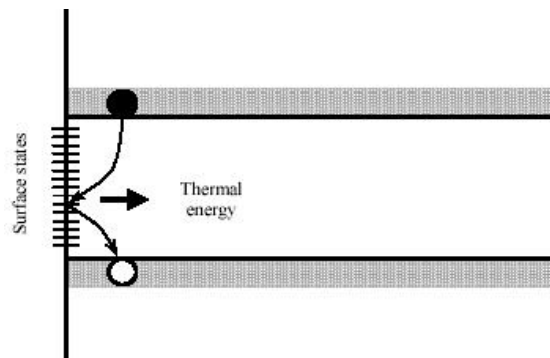


Figure 1-8 – Recombination through levels in the forbidden gap at the surface [17]

At the bare surface silicon dangling bonds are present, and the electron occupation levels here allowed have an energy distribution very different compared with that of the bulk crystal lattice. The surface states density and their energy distribution are very dependent on the environmental conditions and on the chemical treatments at the surface material, so it's generally poorly known. Different is the case of the SiO_2/Si interface, which has been extensively studied and characterized for a number of different environmental reacting conditions [9].

The surface recombination velocity can be calculated, like in the previous SRH lifetime case, with (1.22) [5]

$$s_r = \frac{s_h s_e (n_{h0s} + n_{e0s} + \Delta n_{es})}{s_e (n_{e0s} + n_{e1s} + \Delta n_{es}) + s_h (n_{h0s} + n_{h1s} + \Delta n_{hs})} \tag{1-22}$$

with

$$s_e = \sigma_{es} v_{th} N_{iT} \tag{a}$$

$$s_h = \sigma_{hs} v_{th} N_{iT} \tag{b}$$

The interface density of states N_{iT} is considered constant, and is expressed in cm^{-2} , while the carrier density at the surfaces are in units of cm^{-3} .

The surface recombination doesn't necessarily happen at the surface (interface) of the material. In fact the surface can be in many charge conditions; it can have a surface induced space charge region, as represented in fig. (1-9). It can be accumulated, depleted or inverted, depending, for example, on the charge of the surface states (positively or negatively charged).

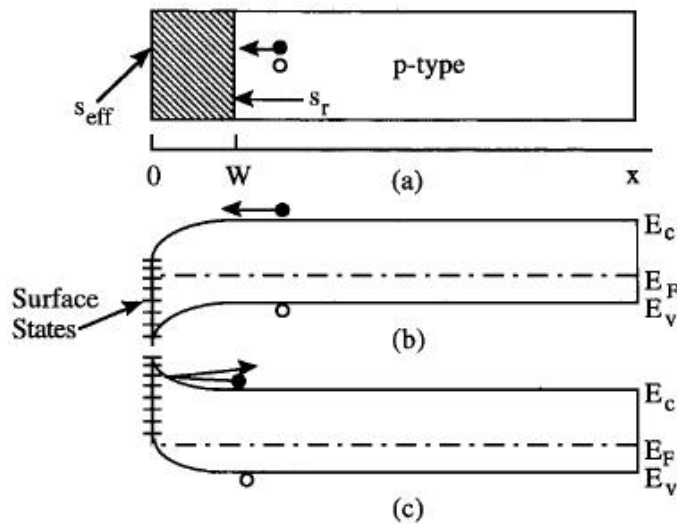


Figure 1-9 – (a) Schematic representation of the region of semiconductor influenced from the depleted surface. (b) Effect on the energy diagram of the depleted surface. (c) accumulated surface.

An accumulated surface repels the minority carriers by a repulsive potential, so the surface recombination velocity is low. This is the effect produced by the back surface field (BSF) in solar cells with the P+/P doping profile at the back surface, with p bulk material. Because of this effect is due to stationary charges, repulsive barrier diminishes with increasing injection level, with consequent increase of recombination. The passivation of the p -type silicon is quite difficult, even with a thermally grown SiO_2 ; this fact is attributed at the higher electron capture cross section than the holes' at the interface of silicon dioxide/ n -type silicon [15].

It's interesting to consider the behaviour of the SRH recombination with the injection level [8]. If we apply (1-19) for the Si bulk lifetime, the behaviour of the SRH lifetime with the energy level of the recombination centre for different injection level is represented in fig.(1-10), where η gives the injection level, being $\eta = \Delta n_e/n_{h0}$. It appears that the lifetime doesn't increase always with the injection level, as frequently stated; however, in the graph, the cross section of the impurities is considered constant; this is in general not true. Has already mentioned, usually the nearer the E_T at the midgap, the higher the capture cross section. In fig.(1-11) is shown how τ_{SRH} depends on the injection level, for an impurity with an E_T near the midgap, for different σ_p values. It appears evident the strong dependence on the capture cross section.

In fig. (1-10) the low level (ll) and high level (hl) injection regime are tagged.

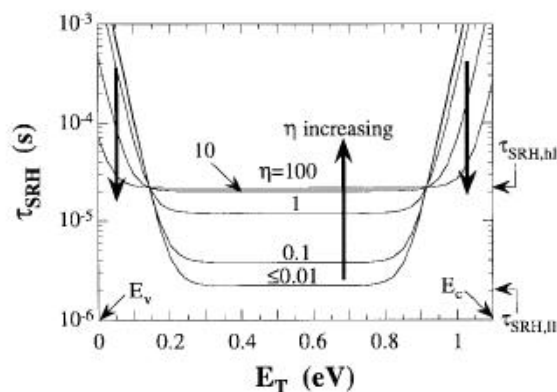


Figure 1-10 – SRH lifetime vs E_T at different injection levels, for $N_T=10^{12} \text{ cm}^{-3}$, $p_0=10^{16} \text{ cm}^{-3}$, $\sigma_n=5 \times 10^{14} \text{ cm}^2$, $\sigma_p=5 \times 10^{15} \text{ cm}^2$ [8]

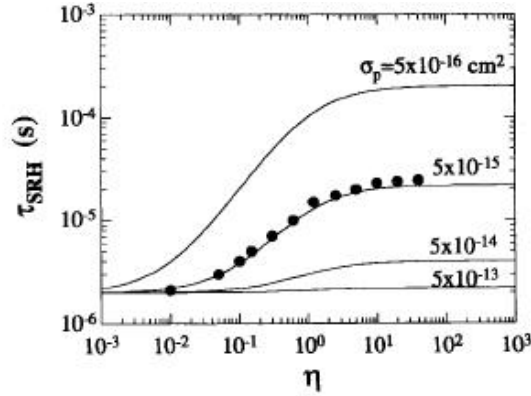


Figure 1-11- SRH lifetime vs injection level for different impurity cross section, for $N_T=10^{12} \text{ cm}^{-3}$, $p_0=10^{16} \text{ cm}^{-3}$, $E_T=0.4 \text{ eV}$, $\sigma_n=5 \times 10^{-14} \text{ cm}^2$ [8]

An analogous graphic regarding the surface recombination velocity is shown in fig.(1-12). The behaviour is opposite at the previous; both indicate that increasing the injection, the recombination by the deep centres is reduced. The dependence, for a fixed E_{Ts} near the midgap, with the injection levels is in fig.(1-13).

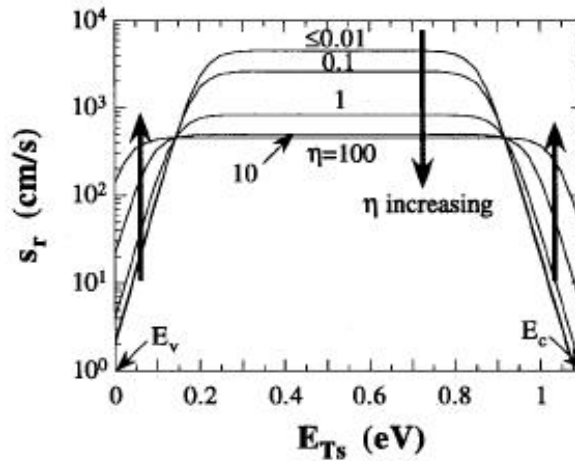


Figure 1-12 – Surface recombination rate vs E_T at different injection levels, for $N_i=10^{10} \text{ cm}^{-3}$, $p_{0s}=10^{16} \text{ cm}^{-3}$, $\sigma_{ns}=5 \times 10^{-14} \text{ cm}^2$, $s_{ps}=5 \times 10^{-17} \text{ cm}^2$ [8]

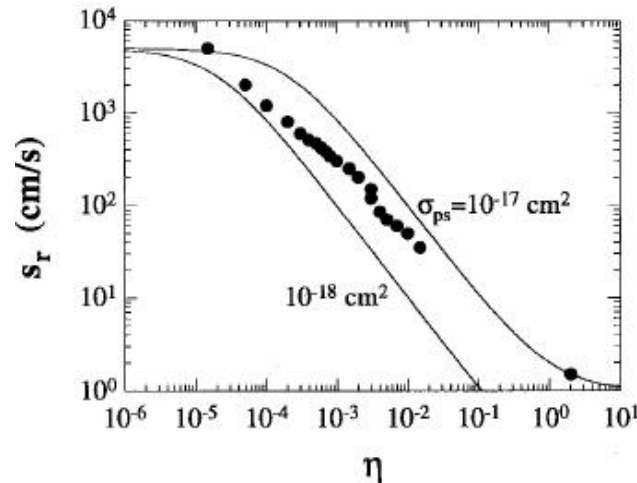


Figure 1-13 - Surface recombination rate vs injection level for different impurity cross section, for $N_{it}=10^{10} \text{ cm}^{-3}$, $p_{0s}=10^{16} \text{ cm}^{-3}$, $E_T=0.4 \text{ eV}$, $\sigma_{ns}=5 \times 10^{14} \text{ cm}^2$ [8]

During lifetime measurements and during devices working conditions, the SRH carrier lifetime is a combination of the bulk and surface effects. The *effective SRH lifetime* is the result of the combination of these effects. This quantity is expressed with (1.24), while the relation between the τ_{surface} and the surface recombination velocity s_r is given in (1.25) [16]

$$\frac{1}{\tau_{\text{eff}}} = \frac{1}{\tau_{\text{bulk}}} + \frac{1}{\tau_{\text{surface}}} \quad 1-24$$

$$\tau_{\text{surface}} = \frac{1}{\beta^2 D_e} \quad \mathbf{a}$$

1-25

$$\tan(\beta t / 2) = \frac{s_r}{\beta D_e} \quad \mathbf{b}$$

Where t is the sample thickness.

Considering low injection regime, the effective lifetimes is inversely proportional to the impurity concentration N_T only if the bulk lifetime dominates the surface lifetime, i.e. at high impurity density. For low impurity density the effect of the surface dominates, as shown, for example, in fig.(1-14), where are introduced Fe atoms as contaminants in a boron doped Si.

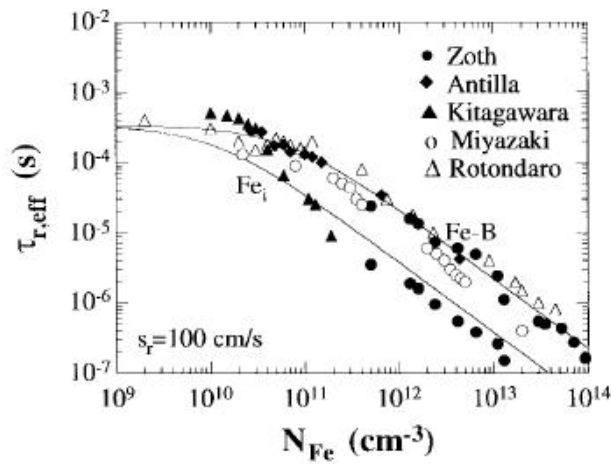


Figure 1-14 - Effective lifetime vs Fe atoms concentration, for $t=650\mu\text{m}$, $p_0=10^{15}\text{cm}^{-3}$, $E_T=0.4\text{eV}$, $\sigma_p=5\times 10^{-16}\text{cm}^2$, $\eta=0.01$, $T=300\text{K}$ [8].

Radiative recombination

The radiative recombination happens when an e-h pair disappears by emission of radiation; the bounding energy is carried away by a photon, in one single step. It's the main recombination effect in direct band semiconductors, but is negligible in indirect semiconductors, at least under low and medium injection levels [9]. τ_{rad} is inversely proportional with the carrier population in the bands, because this band to band process happens when electrons and holes are present simultaneously. A graphic representation is sketch in fig.(1-15)

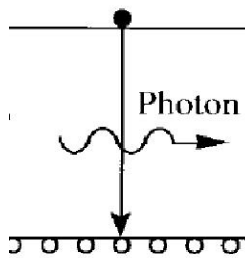


Figure 1-15 - Radiative band to band recombination

The behaviour of this process is described by (1.26) [8], where B_r is the radiative recombination coefficient, typical for each material; for silicon $B_r = 2\times 10^{-15}\text{cm}^3/\text{s}$.

$$\tau_{\text{rad}} = \frac{1}{B_r (n_{h0} + n_{e0} + \Delta n_e)}$$

Auger Recombination

The Auger recombination happens when the energy emitted with the electron-hole recombination is absorbed from a third carrier. It may be of two kinds: direct Auger, or trap assisted Auger. The latter has a functional behaviour like the radiative recombination, but the recombination coefficient must be substituted with B_T , the trap-assisted recombination coefficient, clearly dependent on the material purity. The direct Auger has a different behaviour and, for a p -type semiconductor, follows (1.27), where C_p is the Auger coefficient, for Si equal at $C_p=1.1 \times 10^{-30}$. A sketch of the two Auger effects is in fig.(1-16)

$$\tau_{Auger} = \frac{1}{C_p (n_{h0}^2 + 2n_{h0}\Delta n_e + \Delta n_e^2)} \tag{1-27}$$

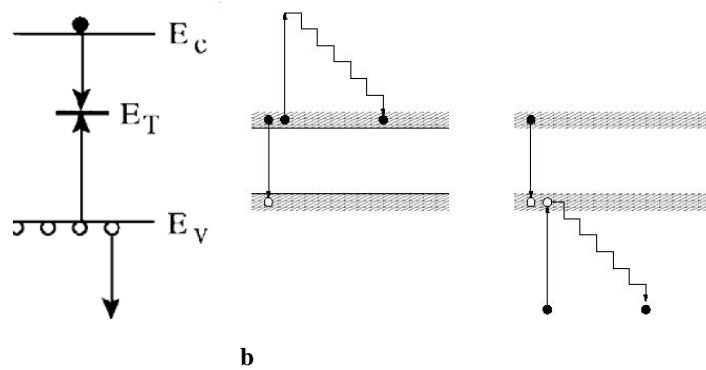


Figure 1-16 - a) Trap assisted Auger b) Auger effect with excess energy delivered at electron in CB or at hole in VB

At high carrier densities the Auger recombination is the dominant effect. The composition of all these different effects is given with (1.28)

$$\frac{1}{\tau} = \frac{1}{\tau_{SRH}} + \frac{1}{\tau_{rad}} + \frac{1}{\tau_{Auger}} \tag{1-28}$$

In fig.(1-17) [17] is summarized the effect of the different recombination mechanisms with the illumination level.

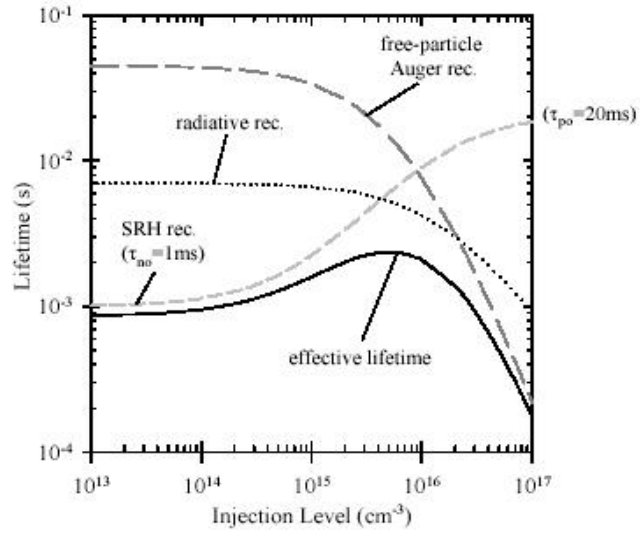


Figure 1-17 – Contributions of different recombination mechanisms at the effective lifetime in silicon [17].

CHAPTER 2 SOLAR CELLS

2.1 Qualitative description

Joining the n and p zones, the two respectively majority carriers diffuse toward the other region by the effect of concentration difference. Associated to this motion, an unbalance of electrical charges is created, producing an internal electrical field near the junction of the two zones. An electrical potential is built-up in order to counterbalance the diffusive motion of the carriers; this electrical potential is accounted by a bending of the VB and CB in the real space energy band diagram until the equalization of the Fermi level for the two regions, which corresponds at the thermal-diffusive equilibrium condition, as shown in (2-1)

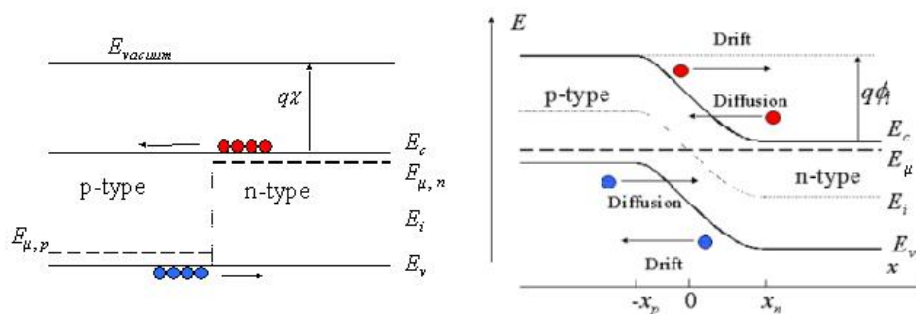


Figure 2-1 – Schematisation of the carriers motion and the consequent bands bending at the metallurgical junction of p and n type semiconductor

In the region of the junction, a strong electric field is present, sweeping the carriers; this region is usually called depletion zone.

The p-n junction is the core of the electronics and of the photovoltaic devices. The fundamental electronic component made of a single p-n junction is the diode. Diodes and solar cells work in different ways: the current in a diode is due by the diffusion of the majority carriers toward the zone where they are minority, by the effect of the concentration difference; the current follows an exponential behaviour with the external voltage applied, because the concentration of majority carriers with enough energy to overcome the potential barrier increases coherently with (2-1). The exponential behaviour is well fit until the device works in low injection conditions, i.e. until the minority carriers concentration is significantly lower than that of the majority.

$$n = N_D e^{-q \frac{(V_b - V)}{kT}}$$

2-1

For a solar cell, the regime of the device is not controlled, as for the diode, only through an external power supply, but is governed from the carrier injection due to the electrons ionized for the interaction with the solar radiation. A number of minority carriers, and consequently also of majorities, equals to the number of converted photons is created. In the condition of doping concentration fairly higher than the concentration of photo-electrons, the variation on the behaviour of the diffusion current due to the majority carrier can be considered negligible; diversely is the case for the minority carriers, which abruptly increase their concentration respect to the non-illuminate condition. This important difference leads to a boost in the current of the minority carriers which can move toward the junction and the zone where they are majority, in opposite direction respect to the diffusion current of the majority carriers present in the diode behaviour (which flows from high concentration region to low concentration region). If a forward bias is applied at the solar cell, the “diode behaviour” of the p-n junction competes with the peculiar “solar cell behaviour” and the current density generated can be expressed as in (2.2-2.3); the diffusion component of the current from the majority to minority region increases in an exponential way; increasing the bias will happen that the current induced by the voltage supply (diode density current) equals the one induced by the light (J_{ph}).

In this description an active load, an external voltage supply, is considered for the solar cell; the same considerations are valid if the external voltage drop is due to the passage of the current produced by the cell on an external passive load.

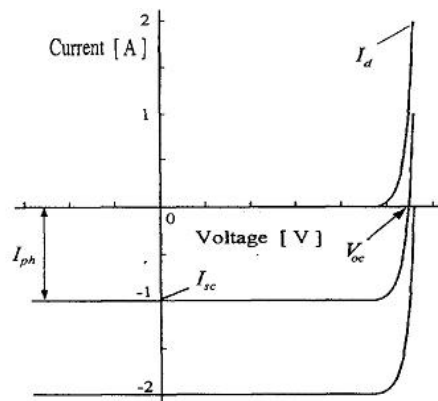


Figure 2-2 – Current – voltage characteristics for an ideal cell at different illumination conditions

$J = J_{ph}$ – “diode density current”

2-2

$$J = J_{ph} - J_0 \left(e^{qV/nkT} - 1 \right) \quad 2-3$$

2.2 Idealized solar cell

In the most simplified configuration, a solar cell can be represented with a semiconductor device made of a p -zone and an n -zone joint together. The model become more sophisticated if, at this basic system, are added the surface effects, the doping profiles, the electrical contacts and different injection conditions. However, even with these complications, the behaviour of a solar cell can be forecasted when some main material parameters are known; indeed, the laws governing the motion of the carriers in the device are the 5 nonlinear equations (2.3) which describe the electric and diffusive behaviour inside the material [7]. They have to be completed with the boundary conditions which are defined specifically under the different electrical loading condition of the cell.

$$\left\{ \begin{array}{ll} \vec{J}_e = e\tilde{\mu}_e n_e \vec{E} + eD_e \vec{\nabla} n_e & \text{electron current} \\ \vec{J}_h = e\tilde{\mu}_h n_h \vec{E} - eD_h \vec{\nabla} n_h & \text{hole current} \\ \frac{1}{q} \vec{\nabla} \cdot \vec{J}_e = U - G + \frac{d\Delta n_e}{dt} & \text{electron continuity equation} \quad 2-4 \\ \frac{1}{q} \vec{\nabla} \cdot \vec{J}_h = -(U - G + \frac{d\Delta n_h}{dt}) & \text{hole continuity equation} \\ \vec{\nabla} \cdot \vec{E} = \frac{q}{\varepsilon} (p - n + N_D - N_A) & \text{Poisson's equation} \end{array} \right.$$

U is the recombination rate and G is the generation rate of free carriers; in steady state condition the terms d/dt in the continuity equations can be neglected. Both U and G depends on the position; while G is dependent on the light source and on the absorption coefficient, U is a function which has strong discontinuities, but it can be considered constant in each separate regions constituting the device, except done for the emitter; the bulk of the material, the depletion zone, the front surface, the back surface and the front and rear metallic contact interfaces are each characterized by own carrier lifetimes or

recombination velocities. The emitter, in a quite precise analysis, has to be considered with a position dependent lifetime; this because it is usual created by diffusion doping process, so the amount of impurities is not space constant and so also the electrical properties. The generation rate $G(x)$ comes by derivation of $I_{abs}(x)$ along the direction perpendicular at the surface, considering that every photon can generate no more than one electron-hole pair, and is given by (2.5).

$$G(x) = \frac{dI_{abs}}{dx} = \int_0^{\lambda_{max}} \frac{I_0(\lambda)}{hc} [\alpha(\lambda)e^{-\alpha(\lambda)x}] d\lambda \quad 2-5$$

The solution of the equations system isn't, in general, analytical. Numerical calculations are required to achieve results for simulated devices working in approximately real conditions. This approach gives good results and is used in conventional solar cell simulators [18]. As counterpart of this method the physical description of the behaviour of the carriers, and consequently of the measured values, as function of the fundamental parameters is not evident. Some aspects referred at particular simplified cases can be pointed out in order to give a better description of the working operations in a solar cell.

One initial assumption is the symmetry of the system along the directions parallel to the junction, in case of flat surface cells (no texturing). So, the mathematical analysis can be carried out with one preferred direction. A second assumption is the approximation (2.5a-2.5b) of drift current negligible in quasi neutral regions [7].

$$\begin{aligned} \vec{J}_e &\cong +eD_e \vec{\nabla} n_e & \mathbf{a} \\ \vec{J}_h &\cong -eD_h \vec{\nabla} n_h & \mathbf{b} \end{aligned} \quad 2-6$$

The continuity equation for electrons in the p -zone becomes (2.7)

$$U - G = \frac{(n_{ep}(x) - n_{ep0})}{\tau_e} - G(x) = D_e \frac{d^2 n_{ep}}{dx^2} \quad 2-7$$

Under these conditions, the behaviour of an excess of minority carriers in a defined position of the bulk region can be described by (2.8) [7], with L_e , the electron diffusion length, given by (2.9). In this particular case, τ_e indicates the bulk lifetime, as result of the different processes previously described.

$$\frac{d^2 \Delta n_e}{dx^2} = \frac{\Delta n_e}{L_e^2} \tag{2-8}$$

$$L_e = \sqrt{D_e \tau_e} \tag{2-9}$$

The solution of this equation depends on the boundary conditions; with the short circuit condition for the solar cell, ($\Delta n_e \cong 0$ at the edge of the depletion zone) it leads at an exponential decreasing behaviour of the concentration with the distance from the generation point, as well as for the minority carrier current. The solution of this case, with generation of the excess of carriers at the position x_1 , is graphed in fig. (2-3).

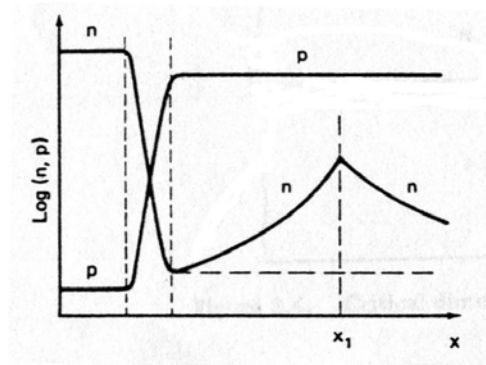


Figure 2-3 – Carrier distribution in a cell with a minority carrier injection at distance x_1 from the surface. [7]

Because of the equation (2.8) is linear, a distribution of excess minority carriers generation gives a superposition of the singular position-dependent injection effects. It follows that the probability for the junction to collect the carriers in short circuit condition is dependent on the generation position as (2.10), for electrons in a p -zone bulk region.

$$\eta_{cc}(x) \propto e^{-x/L_e} \tag{2-10}$$

Except for the case of the back contact solar cells, the junction is near the illuminated surface of the device; combining the (2.10) with the generation function (2.5) appears that

the nearer the junction at the front surface, the higher the number of collected minority charges, considering the emitter region with lower carrier lifetimes respect to the collector region because of higher doping level.

If the electron-hole pair generation rate in p-type silicon of a steady light source is G , then the excess electron concentration caused by the light will be (2.11)

$$\Delta n_{ep}(x) = G(x)\tau_{ep} = n_{ep}(x) - n_{ep0} \approx n_{ep}(x) \quad 2-11$$

The junction acts sweeping the minority charges which collects; in short circuit condition, for the minority carrier population, it can be seen as a surface with an infinite “recombination” velocity; this fact reduces a lot the concentration of carriers, and this is the work required to achieve the same level for the quasi-Fermi level in the two zone, as imposed by the short circuit condition. Actually, the function of the internal electrical field is to move electrons (holes) from the CB (VB) to the VB (CB) of the same zone, by transition throughout the external circuit. The very fast decreasing of the minority carrier concentration in proximity of the depletion region produces a steady gradient in carrier concentration with lower level of particle concentration at the edge of the depletion region, at least for material with lifetime not too small; this fact leads to a “preferred” direction for the generated charges; consequently, it is possible to state that if a carrier is generated at a distance shorter than the diffusion length it has very high probability to be collected, and contributing at the short circuit current. $G(x)$ gives the excess of carriers concentration in a semiconductor material generated by an external source; applying the absorption function for Si with $\alpha(\lambda, 300K)$ and with the solar spectrum AM1.5, the excess of carriers density produced each second at distance x from the surface is obtained; it’s plotted in fig.(2-4).

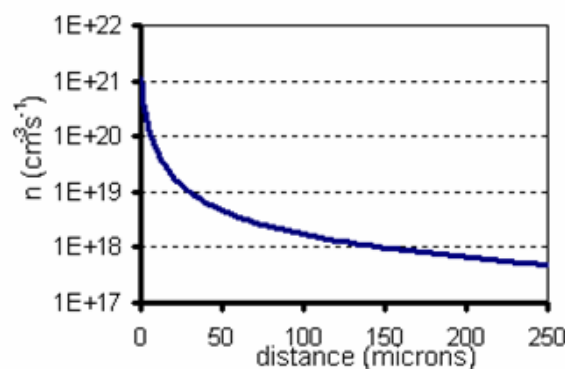


Figure 2-4 – Excess of minority carriers in a second of illumination silicon vs distance from the surface, for a material illuminated with a light source with the characteristics of the Sun.

If $L_e \gg W$, with W sample thickness, and perfect back surface passivation, during a transitory period the carriers moves toward the back of the cell; in the steady condition after this transitory, for the net electron motion there is a preferred direction toward the junction, because the concentration level in the bulk has achieved a constant value. In fig. (2-6) are shown the solutions of eq. (2.12) for the p -zone of a cell $300\mu\text{m}$ thick, for different minority carrier lifetimes, with perfect back passivation. The edge of the depletion region in short circuit condition is supposed to be at 500nm far from the front illuminated surface and is considered for $G(x)$ a function fitting the data obtained from the $G(x)$ profile calculated in a discrete element form, considering the solar spectrum AM1.5 of fig (2-5) for the illumination flux and the absorption function of silicon.

$$\frac{n_{ep}(x)}{\tau_e} - G(x) = D_e \frac{d^2 n_{ep}(x)}{dx^2} \tag{2-12}$$

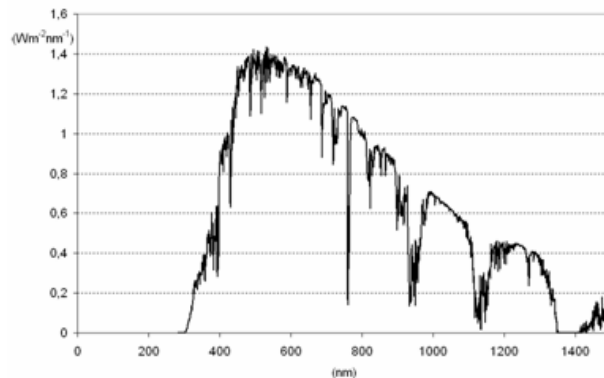


Figure 2-5 – Solar Spectrum AM1.5

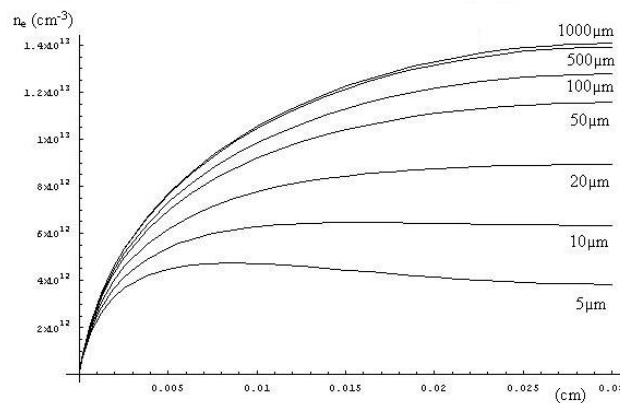


Figure 2-5 – Concentration of minority carriers with the distance from the edge of the depletion region in the p -zone, for different lifetimes of the bulk material.

It appears that the gradient in the excess of minority concentration is higher near the front surface; this allows a better collection of the charges; the effect of directionality for the diffusion motion is stronger with higher carrier lifetimes. The recombination effect reduces this behaviour with consequent reduction of the charge collection and short circuit current generated from the cell. This fact can be considered in the calculation of the generated current, introducing in the collection efficiency factor another dependence on the lifetime, as in (2.13)

$$\eta_{cc}(x) \propto f(\tau_e) e^{-x/L_e} \quad 2-13$$

The concentration of minority carriers in short circuit condition is far below that one of majority, so the low injection assumption is valid, even under concentrated illumination.

The effect of the concentrated illumination has more relevance with moving toward the open circuit condition. Indeed, in the OC case there isn't a net current flow, so the concentration of free carriers has to be quasi constant throughout the zones and the recombination is the limiting factor at the concentration of excess minority carriers. This consideration has as straightforward consequences the evidences of the role of the lifetimes, illumination level and material thickness for the V_{oc} of the solar cell. Because of the minority charges overcoming the junction are counterbalanced by the motion of the majority carriers of the other zone, the only net current inside the device can occur toward the directions opposite the junction, due to the effect of the recombination centres of the material; it occurs in this direction because of the surfaces have usually lower carrier lifetimes and can be seen as a sort of "carriers sinks".

It is significant to show how much the voltage depends on the minority carriers concentration level; in general, the voltage of a device is given by the difference between the quasi-Fermi levels (1.15) at the electrical contacts; referring at the band diagram picture of fig.(2-7) the open circuit voltage of a solar cell is given by (2.14); the V_{bcc} is the built in electric potential in short circuit conditions, i.e. the step between two analogous bands in the p and n region, in short circuit.

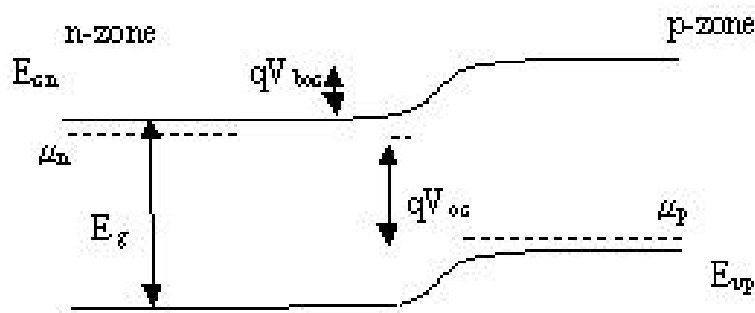


Figure 2-6 – Schematic band diagram of an illuminated PV cell under open circuit condition

$$V_{oc} = \frac{E_g - (E_{cn} - \mu_n) - (\mu_p - E_{vp})}{q} - V_{boc} = V_{bcc} - V_{boc} \quad 2-14$$

While the dependence of the quasi-Fermi levels on the carrier concentration in the two zone are derived from (1.15), the behaviour of V_{boc} , i.e. the voltage step for each band edge at the depletion region under open circuit condition, has to be calculated.

The equilibrium of the electronic density currents between the regions p to n and n to p can be expressed with (2.15), where the first term of the equation indicates the p to n density current, while the second term indicates the n to p contribution. The factors $\eta_{ep}(\tau, V)$ and $\eta_{en}(\tau, V)$ represent the probability of the electrons to reach the depletion region edges from respectively the p and n regions, under external bias V . The n_{ep} and n_{en} are respectively the electron concentration in the p and n zone, while the $\langle v_{ep}(V_{oc}) \rangle$ and $\langle v_{en}(V_{oc}) \rangle$ represent the average velocity component of the electron directed toward the junction in the two zones, in condition of open circuit. In short circuit condition

$$\langle v_{en}(V \cong 0) \rangle \cong \frac{L_{en}}{\tau_{en}} \text{ and } \langle v_{ep}(V \cong 0) \rangle \cong \frac{L_{ep}}{\tau_{ep}} \text{ as in [21].}$$

$$\langle v_{ep}(V_{oc}) \rangle = n_{ep} \eta_{ep}(\tau, V_{oc}) = \langle v_{en}(V_{oc}) \rangle \eta_{en} n_{en} e^{-q \frac{(V_{bcc} - V)}{kT}} \quad 2-15$$

Under low injection condition (2.15) can be simplified with $\eta_{en}(\tau, V) \cong 1$ and $n_{en} \cong N_D$, because the electrons are the majority carriers in the n region. Supposing very good material, we can consider $\langle v_{en}(V_{oc}) \rangle \cong \langle v_{ep}(V_{oc}) \rangle$ so eq.(2.15) becomes (2.16)

$$n_{ep} \eta_{ep}(\tau, V_{oc}) = N_D e^{-q \frac{(V_{bcc} - V)}{kT}} \quad 2-16$$

With open circuit condition, $V_{boc} = V_{bcc} - V_{oc}$; so, V_{boc} results as (2.17)

$$V_{boc} = \frac{kT}{q} \text{Log} \left[\frac{N_D}{n_{ep} \eta_{ep}(\tau)} \right] \quad 2-17$$

Considering the low injection conditions $n_{en} \cong N_D$ and $n_{hp} \cong N_A$, we assume that V_{bcc} doesn't change with the illumination, so the open circuit voltage can be expressed as (2.18)

$$\begin{aligned} V_{oc} \cong V_{bcc} - V_{boc} &\cong \frac{E_g - kT \text{Log} \left[\frac{N_c}{N_D} \right] - kT \text{Log} \left[\frac{N_v}{N_A} \right] - kT \text{Log} \left[\frac{N_D}{n_{ep} \eta_{ep}(\tau)} \right]}{q} = \\ &= \frac{E_g - kT \text{Log} \left[\frac{N_c}{n_{ep} \eta_{ep}(\tau)} \frac{N_v}{N_A} \right]}{q} \end{aligned} \quad 2-18$$

The bandgap narrowing effect due to the doping concentration isn't accounted here, but it can easily be introduced considering the function $E_g(N_A)$, instead of a constant value for E_g .

From (2.18) follows that the voltage decreases with temperature; the ideal coefficient for the V_{oc} decreasing with T can be easily calculated; it depend on the lifetime of the material through n_{ep} and η_{ep} (plus n_{hn} with η_{hn} , if we consider both the region with the opportune weight); this coefficient is lower for semiconductor with higher bandgap, because of the dependence on N_c and N_v , and decrease with the illumination flux for the dependency on n_{ep} , as experimentally proofed by [19,20] for III-V semiconductors and by [21] for silicon.

The conditions of $L_e \gg W$ and perfect back surface passivation can be here used easily to calculate the higher value for n_{ep} , i.e. in conditions of OC, because we can consider the concentration almost uniform in the collector region, as in (2.19)

$$n_{ep} \cong \int_0^W [G(x) \tau_e / W] dx$$

2-19

The voltage calculation requires the contribution of the hole generation in the n region, too. In order to simplifying the description, we consider the system like a cell where almost all the minority carriers are generated in the p -region. With this approximations, the calculation of the Voc of an idealized cell is straightforward; considering τ_{Auger} as limiting minority carrier lifetime for the material, it results of about 1.3ms with a doping level of $1.5 \times 10^{16} \text{ cm}^{-3}$ (corresponding at a resistivity of 1ohm-cm, as from fig.(1-4), applying formulas (2.19 and 1.27)). With perfect surfaces passivation, with this value of lifetime and with a thickness sample $W=300\mu\text{m}$, it is reasonable to consider $\eta_{ep}(\tau, V) \cong 1$, even supposing a random motion of the electrons in the p -region. Under these idealized conditions, $V_{oc}=0.75V$ is obtained under 1sun AM1.5, consistently with [9].

The relation of voltage with lifetime and width of the bulk is confirmed in real devices; for a more accurate evaluation, the real effect of the surfaces has to be considered; for example, the idealized behaviour doesn't take into account the recombinations at the rear surface, which reduces a lot the increasing of minority carriers concentration; the experimental evaluation of the role of the back surface passivation on the voltage is presented in [22].

Through the previous description follows how to draw the I-V curve of an ideal solar cell, without surface recombination and with $L_e \gg W$. I_{abs} limits the maximum current and determines the upper limit for the carriers concentration; this maximum concentration is n_{epoc} ; it corresponds at the maximum value for the minority carriers concentration contributing at the current of the device (n_{ep}^J). If we consider $\eta_{ep}(\tau, V_{oc}) \cong 1$, we can apply the same condition for the collection efficiency for all the voltage of the cell $V \leq V_{oc}$. The electrons concentration in the p -material which doesn't contribute at the current defines the cell voltage following (2.20)

$$V \cong V_{bcc} - V_b = \frac{E_g - kT \text{Log} \left[\frac{N_c}{n_{ep} \eta_{ep}(\tau_e)} \frac{N_v}{N_A} \right]}{q} = \frac{E_g - kT \text{Log} \left[\frac{N_c}{(n_{epoc} - n_{ep}^J) \eta_{ep}(\tau_e)} \frac{N_v}{N_A} \right]}{q} \quad 2-20$$

With the n_{epoc} given by (2-21) and n_{ep}^J varying from 0 to n_{epoc} . The short circuit current results, as function of the carriers concentration, as in (2-22)

$$n_{epoc} = n_{epMAX} \cong \int_0^W [G(x) \tau_e / W] dx \tag{2-21}$$

$$J_{sc} = q[\eta_{ep}(\tau, 0) n_{epMAX} \frac{W}{\tau_e} - \frac{L_{en}}{\tau_{en}} N_D e^{-\frac{qV_{bcc}}{kT}}] \tag{2-22}$$

The solar cell *Fill Factor* $FF = P_{max} / (V_{oc} I_{sc})$, can be calculated maximizing the $J \cdot V$ product.

In fig.(2-8) is shown the I-V characteristic calculated for a silicon cell with the following parameters:

- surface recombination velocity = 0
- minority carrier lifetime=1ms
- $W=300\mu m$
- 1 sun AM1.5
- Front surface reflectance =0
- Material resistivity = 1 ohm-cm
- $T = 300K$
- $\eta_{ep}(\tau, V) \cong 1$

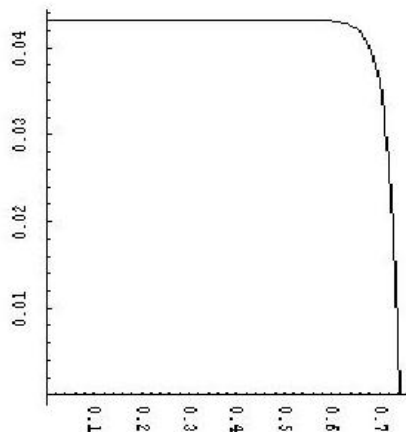


Figure 2-7 – I-V characteristic of an ideal solar cell

With the previous description, the J_e -V relation for the electron current component is derived as (2.23); under low injection condition in the n-region $n_{en} \cong N_D$, so the

thermodynamical equilibrium is achieved when (2.24) is satisfied. In (2.24) n_{ep0} is the electrons concentration in the p -zone due to thermal agitation, in thermal equilibrium conditions. Considering the approximation for very good p -type material of $\eta_{ep}(\tau, V) \cong \eta_{en}(\tau, V) \cong 1$ and $\langle v_{ep}(V) \rangle \cong \langle v_{en}(V) \rangle \cong \sqrt{\frac{D_e}{\tau_e}} f_e(V)$ as in [21], where the diffusivity coefficient and electron lifetime is considered equal in the two regions, the obtained electron contribution at the dark density current assumes the form of (2.26); combining it with the contribution at the dark current of the holes, the J_0 assumes the well known form of (2.27) where $f_e(V) \cong f_h(V) = 1$ is usually assumed.

$$J_e = q \langle v_{ep}(V) \rangle n_{ep} \eta_{ep}(\tau, V) - q \langle v_{en}(V) \rangle \eta_{en} n_{en} e^{-q \frac{(V_{bcc}-V)}{kT}} \quad 2-23$$

$$N_D e^{-q \frac{V_{bcc}}{kT}} = n_{ep0} \quad 2-24$$

$$J_e = q \langle v_{ep}(V) \rangle (n_{ep0} + \Delta n_{ep}) \eta_{ep}(\tau, V) - q \langle v_{en}(V) \rangle \eta_{en} n_{ep0} e^{-q \frac{V}{kT}} \quad 2-25$$

$$J_{0e} = q \sqrt{\frac{D_e}{\tau_e}} f_e(V) n_{ep0} \quad 2-26$$

$$J_0 = q \sqrt{\frac{D_e}{\tau_e}} f_e(V) \frac{n_i^2}{N_A} + q \sqrt{\frac{D_h}{\tau_h}} f_h(V) \frac{n_i^2}{N_D} \quad 2-27$$

In general, the position $\langle v_{ep}(V) \rangle \cong \langle v_{en}(V) \rangle \cong \sqrt{\frac{D_e}{\tau_e}}$ is a fairly rough approximation,

because the behaviour of the average velocity component of electrons toward the junction with the voltage is removed. This approximation can be effective under low V conditions, but it isn't correct near open circuit conditions.

The global electronic density current results as (2.28), where $J_{light_p} = q \langle v_{ep}(V) \rangle \Delta n_{ep} \eta_{ep}(\tau, V)$ is the contribution at the current of the photo-generated electrons in the p -region.

$$J_e = J_{light} + J_{0e} - J_{e0} e^{-\frac{qV}{kT}} \quad 2-28$$

Considering both the electrons and holes contributions at the density current of the cell, the I-V relation assumes the form of (2-29). The term A at the exponent is the *ideality factor* and accounts the recombination in the depletion region by SRH process. In the case of perfect device it is $A=1$; in general $1 < A < 2$ [7].

$$J = J_{light} - J_0 e^{-\frac{qV}{AkT}} \quad 2-29$$

The ideality factor is due to the recombination centres inside the depletion zone [7], region neglected during the previous analysis. Following [7] the (2.29) can be written in a double exponential form as in (2.30) which splits the effect of the depletion zone from the other regions of the cell; the depletion region recombination adds the term $J_{0e2} \exp\left(\frac{qV}{2kT}\right)$ at the (2-27)

$$J = J_L - J_{01} \exp\left(\frac{qV}{kT}\right) - J_{02} \exp\left(\frac{qV}{2kT}\right) \quad 2-30$$

2.3 Real solar cells

The previous description aims to show some crucial points for the solar cells fabrication; another fundamental point, just partially related to the carriers recombinations, is the metal contact manufacturing. A more realistic formula describing the behaviour of a solar cell is (2.31) which takes into account the resistance behaviour due to the metal contacts; two electrical resistance behaviour can be considered: a series resistance, R_s , and a parallel resistance, R_{shunt} . In a simple one dimensional model they are represented using the solar cell equivalent electrical circuit of fig.(2-9). It's a rough electrical schematization of the SC, because of the resistances are lumped; a more precise equivalent circuit should require distributed parameters in 3-D [23].

$$J = J_L - J_{01} \exp\left(\frac{q(V + JR_s)}{kT}\right) - J_{02} \exp\left(\frac{q(V + JR_s)}{2kT}\right) - \frac{V + JR_s}{R_{shunt}} \quad 2-31$$

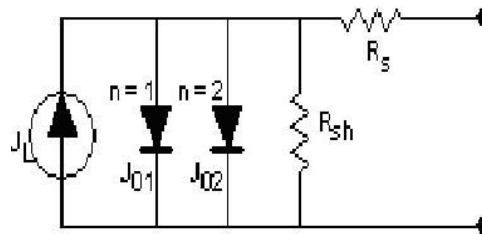


Figure 2-8 – Simplified 1D equivalent electric circuit of a solar cell

This simplified electrical equivalent circuit is enough to explain the importance of attaining R_s as low as possible, especially in the case of concentrator solar cells. Indeed, the higher the current, the higher the voltage drop across the series resistance; in this way, the diode sense a voltage higher than that one on the external load, so it's exponential behaviour reduces the current in the external circuit when the voltage on the diode is closed to its threshold voltage. The discrepancy between the voltage on the diode and the voltage on the external load gives a shortage in the current delivered from the cell in the region of the I-V characteristic of higher V. Diversely, R_{shunt} shows its detrimental effect through all the I-V curve; it's a resistance in parallel at the external load, so it drains off current in every load condition, with a linear behaviour; for this reason, it can be easily recognized and measured, considering, for example, the slope in the low voltage region of the I-V curve, where it's effect doesn't mix the series effect, at least in the more common conditions [24]. This resistance effects are represented in fig.(2-10).

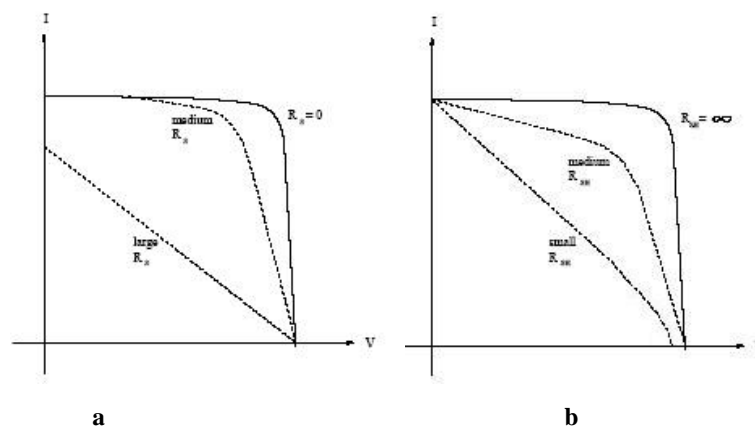


Figure 2-9 – (a) 3 different curves correspondent at three series resistance; (b) effect of the shunt resistance on the I-V characteristics

Obtain a low series resistance is fundamental in concentrator solar cell; this because the current reduction due to the diodes direct polarization depends on the diodes sensed voltage; this value is directly proportional at the generated current, for a constant value of R_s . If we define a threshold R_s to permit good FF at the cell under 1 sun of illumination, it follows that R_s has to decrease linearly with the concentration factor if we want maintain the same FF.

The series resistance is composed of 4 main components:

- emitter sheet resistance
- metal-semiconductor Schottky barrier
- Metal contact resistivity
- Bulk resistivity

Emitter sheet resistance – In front contact solar cells the emitter is near at the front surface; in order to cover the minimal area with metal contacts on the illuminated side, the current has to flow parallel at the surface in this shallow region, from the point where the charges cross the junction until they reach the contacts, as schematically depicted in fig.(2-11)

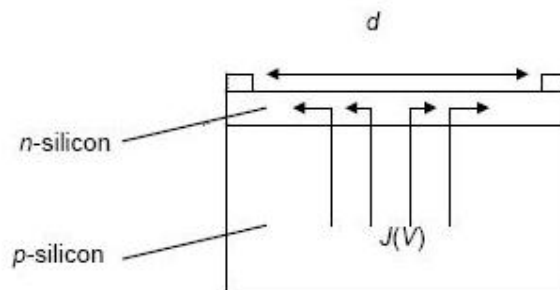


Figure 2-10- Current produced in the p-region flowing on the emitter layer of the cell toward the metal contacts

If the cell has the structure of fig.(2-11), with bulk of *p*-type and *n*-type emitter, the arrows represent the electrons motion; in the emitter they move as majority carrier, so the resistance of this layer can be measured under dark condition by a four point probe set up. The influence of the holes current in this region can be neglected being the holes the minority, at least under low injection conditions, so they move toward the junction and not toward the contacts, covering a very short path. If the sheet resistance is known, it is

possible to calculate the optimal distance between the fingers of the metal grid in order to reduce the contribution of this resistance on the overall R_s [23].

Metal-Semiconductor Schottky barrier – The ohmic behaviour of the electrical contact depends on different features of the two connected materials; the thermodynamic equilibrium between the semiconductor and the metal is reached by a deformation of the bands near the interface as in fig.(2-12), respectively for metal contacting an n-region and a p-region. This band bending is due to the different carriers concentration in the two separate materials, with physical processes analogues at these for the bands bending at the p-n junction.

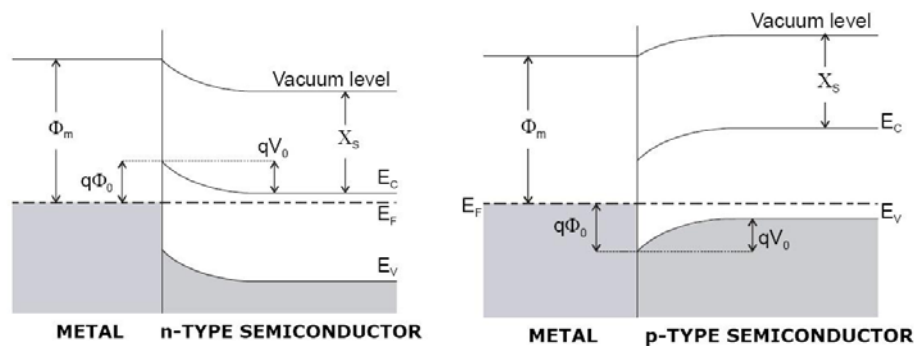


Figure 2-11 – Band bending in the semiconductor near the metal-semiconductor interface for n and p type materials

A Schottky barrier is built up at the semiconductor side of the interface and it works as an obstruction at the current flow. There are two possible way to reduce this effect: one consists in choice a contacting metal with a *working function* Φ_m closed to the *electron affinity* of the semiconductor X_s (or $X_s + E_g$ for contacting p-type semiconductor), in order to get a lower potential barrier V_0 . The second possibility consists in passing throughout the potential barrier by tunnelling; to achieve this result a narrowing of the barrier is required. The use of a metal which permits a lower V_0 is recommended in any case, but the metal selection has to satisfy also other characteristics; the more important requirements are to do not introduce deep recombination levels in the semiconductor and, for the metal contacting the front diffused region, to don't diffuse inside the semiconductor (or vice versa).

The qualitative ohmic behaviour of contacts where the current surmounts or pass through the barrier is slight different, and is depicted in fig.(2-13)

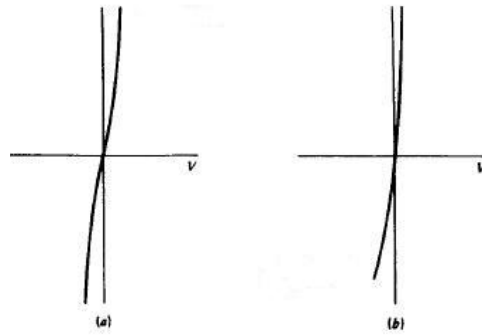


Figure 2-12 -a) tunnelling b) Low V_0

The ohmic behaviour is achieved when the condition (2.32) is satisfied [25]; in this case the resistance has a definition different respect to the generally adopted; this because, as appear in fig.(2-13), the classical resistance is function of the voltage applied.

$$R_c = \left(\frac{dJ}{dV} \right)^{-1} \Big|_{V=0} \cong 0 \tag{2-32}$$

In the case of negligible tunnel effect, the current passes the barrier by thermoionic emission; the resistance is inversely proportional at the probability of the charge to surmount the obstacle, so, for this case, R_c as the behaviour of (2.33). If the tunnelling is the dominant effect, the charge transmission is a field emission and depends on the doping of the semiconductor; the resistance follows (2.34), where C is a constant depending on material parameters. The two effects are represented in fig.(2-14)

$$R_{c_thermoionic} \propto e^{\frac{qV_0}{kT}} \tag{2-33}$$

$$R_{c_tunnelling} \propto e^{\frac{qV_0}{C\sqrt{N_D}}} \tag{2-34}$$

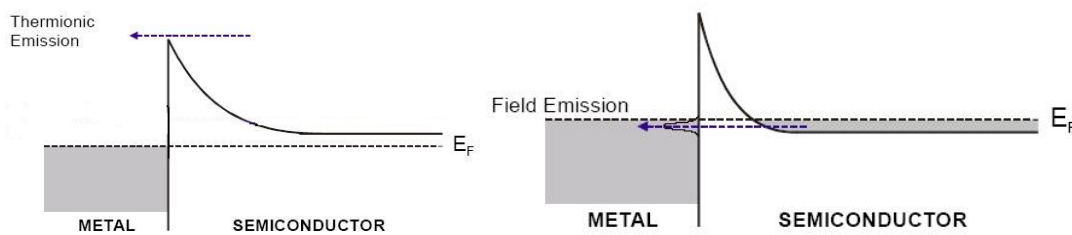


Figure 2-13 – Mechanisms for the electron transport from the n-type semiconductor to the metal

An heavy doping of the semiconductor is a way to reduce the R_c . An usual method to attain a good ohmic contact consists in doping heavily the region under the contacts, in order to produce a degenerate semiconductor for a narrow region of the semiconductor material, as sketch in fig.(2-15) for n -type material. In this way a plenty of energy levels are created inside the semiconductor forbidden gap, at the interface; this fact works helping the conductivity, so the global dominant transport process is a tunnelling, defect assisted current.

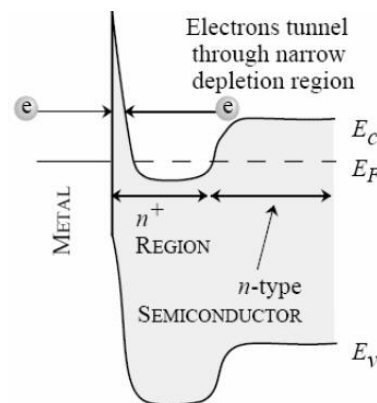


Figure 2-14 – Tunnelling in the potential barrier at the metal-semiconductor interface; the narrowing of the barrier is achieved heavily doping the material near the surface

Depositing aluminium as contact on the p -type Si and annealing it at temperature higher than the eutectical temperature (577°C) it produces a p^+ doping just at the interface; this helps the tunnelling mechanism, decreasing the contact resistance.

Metal resistivity – The current collected by the contacts has to be carried in the grid up to the wires soldered on the cell; this path through the metal contacts introduces a voltage drop because of the resistance of the metal. Although the resistivity is fairly low, the fact of carry all the generated current in very thin metallic lines leads to a voltage drop which can became significant, especially under concentration. In order to reduce this detrimental effect is convenient to select the lowest resistivity metal and deposit fingers as higher as possible; this enhances the contact cross section, without increasing the covering of the semiconductor surface. Another useful solution for the same purpose is finding a contact layout and a cell size which permits to short the fingers.

Bulk resistivity – As bulk region is here intended the thicker type of semiconductor in the solar cell; it's the region used as substrate for the process in the device manufacturing. Its resistance detrimental contribution at the I-V characteristics cannot be evaluated in every condition just considering the voltage drop given by the material resistance multiplied with the current generated from the cell. This because the material has, in general, a conductivity dependent on the illumination. However, under low injection conditions this approach can be used, also if it's not exact; if the total current produced is considered, the calculation overestimates the voltage drop. This because the so adopted resistance is for the current of the majority carriers; supposing a p-type bulk material, the electrons generated in this region doesn't feel the electrical resistance as measured in dark conditions, because they are in a quasi-empty band, and for their diffusion current the conductivity grows with the electrons concentration, as in (1.1). This means that increasing the number of minority carriers, and consequently their diffusive current, there shouldn't exist a significant voltage drop, at least in the material where they are minority. Consequently, the current which contributes at the voltage drop is principally the current of carriers injected from the other zone, which passes from a current of minorities to a current of majorities. The electrical current which has to be multiplied by the bulk resistance material is that one produced in the front, *n*-region.

From $J_e = q \langle v_{ep}(V) \rangle \Delta n_{ep} \eta_{ep}(\tau, V)$, appears in which way the electrons current in the *p*-zone is influenced by the voltage applied, in a quasi-ideal cell; the resistance introduced by this region on the electron current can be calculated as in (2.35), where $\rho_{lattice}$ (2.36) represents the effect of the lattice for free charges, as in every crystalline material, with ν frequency of electron "collisions" with the lattice and m_e^* is the effective electron mass for the semiconductor.

$$R_{e_p\text{-zone}} = \left(\frac{dJ_e}{dV} \right)^{-1} = \frac{1}{q \Delta n_{ep}} \left(\frac{d[\langle v_{ep}(V) \rangle \eta_{ep}(\tau, V)]}{dV} \right)^{-1} + \rho_{lattice} \frac{W}{S} \quad 2-35$$

$$\rho_{lattice} = \frac{m_e^* \nu}{\Delta n_e q^2} \quad 2-36$$

This means that the higher the purity of the bulk material, the lower the resistivity for the minority current, because the terms $\langle v_{ep}(V) \rangle$ and $\eta_{ep}(\tau, V)$ can be considered approximately constant if $L_e \gg W$; it implicates more current reaching the junction.

This term is not a resistive effect like the other enumerated, because it's not the same in every illumination condition, but it comes out only in working situations for solar cell; the produced effect, however, is the reduction of the current at higher voltage, as well as all the series resistance components.

In general, in non illuminated semiconductors, the thermal energy dissipation is not just produced by the interaction between electrons and lattice (Joule effect), but also by the thermal processes related to the recombinations, i.e. multiphonon process or thermalization of carriers excited by Auger effect.

In the low injection approximation, the carriers introduced in the p-zone from the n-region doesn't change significantly the hole concentration. Therefore the conductivity of the material for this holes current is the one measured in dark conditions. If the low injection approximation is not matched, a dependence on the voltage similar at that for minority carriers has to be taken into account.

Because of the diffusion component of carriers motion toward the junction diminishing increasing the voltage, $\langle v_{ep}(V) \rangle$ decreases with the V , and $\eta_{ep}(\tau, V)$ decreases if τ decreases. It follows that the resistance for the diffusion minority carriers current in the p-region is voltage and lifetime dependent. It's higher with higher voltages, so it's effect is more evident in the part of the I-V cell characteristic where the R_s is usually more deleterious; its highest value can be estimated in the open circuit condition.

The emitter depth is a parameter playing an important role for the fabrication of concentrator solar cell also for the determination of the bulk resistance; this because, in a p-type substrate cell, the thinner the n-region, the higher the electron current generated in the p-zone. If the n region, as usual, is created by a diffusion step, the donor concentration is very high; therefore the low injection condition is here practically always achieved and the emitter resistance doesn't change. Diversely, if a great current fraction is generated in the n-zone as holes current, it transforms itself in majority current crossing the junction. If the concentration of minority carriers current injected in the p-zone in steady state conditions is higher than the N_A , the low injection in the p-region cannot be assumed and the bulk resistance calculation has to be corrected.

An important effect of the contacts metallization in Si SC concerns the recombination rate at the interfaces, because it is usually fairly high [9]. In particular, ensure a good back surface passivation in Si solar cell is fundamental to get a good minority carrier collection function in the bulk of the cell. Many approaches can be followed to achieve this result [26,27], but usually they require additional process steps which lead to a longer fabrication process and therefore higher cost in the production. Generally, to decrease this recombination rate in silicon, the fraction of metal covering the surface is reduced; the rest of the back surface can be passivated with a number of different ways: saturating the dangling bonds growing thermal oxide, using Si_3N_4 with forming gas annealing, Al-nealing, creating back floating junction, creating a p^{++} back region to build up an additional local electrical field (BSF), or combinations of these methods [28,29]. In particular, the best results have been achieved, for non concentrated solar cells, with back surface locally contacted and a floating junction [30]. As described in par.(1.3), the electrostatic passivations (coming with the BSF, Al-nealing) lose their effect with increasing the carriers concentration, i.e. with increasing the illumination; the floating junction acts as electrostatic passivation, but the concentration of dopant is enough to ensure repulsion for the the minority carriers even under concentration. However, create a p^{++} layer at the silicon-metal interface is very useful for the ohmic contact behaviour; a favourable aspect is that it can be produced in the p-type semiconductor, as already mentioned, by thermal annealing of Al; for this reason aluminium is the more used metal for contacting the p-type bulk of Si solar cells.

As well as for the rear contact, the recombination rate is very high, closed to the scattering limited velocity (order of 10^7cm/s)[9], also at the front silicon-metal interface. Decreasing the fraction of metal surface cover is a way to reduce the weight of this effect. However, especially for concentrated solar cell, this method cannot be heavily pursued, to avoid increasing of series resistance. Because of this high recombination rate influences partially only the region in a distance range of less than one diffusion length in the diffused material (for holes, in an n-type diffused material), and because of under the contact the light, in first approximation, doesn't generate minority carriers, the effect of recombination at the front contact metal-semiconductor interface can be considered of secondary importance.

2.4 Strings of solar cells

Because the voltage produced by single solar cells is too low for the most common applications and for the inverters, the cells are series connected in strings. This leads to the necessity of having all the cells of the string producing the same current; considering devices with analogue characteristics, they have to receive the same illumination flux. Indeed, the lower illuminated cell limits the current production of the string; the reason of this fact can be illustrated considering the band diagram in the real space of connected cells; in fig.(2-16) is depicted for 3 cells series connected, with a resistive load on the external circuit. Here, one cell (A) produces less current than the others, as happen in the case of shadowing.

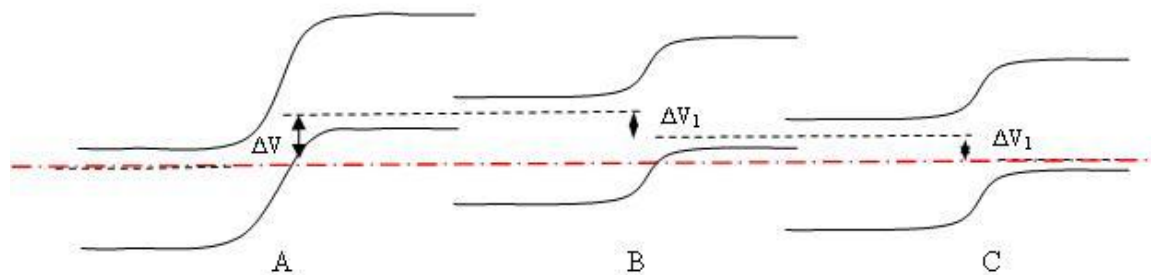


Figure 2-15 – Band diagrams of 3 cells series connected; the A cell is less illuminated than B and C

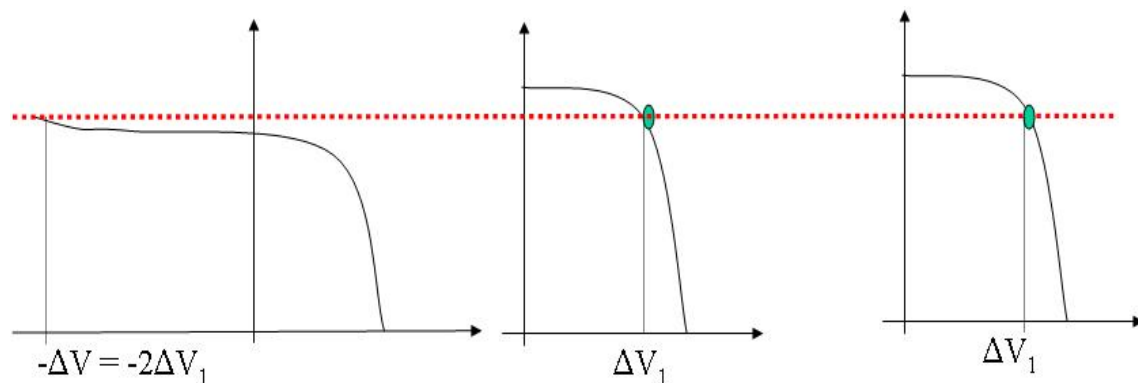


Figure 2-16 – Current-voltage characteristics and working points of the cells in different conditions of illuminations

The current produced by A is reduced, so the electrons flux in the circuit is limited because this cell doesn't deliver enough current at the next cell B. A reduction of the junction potential barrier in the cell B and C allows the correct net current to flow in the circuit; the resulting potential step will be such high to set the two cells in the point of their I-V characteristics correspondent at the current furnished by cell A, as in fig.(2-17). The voltages produced by the illuminated B and C cells give an inverse polarization on A. If

the voltage becomes high enough, for example considering longer string of cells, the inverse polarization of the not illuminated solar cell can become so high to produce breakdown in the A cell. This can lead at very high current density damaging the module materials by overheating and degrading the cell behaviour in normal, operative conditions. For this reason by-pass diodes are used in photovoltaic strings of cells.

Small fluctuations in the light flux impinging different series connected solar cells don't affect very much the efficiency of string; in some cases the small inverse voltage induced in some cells of the string increase the carrier collection efficiency of these devices; however, the behaviour of the module response depend strongly on the kind of cells mounted on, especially on their performances in reverse conditions [31]. If the cells present a quite low shunt resistance, for small flux fluctuations there's an almost constant FF and a slight I_{sc} decrease, while if the shunt resistance is high, the I_{sc} decreases proportionally with the shaded fraction, but the FF can even increase. This happens at least if the illumination variation ΔI_{max} results in less than (2.37), with I_{max} as the maximal light flux intensity. It is usually well recovered if it's in the range of 10-15% of I_{max} .

$$\frac{\Delta I_{max}}{I_{max}} = \frac{(J_{sc} - J_{mp})}{J_{sc}} \quad 2-37$$

The influence on the module efficiency of the uniform illumination level has a great importance in concentrated photovoltaic, bearing to the necessity of optical and mechanical solutions able to ensure the light uniformity for all the cells mounted on the series connected strings.

CHAPTER 3 SOLAR CONCENTRATION

3.1 Silicon solar cells performances under concentrated illumination

Increasing the light flux impinging the semiconductor, the number of electron-hole pairs produced increases as well. This means that the concentration of minority carriers raises and, following the (2.18), the voltage increases logarithmically with the illumination. Because of the short circuit current enhances in a linear way, the conversion efficiency of the device, not just the power delivered, increases with the light concentration; however, with this conclusion, some important aspects have been neglected: the temperature effect, the behaviour of the lifetime with the illumination and the electrical resistances of the cell.

Resistance

Regarding this point, the importance of having a resistance as lower as possible has been already motivated. To give the order of magnitude of the resistance required, we can consider this calculation: for a cell of 1cm^2 under a solar light flux equivalent at 100 AM1.5 suns, the current produced in short circuit condition from a good Si cell is of about 4A. To ensure a fill factor variation in the order of $\frac{\Delta FF}{FF_{\max}} = 5\%$, corresponding for example at a decreasing from the higher $FF=80\%$ at a $FF_{100x}=76\%$, the resistance should be of about $0.01 \frac{\text{ohm}}{\text{cm}^2}$; so, at higher concentration it's important to keep the resistance in the order of the milliohm/cm². The technological solutions proposed to achieve this result will be discussed later.

Lifetimes

The lifetime, as already described in chapter 1, depends on different processes; the τ_{SRH} improves with the concentrated light, as shown in fig.(1-10), considering that the capture cross section of the defects near the midgap of the semiconductor are, in general, significantly higher than that near the edge, and the behaviour of the lifetime with this last parameter is that of fig.(1-11).

Diversely, the τ_{Auger} decreases, because of the number of carriers in each band raises and so also the probability for these particles to collide. The τ_{rad} increases as well, because of

the higher the number of carriers in both the bands, the higher the probability to find particles in the right conditions for the band to band recombination.

Evaluating these facts, it appears that, under concentration, in conventional front contact silicon solar cells there isn't need of extremely pure bulk material. Indeed, the Auger process, except done for the trap-assisted one, doesn't depend on the defect concentration of the material; it's the first factor limiting the τ at high illumination levels, as follows from fig.(1-17).

The surface recombination rate decreases with the light concentration, so this aspect can be regarded with less attention than in the low illumination regimes. Moreover, the surface passivation by accumulation is not very useful in these cases, because its effect decreases with the minority carrier concentration; a more successful solution is the floating junction, because the concentration of the introduced carriers with the doping is higher than that produced by the illumination, even under concentration, so it can act as electrostatic repelling for the generated minority carriers. This is the method adopted at the front surface in some interdigitated back contact (IBC) silicon solar cell to reduce at the minimum level the recombinations at the interface.

In all the recombination processes the energy is released by heat dissipation, except done for the radiative one; even if they contribute with a minor part in the thermal budget of the solar cell, it is an additional term increasing the temperature of the material. This energy fraction has low practical interest, but has an important physical meaning, because it ensures that cannot exist any theoretical structure composed of solar cells array with global conversion efficiency higher than that imposed by the thermodynamic.

Temperature

This issue is one of the main enemies for the photovoltaic cells, because the efficiency decreases almost linearly with the temperature of the material, for fixed light flux. It can be seen through formula (2.17); the coefficient of proportionality (3.1) is only slightly implicitly temperature dependent; (3.1) is derived by the contribution given from the p-region of the solar cell; the contribution from the n-region has an analogue form.

$$\frac{\partial V_{oc}}{\partial T} \cong - \frac{k \text{Log} \left[\frac{N_c}{n_{epoc} \eta_{ep}(\tau)} \frac{N_v}{N_A} \right]}{q} \quad 3-1$$

In the fig.(3-1) from [32] is sketched the behaviour of the open circuit voltage for commercial, 1 sun Si solar cells with temperature, for slightly different illumination levels.

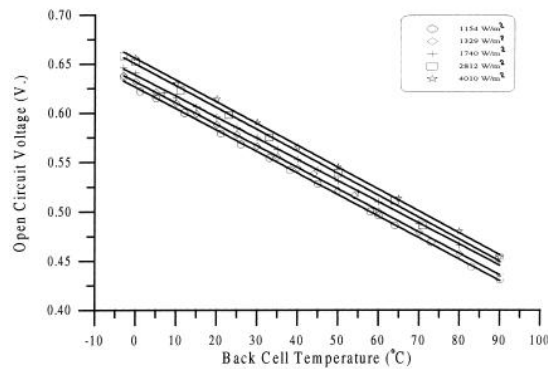


Figure 3-1 – Open circuit voltage vs. Si cell temperature for slightly different illuminations from [32]

This value can vary a lot among silicon cells of different lifetime properties because the dependence on τ of the terms $n_{ep} \eta_{ep}$. Deriving (2.19), (3.2) is obtained; it means that the voltage dependence on the temperature is not constant for every voltage conditions. This implies that the V_{mp} , i.e. the voltage at the maximum power point, has a voltage-temperature coefficient higher than that for the V_{oc} , in general. It leads to a decreasing of the FF with the temperature. This variation measured for GaAs solar cell from [33] is in fig.(3-2).

$$\frac{\partial V}{\partial T} \cong - \frac{k \text{Log} \left[\frac{N_c}{(n_{epoc} - n_{ep}^J) \eta_{ep}(\tau_e)} \frac{N_v}{N_A} \right]}{q} \quad 3-2$$

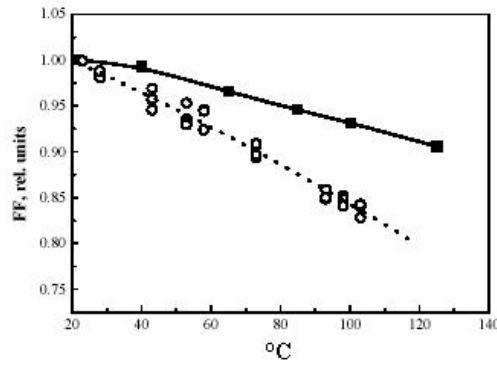


Figure 3-2 - FF vs. temperature for GaAs solar cells, in relative unites [33]; the dashed line represent the effect with non-uniform illumination

A more precise analysis should consider the temperature variation throughout the cell; indeed, the establishment of the global potential difference at the cell contacts is given by three different contributions, as in (2.17). In (3.3) each term is characterized by the proper temperature; because of, in front contact solar cell, the junction is closed at the front surface, it's possible to gather these two terms; the rear of the cell can have a different temperature, if an heat exchanger is connected at the back of the device, as usually done, especially in PV receivers for concentration. The resulting V_{oc} function, considering negligible the light absorbed in the emitter, is (3.4).

$$V_{oc} \cong V_{bcc} - V_{boc} = \frac{E_g - kT_{front} \text{Log}\left[\frac{N_c}{N_D}\right] - kT_{rear} \text{Log}\left[\frac{N_v}{N_A}\right] - kT_{junction} \text{Log}\left[\frac{N_D}{n_{ep}\eta_{ep}(\tau)}\right]}{q} \quad 3-3$$

$$V_{oc} \cong V_{bcc} - V_{boc} = \frac{E_g - kT_{front} \text{Log}\left[\frac{N_c}{n_{ep}\eta_{ep}(\tau)}\right] - kT_{rear} \text{Log}\left[\frac{N_v}{N_A}\right]}{q} \quad 3-4$$

The front junction is a disadvantage, for concentration solar cell; the photons with higher energy are absorbed in the few microns down the front surface; all the exceeding energy is dissipated by heat in the crystal lattice, increasing the temperature. So, the temperature is higher in the junction region, reducing the voltage of the device without permits to drain off the heat in the most efficient way, with external cooling systems. One of the IBC solar cells advantages is their less voltage-temperature coefficient because it can work with junction and contact regions closed at the cooling system; besides, they must be fabricated on very high τ materials with the consequent high collection efficiency.

However, IBC Si solar cells have also disadvantages [34]; the mainly problems are not related to working situation, but to their fabrication. Indeed, the necessity of very high minority carriers lifetime for good collection efficiency and the complexity of the microfabrication process lead to a quite expensive product, with prices in the order of MJunction solar cells, for concentration.

As already explained in cap.2, the temperature coefficient improves with the concentration level, so the detrimental effect of temperature is partially limited; for example, the HCPV Amonix silicon solar cells have a voltage temperature sensitivity of about $-1.78 \text{ mV}/^\circ\text{C}$ at one sun and of about $-1.37 \text{ mV}/^\circ\text{C}$ at 250 suns [20], while for GaAs from $-2.4 \text{ mV}/^\circ\text{C}$ to $-1.12 \text{ mV}/^\circ\text{C}$ at 250 suns [19].

3.2 Non-silicon semiconductor solar cells under concentration

Not every kind of solar cell can work under high flux illumination; some type of material become instable under high flux, losing their photoelectrical properties. In particular, amorphous Si, II-VI semiconductors and organic solar cells have this problem [35]. Diversely, III-V semiconductors can works even under very high light fluxes (several thousands of suns) [36]; the Auger recombination process which limits the efficiency for silicon solar cells is here dominated by the band to band radiative recombinations. This opportunity for III-V solar cell has opened new prospects for the market of this kind of cells, up to now dedicated only for space applications because of their very high costs. The reduction of the amount of required material in the concentrated PV decreases the cost impact of these cells; however, it remains significantly higher than for Si solar cells, and it is relevant in the overall costs of a complete concentrating system, if the concentration factor is lower than about $400\times$. This latter illumination level combined to high optical efficiency leads to quite sophisticated system solutions; a trade off between cost and efficiency is then required.

III-V materials grown epitaxially gives the possibility to fabricate multijunction (MJ) solar cells, i.e. photovoltaic cells made of stacks of different crystalline materials series connected, like that sketched in fig.(3-3), representing a triple-junction solar cell. P-n junctions of different material are connected through heavy doped layers crossed by the current for tunnelling effect [37].

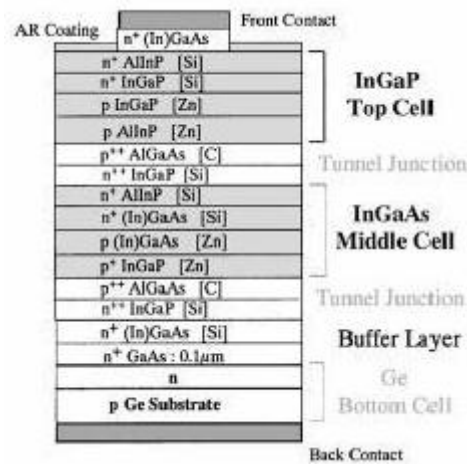


Figure 3-3 – Example of a stack of layers for an high efficiency triple-junction solar cell [37]

The lattices of the different materials of the stack have to be similar to permit a growth of the structure without pinholes and dislocations, which compromise the efficiency of the device. The higher the number of the layers, the higher the difficulties to achieve good results; up to now, very good performance (37% at 175 suns and 35°C) has been obtained from triple-junction solar cells, with Ge, InGaAs and InGaP as photoactive materials [38], while devices with more junctions are currently only under development [39]. Other epitaxial configurations have been studied with good result, also under concentration, with, for example, $\text{Al}_x\text{Ga}_{1-x}\text{As}$ as top layer [21].

Because of the different materials are series connected, while the device voltage is the sum of the voltages of each junction, the current is limited by the lower current produced among the material sectors. For this reason thickness and bandgap of every material have to be calibrated in order to maximize the generated current.

The major problem of this kind of cells for terrestrial application is their high cost; indeed, the base material (usually Ge) and the fabrication process are very expensive for energy production purposes; one very promising way to reduce this problem consists in replacing the high cost Ge substrates with cheaper Si wafers. With particular technological techniques [40], the possibility to grow good efficiency III-V solar cells on virtual substrate (i.e. Ge layers grown on silicon substrate) has been demonstrated [41]. Up to now, this approach seems one of the more interesting for the cost reduction of III-V solar cells; however, the quite high concentration of dislocations in the large area virtual substrates leads to strong difficulties in growing high efficiency multijunctions stack [42].

Currently, a big fraction of the research and development on concentration photovoltaic adopts MJs as solar cells [43,44,45]; all these systems aim at high concentration levels, in

order to reduce the global costs; this approach has advantages and disadvantages. Advantages: in the III-V devices the efficiency increases with the injection level logarithmically, but with an higher coefficient than Si, and haven't the same Auger limitation [21]; moreover, the materials with higher bandgap less suffer the temperature increasing. For example, GaAs has a temperature coefficient of $-2.4\%/^{\circ}\text{C}$, while for Si it's from $-2.6\%/^{\circ}\text{C}$ [20] for high efficiency cells, up to $-3.7\%/^{\circ}\text{C}$ for traditional, commercial PV cells [7]. Disadvantages: even if the detrimental effect of the temperature are weaker than for silicon, the high concentration raises a strong cooling problem. Indeed, the fraction of energy flux not converted in electrical power produces heat in the device; for high efficiency MJ of 30% of efficiency, about the 55-60% of power is heat (c.ca 10-15% is considered reflected by contacts). For a device of $5\text{mm}\times 5\text{mm}$ under a flux of 400 suns, the thermal budget to drain off is approximately $0.6\times 10\text{W}=6\text{W}$, which corresponds at an heat flux of $24\text{W}/\text{cm}^2$. For comparison, a medium level concentration of 100 suns on 20% Si solar cell produces an heat flux of approximately $7\text{W}/\text{cm}^2$, which can be easier managed. Another important disadvantage for the high concentration approach is the very high precision alignment required for the optical components of the system along the Sun-cells axis; small mis-alignments lead the focus of the concentrating system out of the target, with consequent power losses for the single cells and for all the series connected string; optical recoveries for these situations are then compulsory.

Other device configurations discussed in literature are the mechanically stacked solar cells [46,47]; they are stacks of one junction cells, series connected, made of semiconductors with different bandgaps. This approach doesn't seem very effective considering the cost of each devices and the precision required for the alignment among them.

The best conversion of the full solar spectrum using different semiconductor materials can be also pursued with the approach of the solar light spatial spectral splitting, as will be extensively discussed in Cap.4.

3.3 Solar concentrators

There's a large number of different kind of solar concentrators; here we consider optical systems with medium and high concentration factor, i.e. $\geq 30\times$. The classification can be

made with the physical principles used to converge the light (refraction or reflection), on the symmetry of the systems (1D or 2D) and on the module packaging (dense array or separated solar cells). An extra class not taken into account in this list is that of photoluminescent photovoltaic solar concentrators [48]; they are static concentrators using physical processes completely different than in the other cases.

Because of the system considered in this study is 2-axis tracking (2D symmetry), will carry out a brief summary of the currently investigated systems of this category. Their prerogative is the possibility to achieve high concentration levels, because of they move holding the optical axis always directed toward the Sun dish centre. In fig.(3-4) are sketched two classical optical solutions.

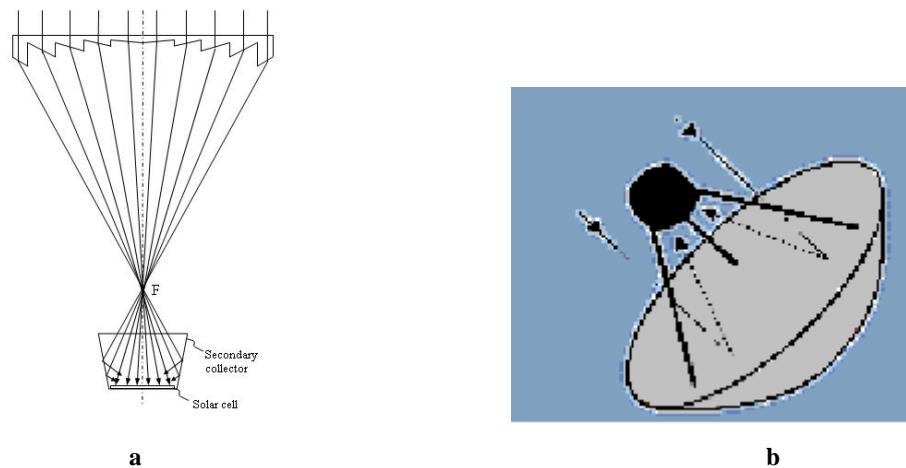


Figure 3-4 – (a) Fresnel lens with a secondary optical element; (b) parabolic dish reflector

These two approaches, one using lenses and one using parabolic shaped mirror dishes as primary concentrators, are the main widely considered solutions in the field of solar PV concentration; besides, these are the configurations used from the only two currently commercial player in the field (AMONIX for lenses and Solar Systems for mirrors). Their respective concentrators are shown in fig.(3-5).

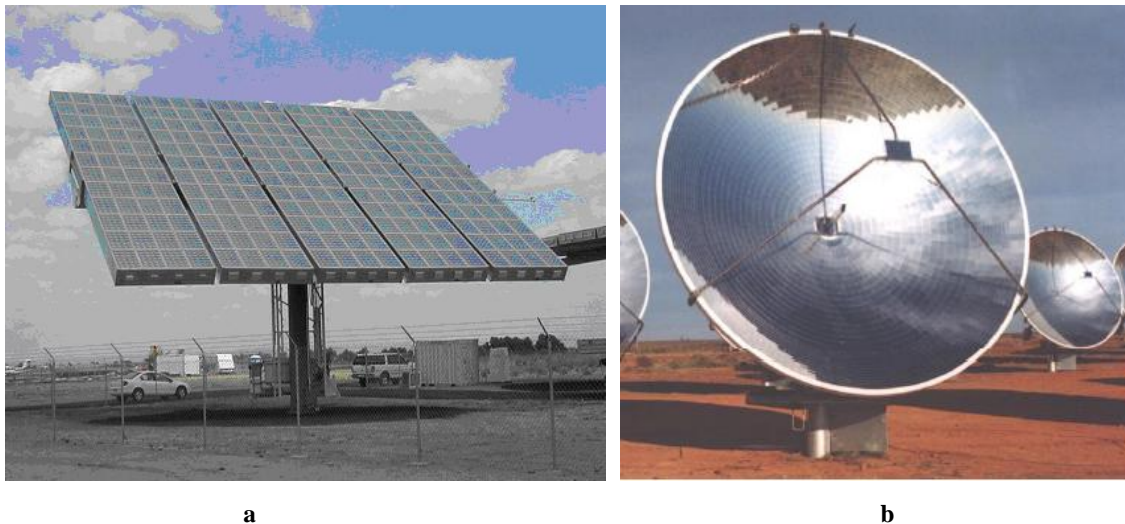


Figure 3-5 – (a) Amonix solar concentrator; (b) Solar System concentrator dishes

In general, the aim of the study of these optical configurations is to obtain the solution for low cost mass production and high efficient objects; here, the useful efficiency is not just the optical efficiency of (3-5) generally considered in non-imaging optics [49], but is an illumination efficiency which has to ensure the good performances of the PV module, defined as in (3-6).

$$\eta_{opt}(\theta) = \frac{\text{RADIATION ON THE TARGET}}{\text{TOTAL IMPINGING RADIATION}(\theta)} \quad 3-5$$

$$\eta_{ill}(\theta) = \frac{\text{USEFUL RADIATION}}{\text{TOTAL IMPINGING RADIATION}(\theta)} \quad 3-6$$

Because of the behaviour of series connected cells, the useful radiation has to be considered regarding each separate string of PV devices; as described in cap.2, not every cell typology works in the same way if series connected, under non-uniform illumination; however, to give a more general definition, it is possible to consider as *useful radiation* the value of uniform illumination on a single cell limiting the I_{mp} of the string, considering all PV devices equals, in the same thermal conditions. This illumination level has to be considered as the useful radiation on all the target area, because it's the limiting factor.

The branch of optics studying these applications is the non-imaging optics; it concerns the applications where, generally, the aim is to achieve the higher light transfer, without take care of information transmissions with images [49]. The more involved fields on the non-imaging optics are the light concentration and the illumination engineering.

The functions (3-5, 3-6) depend on the incidence angles of the impinging radiation. For systems with optical efficiency at incidence angle $\theta=0$ of $\eta_{opt}(0) = 1$, an *acceptance angle* (θ_m) is usually defined; it represents the maximum angle for the radiation out to the direction of the optical system axis ensuring $\eta_{opt} = 1$. The limits of this acceptance angle for the different concentration level are given by the thermodynamic, as explained in [49]. For solar concentrators, the lower acceptance cannot be less than $\theta_m \geq 0.26^\circ$, because of the solar divergence; this angle is due to the not negligible transversal dimension of the solar diameter, respect to the distance Sun-Earth. The higher the acceptance angle of the system, the higher its tolerance at tracking errors. In general the concentration factor is limited from the relation (3-7, 3-8) for 1-D and 2-D concentrators.

$$C_{1D} \leq \frac{n \sin \alpha}{\sin \beta} \quad 3-7$$

$$C_{2D} \leq \frac{n^2 \sin^2 \alpha}{\sin^2 \beta} \quad 3-8$$

While the optical efficiency and the (θ_m) are values characteristics only of the optics of the systems, the illumination efficiency depends on factors related to the PV module and to the PV cells. It is possible to introduce an angle analogue to (θ_m) for the PV concentrators; we call it (θ_{mPV}) and it represents the maximum angle for the radiation which ensures good performance at the systems, for a given value of $\eta_{ill}(0)$. This definition is not absolute, because the “good performance” is not well defined; a tolerable decreasing of efficiency can be considered of the 10%.

Generally, lenses and reflective dishes have different PV module configurations; while lens concentrator systems have one cell for each lens and all the cells are well separated, reflective dishes use dense array modules, because the light beam is unique (except done for some particular approaches, like the mini-dish approach of [50]). Two example of PV module arrangements are sketch in fig(3-6), representing the module of the Phocus System of ENEA and a dense array receiver of Spectrolab, for a dish concentrator.

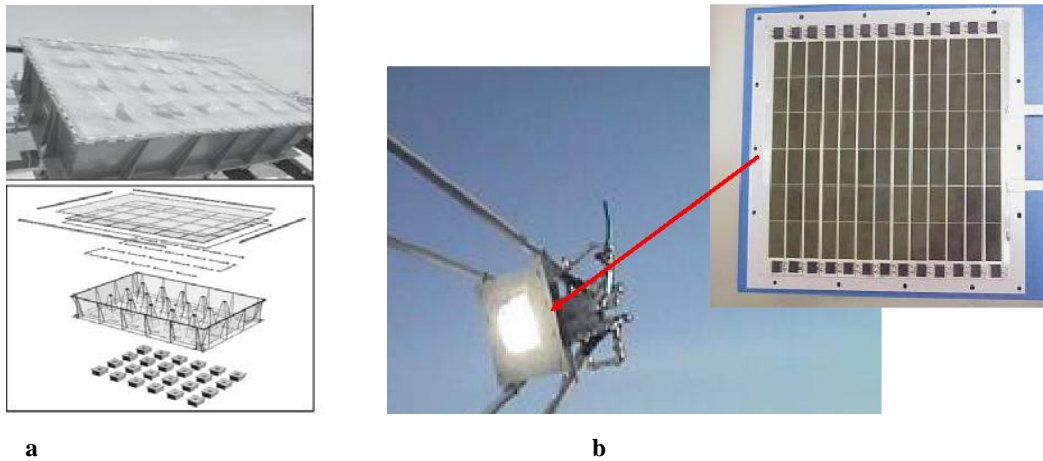


Figure 3-6 – (a) Lens module of the Phocus system of ENEA; (b) dense array module of 3-junctions Spectrolab solar cells mounted on the receiver of a parabolic dish

These different configurations lead to different problems in the panel assembly, in optics constrains and for the thermal management in operating conditions.

The efficiency of a string of solar cells is strongly function of the illumination uniformity in the module; so, considering the dish mirror configurations, the produced beam has to strike the PV dense array panel with the most uniform illumination profile. One currently adopted solution to achieve this result is the implementation of a secondary homogenizer collector which uniformes the light passing through it [51]; the configuration of this optic element can vary, depending on the primary concentrator and on the grade of recovery required. In fig. (3-7) are shown the solution and the corresponding results studied by [50], while those of Solar System [52] are in fig.(3-8). Alternatively, we propose an appositely designed shape for the primary collector composed of flat shaped surfaces [53,54], as will be widely described in the next chapter.

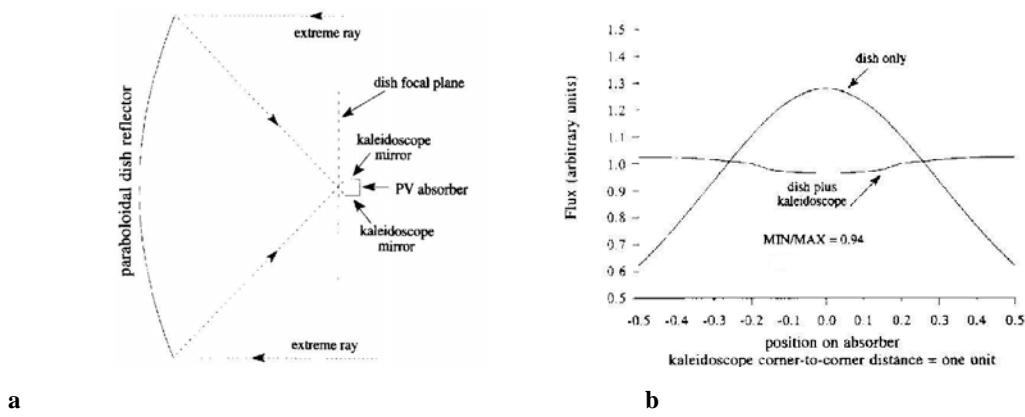


Figure 3-7 – (a) Scheme of the optical concentrator system, with a parabolic dish and a kaleidoscope secondary element; (b) illumination flux profile with and without the secondary [50]

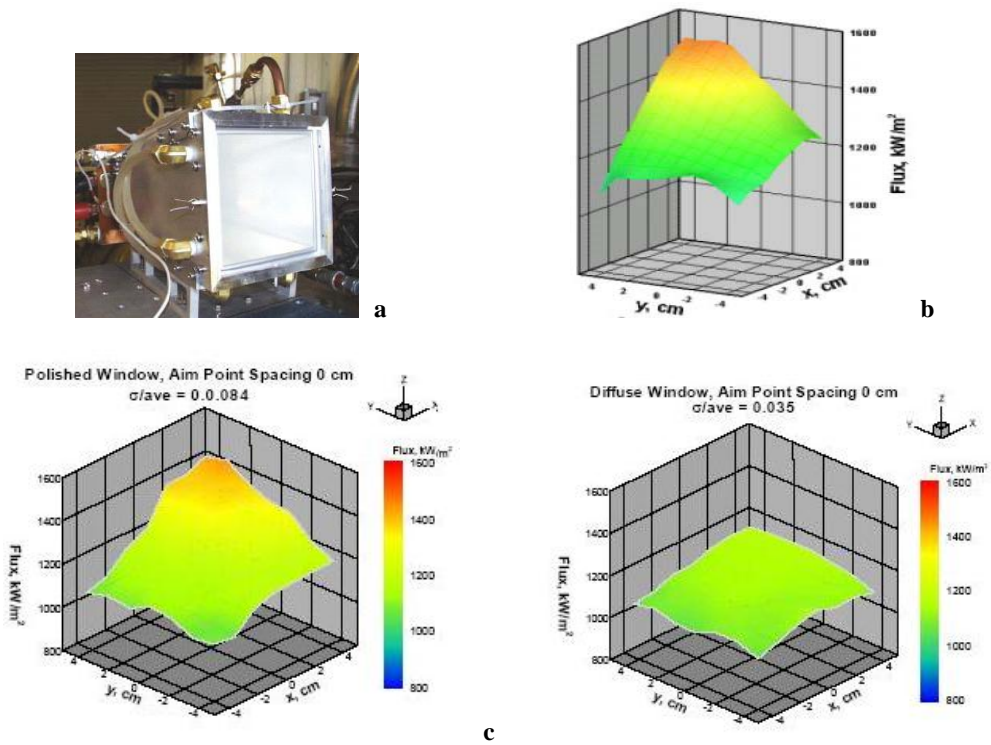


Figure 3-8 – (a) Secondary optical element used in the Solar System concentrator; (b) illumination flux profile without secondary; (c) flux with secondary and polished window; (d) with diffuse window.

The optical and illumination efficiencies for systems with one cell for one concentration element (usually lenses) can not be considered just as the efficiency of the single, elementary unit; it's only a component of the object of interest. The useful radiation accounted in the definition of useful illumination can be considered here like that produced by the less efficient unit in a string, again considering the same electrical and thermal characteristics for every cell. Up to now, each elementary unit of the system is considered to be rigidly connected to all the others; the mechanical flexibility of the array has to be as low as possible to ensure the same pointing conditions for each unit, in a wide range of tracking conditions. Indeed, following the Sun in its elevation, the different positions on the module are under different mechanical conditions, due to the gravity effect. Another important effect is the wind, again for the different elevation conditions of the systems [55]. These points affect the illumination efficiency both for dishes and lenses systems; consequently, η_{opt} and η_{ill} can be expressed in a more general form, as in (3-9) with θ^1 function of the azimuth angle φ and of the wind speed w_s , as in (3-10).

$$\eta_{ill\ string} = \eta_{ill}(\theta^1) \quad 3-9$$

$$\theta^1 = \theta^1(\varphi, ws) \quad 3-10$$

Besides these considerations, some points can be treated to highlight differences, advantages and disadvantages of lenses concentrators and mirror dishes [56].

Considering the lenses systems, the principal advantages are a more compact structure, fairly high tolerance at non-uniform illumination on single solar cell of each unit and the modularity of the structure. Moreover, depending on the concentration conditions and on the cell type mounted, the PV devices can be cooled down to reach quite good working conditions with passive cooling heat exchanger [57]. Disadvantages of this approach are the problems related to the fabrication of high efficiency lenses, especially for high concentration, at low cost; in fig. (3-9) is shown the effect of one typical problem, related to the not infinitesimal radius of the point features of the lenses.

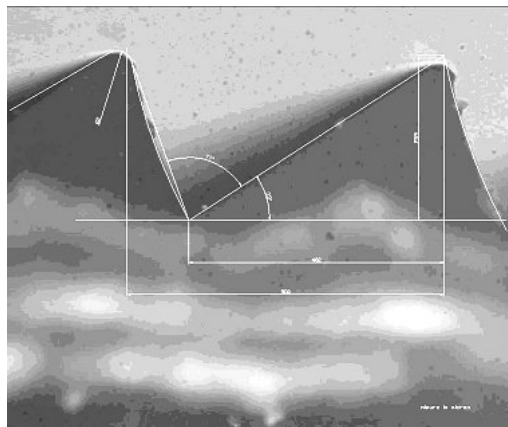


Figure 3-9 – Cross section of prisms of a lens

However, some high efficiency non-imaging lenses have been manufactured for PV applications [58], but not yet commercialized. An important characteristic of high concentration lenses systems, especially using III-V MJ solar cells, is the very high precision required in the fabrication procedure to align every part along the optical axis, ensuring this in working conditions; in fact, the errors in the mounting of one unit compromises the working operations of all its string [57]. The module configuration makes the system sensible at the shadowing of the units (due, for example, at dirty), like in flat, non-concentrating solar panels, as described in cap.2. Moreover, the fact of using passive

cooling can be seen as an advantage but also as a disadvantage. This because the flux of drained out heat can not overcome some limits, and an high efficiency passive cooler has to be set for each cell. The configuration of the system doesn't allow to use active cooling with an economical solution.

On the other side, the mirror dishes, having an unique concentrator surface for series connected cells, has the advantage to don't suffer on partial shadowing in the collector because of the necessary light homogenization of this approach. The possibility to find low cost, very high reflectivity materials permits to produces systems with high optical efficiency at low cost. The single concentrated beam requires an high efficient cooling system; a liquid heat exchanger can be here used, for the lumped nature of the focus. The warmer water obtained can be used for co-generation purposes[59, 69]. Disadvantages of this approach are the non compact system structure and the non-modularity; these points, however, can partially be corrected. Indeed, instead of using an unique concentrator to deliver all the power required, is possible to split the system in many concentrator dishes, each one for a string of series connected cells; so, the system becomes more compact and modular, as, for example, in fig.(3-10). Another critical issue is the illumination efficiency, both as light uniformity and as cells packaging in the PV receiver.

An additionally advantage for the reflective approach is the possibility to introduce dichroic materials as reflectors; this point will be extensively discussed in cap.4.

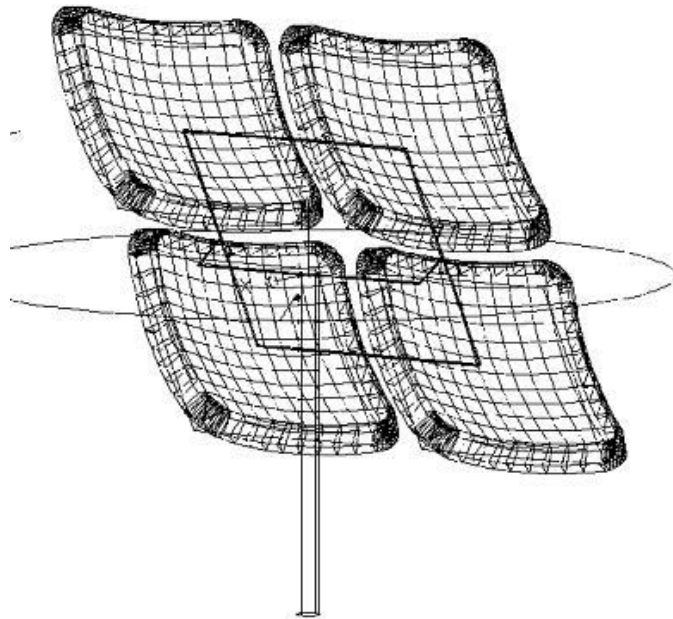


Figure 3-10 – Four dishes mounted on a single tracking system

3.4 Efficiency of PV concentrators

In the flat-plate PV applications, the efficiency is generally given in the Standard Rating Conditions (SCR), i.e. 1kW/m^2 and AM1.5 light flux, with the solar cell kept at 25°C . These conditions are quite unrealistic in outdoor working modules, both for the peculiarity of the supposed illumination flux and for the temperature considered. Also if the efficiency is considered the same for the different fluxes which can impinging the module, the temperature of the cells is usually higher than the 25°C if the illumination level is considerable, especially in the good season at the sunnier latitudes; A study of the nominal operating cell temperature (NOCT) as a function of ambient temperature and wind speed concluded that a cell temperature of 44°C corresponded to a 20°C ambient temperature for common rack-mounted, crystalline-silicon cell, glass-on-Tedlarframed, modules at 800W/m^2 irradiance and a 1 m/s wind speed [61]. A more useful standard for the definition of the efficiency of PV panels is given under the PVUSA Standard Conditions (PTC); in this standard the PV modules or systems are tested under more real conditions: 1kW/m^2 , AM1.5, 20°C ambient temperature and 1m/s wind speed. With this second standard, the performances of the commercial, flat-plate PV modules suffer a strong efficiency decrease; PTC efficiency of commercial PV with mono-crystalline silicon technology are usually comprise in the range of 7-11% [62]. Moreover, the efficiency is calculated as $\text{electrical } P_{out} / P_{in}$; this data is not the most interesting for the PV user. Usually, the most significant data is the average amount of energy delivered from the module in an years; this data is different from the previous one, because the light flux varies during the day and during the year, and the standard conditions are not always matched. The cumulative energy, instead of the peak power, is the most relevant data. In particular, for the fixed flat-plate PV module, the incident power is reduced for the perspective effects, i.e. the fraction of light impinging the module is given from (3-11), where δ and ψ are the angle of the module plane respect to the Sun-module direction.

$$I = I_{\max} \cos(\delta) \cos(\psi)$$

3-11

So, even if the cells have high efficiency and high angular acceptance, the power produced is lower than in the standard conditions. Considering the energy produced from

flat plate PV modules with 2 axis tracking, the difference can be estimated in about the 50% of kWh/y produced at a latitude of $\sim 45^\circ$.

The efficiency of PV concentrators cannot be directly compared with the efficiency of modules measured in STC. The useful impinging radiation is lower than that for the flat modules, because only the direct component of the flux can be concentrated; in general, it's considered the 85-90% of the global one. This reduction of the solar light limits the power production of the PV concentrators; however, the tracking of these systems allows an higher energy production during the days; in fig.(3-11) there's the power produced during a day of a concentrator system and of a flat plate multicrystalline silicon module located in Sunnyvale, 37° of latitude, in North California, while in fig.(3-12) there's the kWh/m² of energy produced during about 6 months [63]. The total amount of energy produced by the concentrator is 37% greater than the energy produced by the flat plate on a kWh/m² basis. The measured efficiency of the concentrator and of the flat panel was respectively of 16.5% and 10.7% under operative conditions. Independently on the efficiency but basing on the amount of produced energy per rated power(kWh/kWp), the concentrator system outperforms the fixed flat plate by more than the 24%.

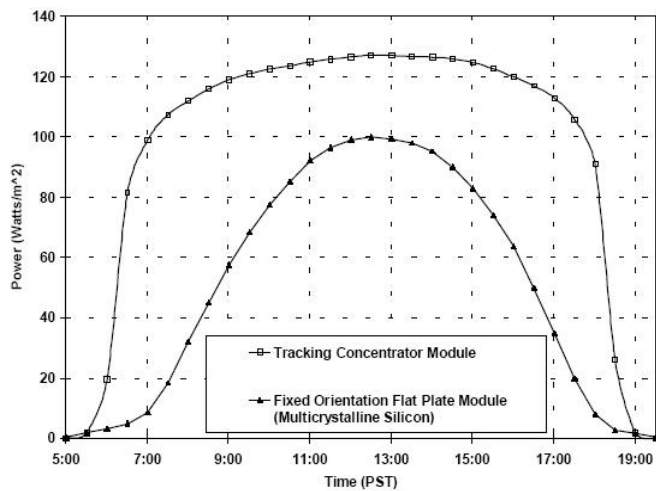


Figure 3-11 - Power produced during a day of a concentrator system and of a flat plate multicrystalline silicon module located in Sunnyvale, 37° of latitude, in North California [63]

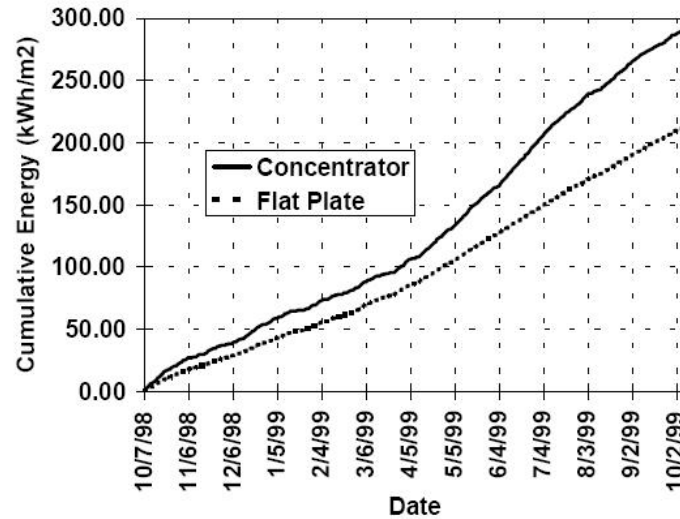


Figure 3-12 – Cumulative kWh/m² of energy produced during about 6 months for a concentrator system and of a flat plate multicrystalline silicon module located in Sunnyvale, 37° of latitude, in North California [63]

Another fundamental issue is the cost of the systems, and so of the produced energy; indeed, as well as for the thin film solar cells approach, a low cost systems can be more effective than an high cost system, even with a low efficiency. As final analysis, for terrestrial, large scale energy production, the most important data is the fraction $\frac{\text{electrical energy produced}}{\text{PV system cost}}$; for concentrator systems, this data is not yet well defined,

because it strongly depends on the kind of systems and because a large number of PV concentrators are currently under development.

CHAPTER 4 - FLAT FACETTED SOLAR CONCENTRATOR DISHES: GLOBAL AND DICHROIC REFLECTIVE APPROACHES

4.1 Flat faceted profiles for PV concentrator dishes

As previously described, the illumination uniformity on the panel is a critical issue; to achieve this result, an alternative at the utilization of a secondary homogenizer collector consists in a particular primary concentrator design able to produce directly the uniform illumination at the target, without other recoveries. To construct it, it's useful to think how a parabolic dish produces its focus: the reflector sends every incident ray parallel at its symmetrical (optical) axis toward a single point. Because we don't want a point size hot spot, we change the surface in such a way to haven't every ray with different deflected directions, but beams of rays with this behaviour. These beams of light are obtained with flat mirrors opportunely placed on a concentrating surface profile. The easier geometrical procedure to get it is depicted, for a one dimensional case, in fig.(4-1); segments, each one approximately with the length of the target, are formed by drawing the tangent at the parabolic curve in equally spaced points. These segments are the actual mirrors and their projected image coincides, in first approximation, with the receiver.

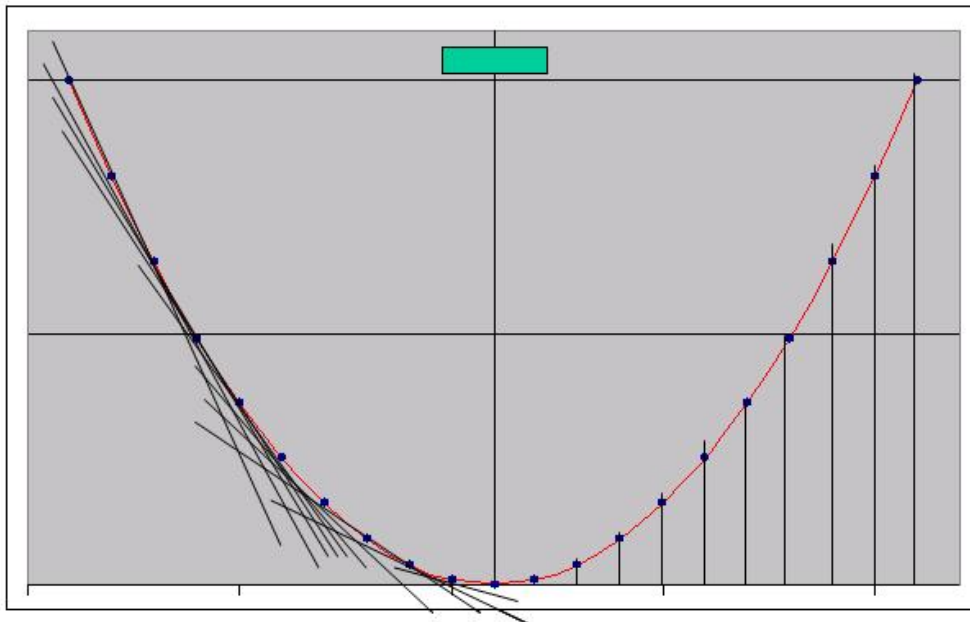


Figure 4-1 – Geometrical construction of a 1D flat faceted parabolic concentrator

The two dimensional procedure is straightforward, considering a paraboloidal surface instead of the parabolic 1-D design; the result of this procedure, for a concentrator of about $116\times$, is sketched in fig.(4-2). It comes out from an automated algorithm which implies the same conceptual procedure described for the 1-D case.

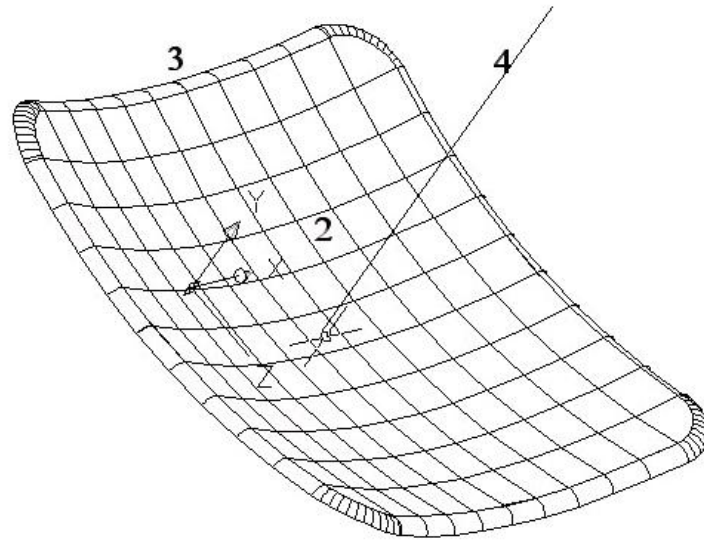


Figure 4-2 – CAD design of a 2D flat faceted concentrator

This concentrator design produces an illumination profile on the target quite close at a pillow box, but this characteristics degrades when the enveloping paraboloidal curvature rises. The weight of this effect can be evaluated with the trigonometric formula (4-1), where T is the target size, L is the mirror size and ϕ is the angle between the optical axis of the system and the mirror segment; the effect is graphically represented in fig.(4-3)

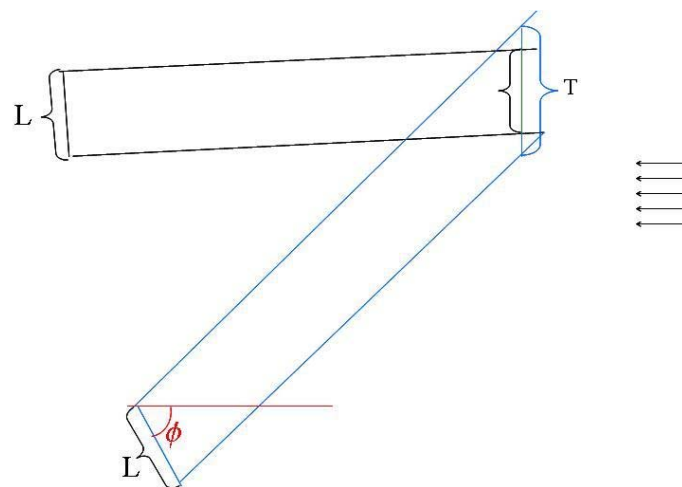


Figure 4-3 – Enlargement effect due to the laterals flat mirrors in the faceted design with all equal size mirrors

$$T = \frac{\sin(\phi)}{2 \cdot \sin^2(\phi) - 1} L \quad 4-1$$

Considering a fixed dish-receiver distance, the focus spreads itself with the concentration level in a similar way as happen with the enveloping curvature, because of a larger fraction of paraboloid is required; so, more oblique mirrors are accounted in the design.

The illumination profile produced with the theoretical surface of fig.(4-2) is sketched in fig.(4-4); this 3-D graphic is produced with the software TracePro Expert 3.1 of the Lambda Research Corporation, considering ideal alignment conditions and solar angular distribution for the incoming radiation flux.

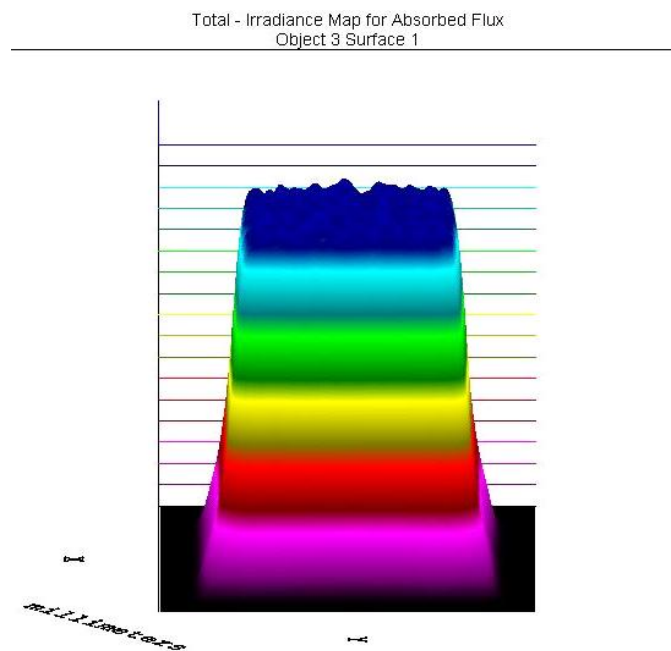


Figure 4-4 – Illumination profile generated at the focus of the concentrator in fig. 4-2, for an incident radiation with the solar divergence

Also a parabolic dish produces a quite uniform illumination profile, if the considered concentration factor is not very high; in particular, for a dish of 120× with the same target-concentrator centre distance as considered for the flat faceted configuration, the simulated flux profile is shown in fig.(4-5a); the receiver is placed at that coordinate along the optical axis between the dish and the focus allowing the same lateral size for the illuminated region as in the previous configuration. Practically, for fabrication simplicity, the

paraboloidal surfaces are often approximated with spherical profiles. This fact leads to a strong difference in the uniformity flux, as sketched in fig.(4-5b) for a spherical reflective dish with target in the same position as for the paraboloidal configuration.

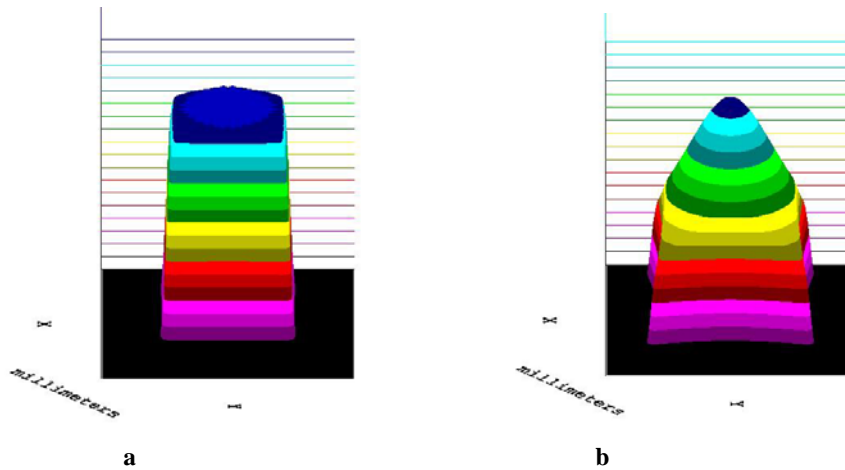


Figure 4-5 – (a) Flux distribution for a perfect parabolic dish at the distance dish centre-target equal at the focus distance of the concentrator of fig.4-2; (b) flux distribution for a spherical dish with target in the same conditions of (a)

The theoretically flux uniformity of the flat faceted dish has been tested on the prototype structure of 2.43m^2 in fig. (4-6), with the focus at 114cm from the dish centre. This model has been fabricated by moulding a fibreglass shell by bubble forming; the obtained dish has been covered with flat mirrors, one in each flat location; the final result is that in fig.(4-6b)

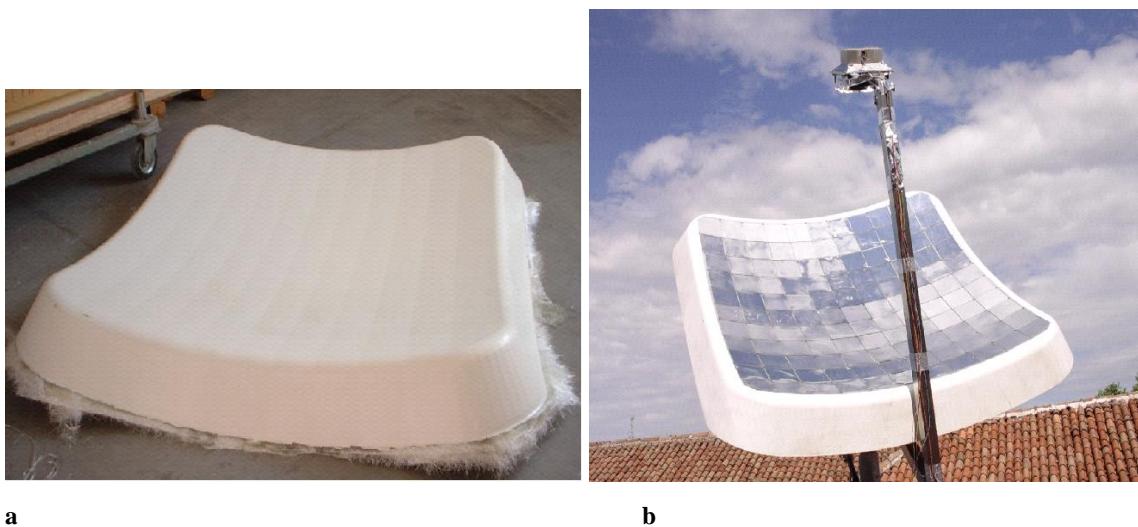


Figure 4-6 – (a) Fibreglass shaped concentrator as result after bubble forming; (b) concentrator dish with mirrors mounted on their proper locations

In reality, it is difficult to achieve a uniform flux profile: the mirrors are not perfectly specular and more significantly, the mirror substrate is not precisely fabricated as per the design.

Measurement of the intensity of light at the focus of the dish was carried out by taking images of a white lambertian target using a Hamamatsu CCD video camera. As the camera was mounted on an angle relative to the target, the flux profile was corrected for geometrical perspective and light intensity using the method described by [64]. The schematic, general set up is shown in fig.(4-7).

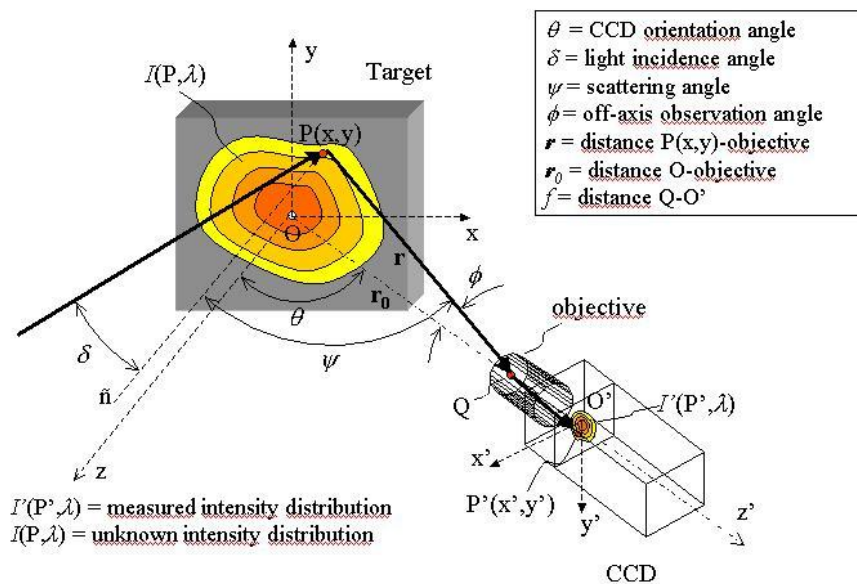


Figure 4-7 – Schematic diagram of the methodology for the flux uniformity measurement on the illuminated target

To investigate in detail the reasons of the discrepancy between the simulated flux profile and the real one, the precise shape of the fibreglass mirror substrate, after the application of mirrors, was measured using the photogrammetric method developed by Johnston [65], with accuracy in displacement estimated to be 70 microns. The photogrammetric method involves taking a series of photographs of target points on a mirror from different positions, establishment of reference coordinate system with known target points on the mirror, and complex trigonometric calculations using custom developed software called VMS to create 3-dimensional coordinates for the target points. The resulting reconstructed surface is used in ray-tracing to establish the effects of the fabrication process on the optical properties of the system [66]. The uniformity flux results are summarized in fig.(4-9); these graphs represent respectively the flux maps for the ideal and for the measured

cases without and with a flat faceted reflective secondary collector. The experimental arrangement is shown in fig.(4-8); the tilting in the fig. (4-9c) is due to a slight tilt of the camera along its optical axis; it doesn't compromise the flux measurement.



Figure 4-8 – Elements of the experimental set-up for the measurement of flux uniformity of the dish in fig.(4-6b). The CCD camera, the lambertian diffuser and the diffuser with the employed secondary collector are shown.

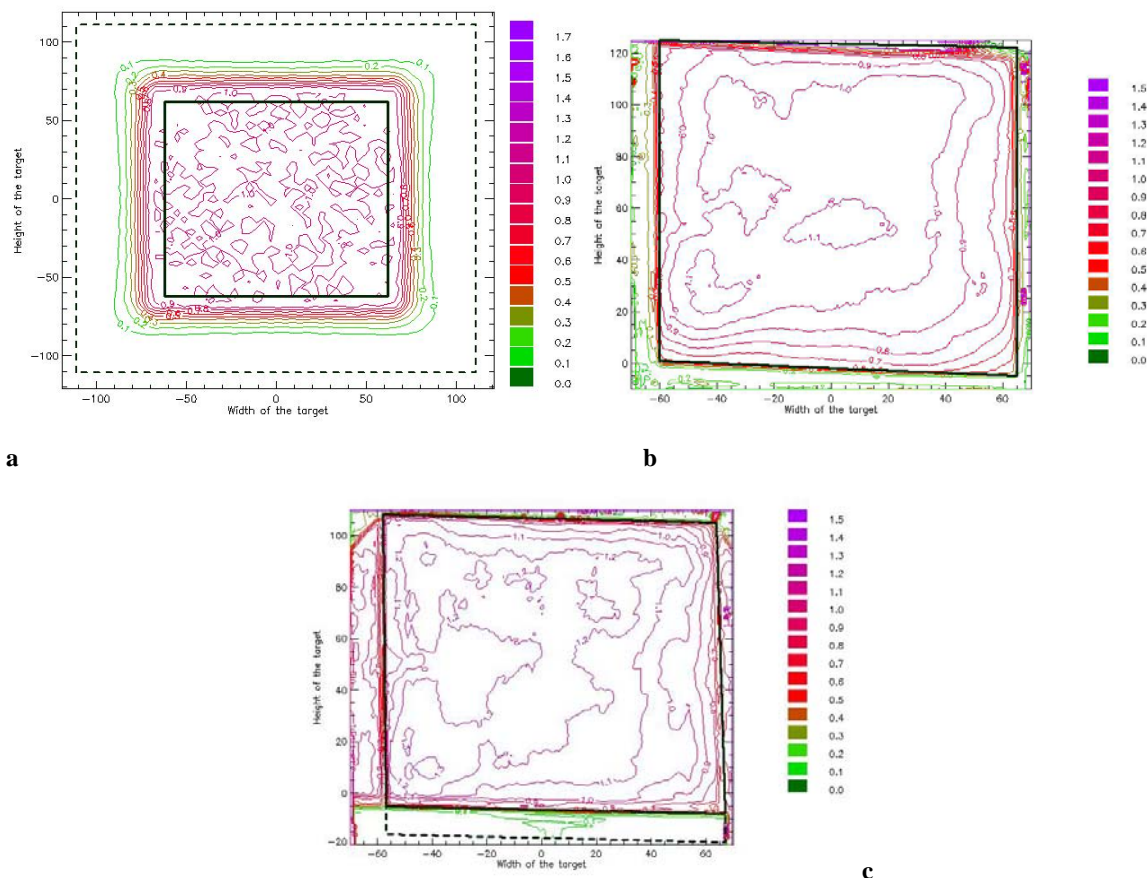


Figure 4-9 – Illumination flux maps, corrected from perspective deformation effects, of the concentrated light on the receiver; the black line enclose the target zone. (a) represent the flux map for the CAD geometrical shape; (b) is the obtained flux distribution without the secondary collector; (c) is the map flux with secondary; portion of the target was covered from the secondary, from the point of view of the camera.

A secondary optical element is used to collect the radiation directed out of the target; these rays can be due to fabrication errors, to misalignment of the system or can be part of the ring of light out of the target accounted even for the ideal design. Its project has been carried out using the ray-edge principle largely utilized in non-imaging optics [49], and it is composed of three different flat reflective surfaces with proper inclination, for each side. A profile composed of flat surfaces has been selected to simplify the fabrication process of the secondary; the inclinations was calculated considering hypothetical cases as represented in fig.(4-10); the ray reflected in (A) should go, in the ideal conditions, in (C), but because of errors in the concentrator surface fabrication or misalignment, it is sent out of the receiver area. A proper designed secondary element has to redirect the ray with the worst direction inside the target area; if this ray is sent to the opposite edge of the receiver (D) all the other out of target rays will be reflected inside the receiver region. This aim cannot be always reached, especially with the more simple geometries. An improvement is obtained using more inclination for the secondary reflective surface; as appear from fig.(4-11), if the leaning is good for the reflection of rays coming from the opposite side, some radiation can be lost for a shadowing effect of the secondary, as, for example, represented with the dashed line from the right in fig.(4-11a). An additional, more leaned surface can recover this effect as shown in fig.(4-11b).

The secondary project is strictly dependent on the geometries of the primary collector and the receiver. The inclination angles and the lengths of each part have been calculated from the geometrical characteristics of the concentrator system imposing the mentioned constrains for the edge rays.

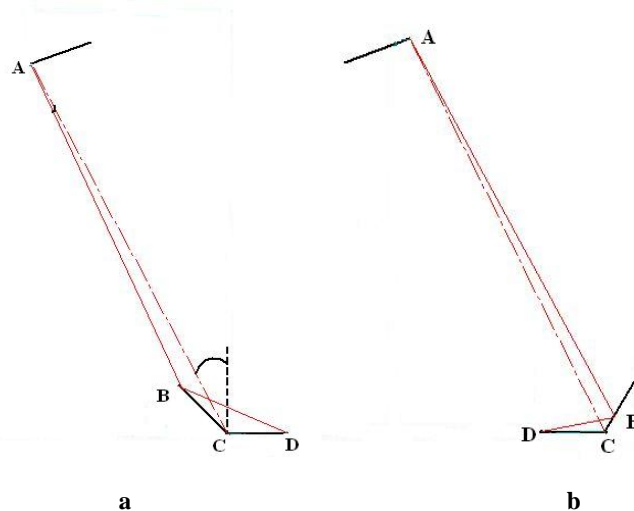


Figure 4-10 – Geometrical construction of the secondary collector for the flat faceted concentrator, with one leaned reflective surface for each side of the receiver

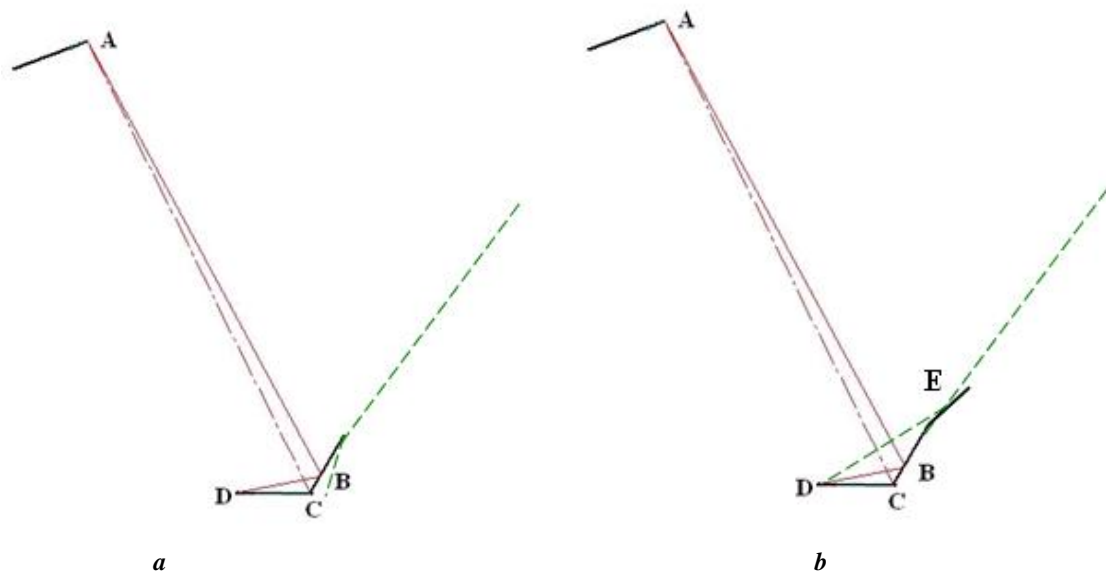


Figure 4-11 - Geometrical construction of the secondary collector for the flat faceted concentrator, with 2 leaned reflective surfaces for each side of the receiver

A CAD view of the cross section of the fabricated secondary and its recovery effect is shown in the ray-trace of fig.(4-12)

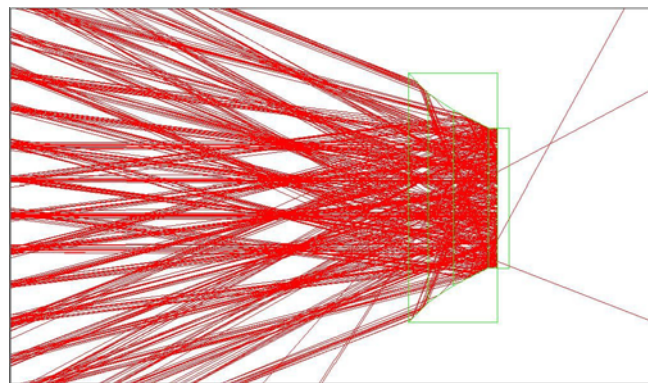


Figure 4-12 – Cross section of a raytrace simulation near the receiver, with the secondary employed

The results in fig.(4-9) show an improved uniformity in the configuration with the secondary light recovery; however, even with this optical element, the light flux uniformity has some leakages which can create problems if the PV cells are fairly small; especially near the receiver perimeter the strong flux gradient has to be taken into account. More efficient cells or slightly larger devices has to be placed in these positions to balance the current reduction.

To overcome the limitations in the optical illumination efficiency described in (4.1) of this squared faceted design even in the theoretical model, a new collector profile has been calculated and produced. The geometrical-computational procedure for its creation is based on the calculation of the array of flat quadrilateral surfaces which allows each corner of them to map a solar ray incoming with the same direction of the optical axis of the dish, on a corner of the target. The obtained draw for a concentrator of $140\times$ is shown in fig.(4-13) [54]. The correspondent intensity profile is sketch in fig.(4-14a), directly compared with the already shown draw for the $116\times$ dish with all squared mirrors of fig.(4-2). Considering the solar divergence, the theoretical illumination efficiency of this system is slightly over 92% without any secondary, while the first one configuration has the corresponding value at 84%.

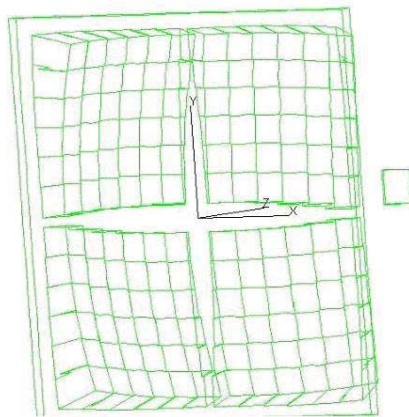


Figure 4-13 – Concentrator with an optimised profile to achieve an uniform light flux at the receiver

Using the possibility of this design method for increasing the theoretical illumination efficiency even at higher illumination levels, prototype collectors of about 1m^2 with a concentration factor of approximately $200\times$ have been designed and fabricated in ABS thanks to an industrial partnership. The as produced dish concentrator without reflective cover is sketched in fig.(4-15a), while in (4-5b) there's a small ($30\text{cm}\times 30\text{cm}$) prototype with a mirror film.

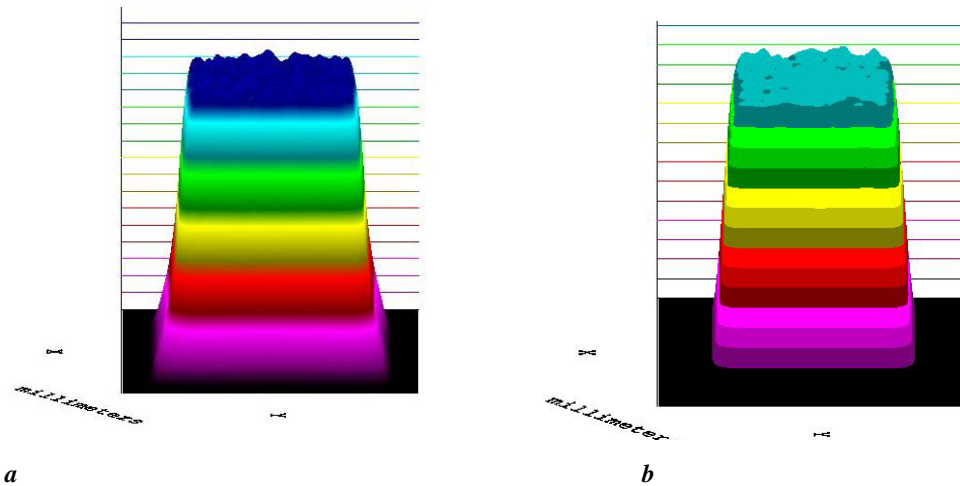


Figure 4-14 – (a) Flux distribution for the flat faceted dish of fig.4-2; (b) flux distribution for the flat faceted dish of fig.(4-13)



Figure 4-15 – (a) Optimised flat faceted dish in ABS before the reflective cover; (b) small prototype of the dish in (a) with reflective surface

The reflective materials for solar concentrators have been extensively studied [67,68,69], because they have a fundamental role in the overall system efficiency of every reflective concentrator; three points are necessary for their implementation in large scale solar applications: they must be durable in external environment, must be cheap and with high direct reflectivity in the interested range of the spectrum. Many low price materials have been investigated using a spectrophotometer, in collaboration with ENEA; the results are shown in fig.(4-16)

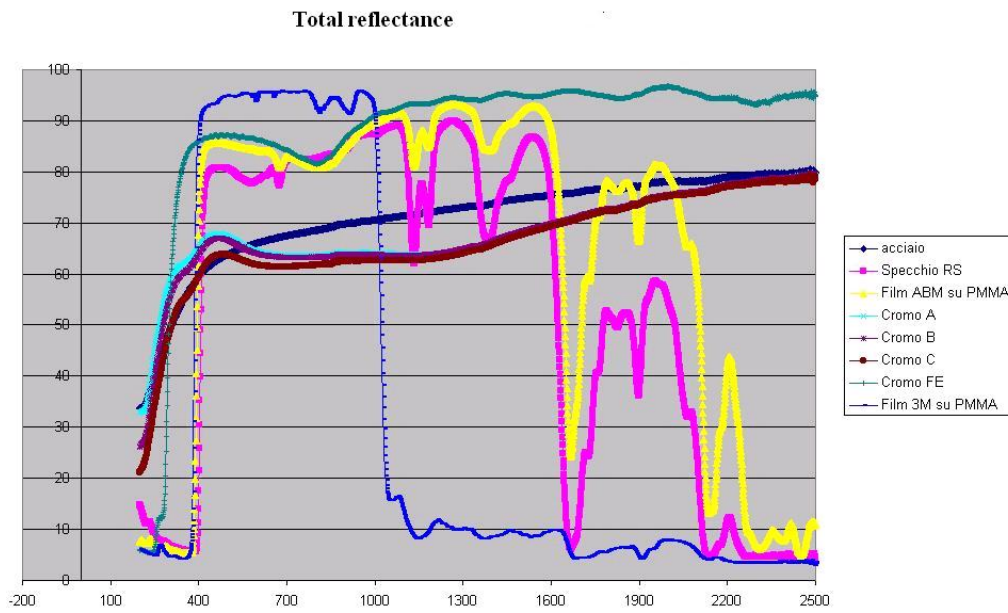


Figure 4-16 Total reflectance vs. wavelength for different materials

The selected material is the 3M VM2002 mirror film; it's a commercial, polymeric adhesive film with dichroic properties, with extremely high direct reflectance (about 96%) in the wavelengths range between 400nm to 1050nm. Its dichroic properties permit to have a lower thermal budget at the PV receiver.

4.2 Dense array PV panel and cooling

The PV panel, as in all the dish concentrator systems, is a dense array. This because the higher the packaging fill factor, the higher the optical efficiency. Two approaches have been investigated and partially tested; both use front contact solar cells.

The first configuration consists in the packaging of 1.1cm×1.24cm series connected Saturn BP solar cells on an alumina substrate for power electronics, as in fig.(4-17a). This small module covers a quarter of the illuminated target of the concentrator of fig.(4-2); it's the unitary element for a modular approach in the panelling. The cell to cell interconnections are made with aluminium wires in number and size appositely selected to give a negligible resistance(2-3 mOhm) and the cells are placed by an automated process; these fabrication process steps have been carried out by Hybritec S.r.l..

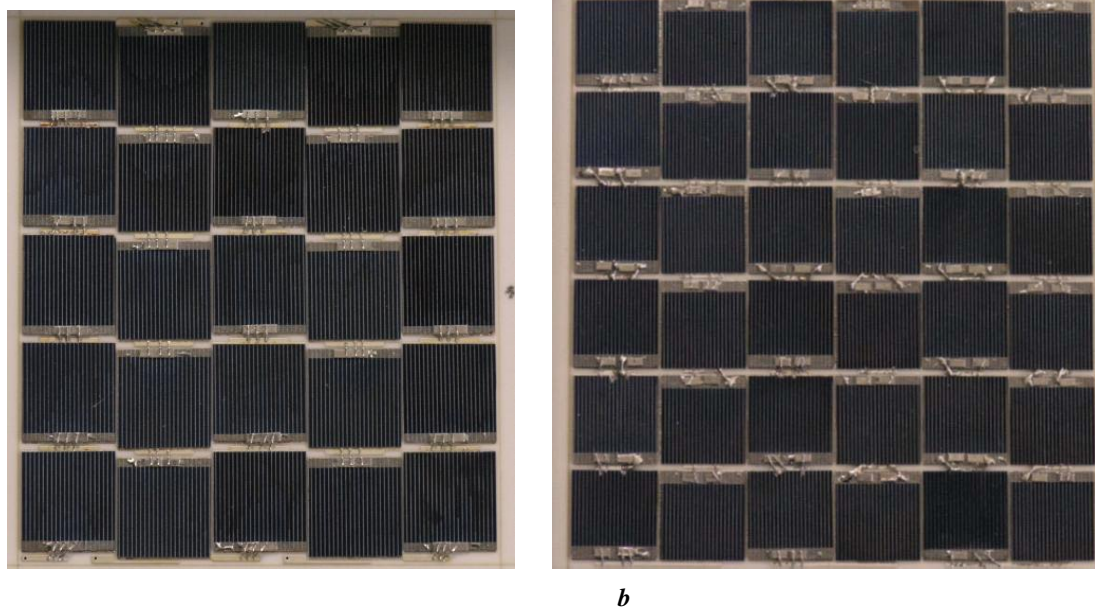


Figure 4-17- (a) 5×5 dense array module of Saturn cells; (a) 6×6 dense array module of Saturn cells

Higher packaging configurations have been fabricated as in fig.(4-17b), but in some cases the wire bonding has produced short circuits, contacting simultaneously front and rear side of single cells, as in fig.(4-18); more precise fabrication steps can recover this problem.

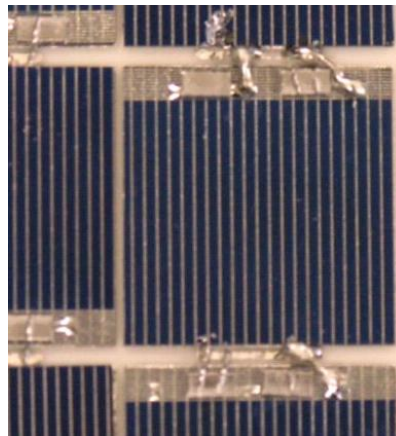


Figure 4-18 – Feature of a fabrication error in the soldering of the cells of the dense array

The cell arrangement is function of the cell dimensions, of the output voltage required and of illuminated area, so also other configurations are possible.

The panel has to be mounted on an active heat exchanger; this one can be an air forced or a liquid cooler element. Preliminary tests on one of these modules have been carried out

with an air active cooling; the assembled system tested is sketch in fig.(4-19). The results of this panel are discussed in cap.6.

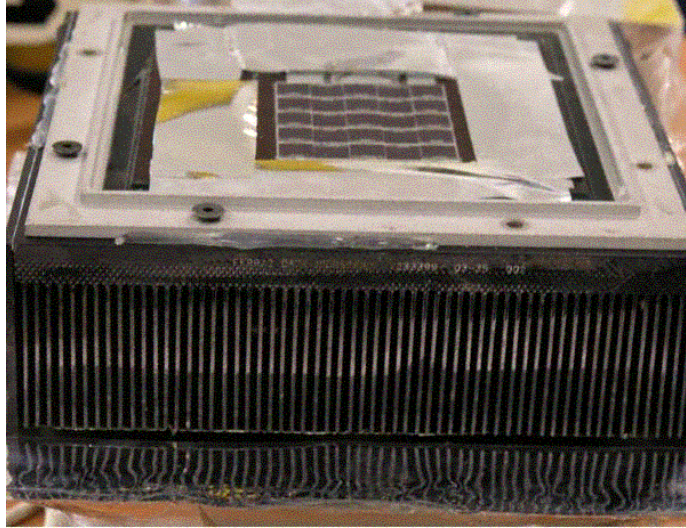


Figure 4-19 - 5×5 dense array module of Saturn cells mounted on an air heat sink

As illustrated in cap.3, the cells refrigeration is a very important issue in operative conditions; to achieve this goal, the optimisation of the panel thermal contact on the cooler is necessary. The ceramic substrate for the cells circuit has been attached at the heat exchanger with the high density polysynthetic silver thermal compound “Arctic Silver”; it isn’t an electrical conductor and have a thermal resistance $<0.0045^{\circ}\text{C}\cdot\text{in}^2/\text{Watt}$ per 0.001 inch layer.

A second approach developed in collaboration with ANU (Australian National University) is under evaluation: the optical losses due to bus-bar and cell to cell back-front connections are eliminated by a proper manufactured substrate with stair configuration; an analogue module is presented in [70], for TPV (thermophotovoltaic) application. The step highness corresponds at the thickness of each cell; the cells have been fabricated at the ANU appositely to work under 100 suns and they have been soldered together in a particular jig. The resulting string are shown in fig.(4-20).

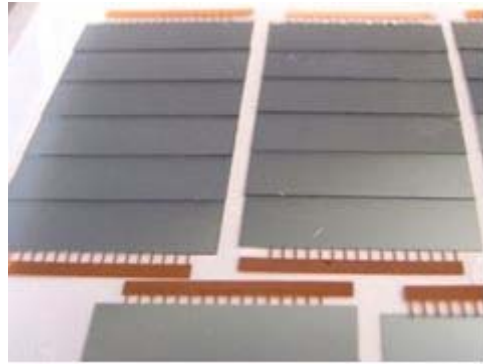


Figure 4-20 – ANU silicon solar cells shingle soldered together in series connected strings

The stepped substrate was fabricated on an aluminium plate and is shown in fig.(4-21); to avoid the short circuit of every cell rear sides, a thin (0.1mm) layer of good thermal conductor but electrical insulator, with typical applications in power electronics (Keratherm 86/90 heat conductive film), has been placed under the cells. The thermal properties of this layer have been tested at ANU; despite the claimed performances in the product data sheet, the obtained results are poorer, probably because of the difficulty in lay down the foil avoiding the introduction of air voids under it. The conductivity is stated by the manufacturer to be $10 \text{ Wm}^{-1}\text{K}^{-1}$, however it is found that the measured conductivity is $0.3\text{-}0.4 \text{ Wm}^{-1}\text{K}^{-1}$ (depending on the applied pressure) for silicone free samples and is $0.6 \text{ Wm}^{-1}\text{K}^{-1}$ for encapsulated samples. The conductivity of the used silicone rubber is stated by the manufacture, Wacker, to be $0.2 \text{ Wm}^{-1}\text{K}^{-1}$, then a layer of silicone of thickness around $30\mu\text{m}$ can be considered to give a net thermal impedance the same as that measured in the tested sample.



Figure 4-21 Stepped substrate for the ANU strings of cells

Although the string positioning was carried out manually, the optical losses for the receiver are strongly reduced, as shown in fig.(4-22); moreover, the cell efficiency can here

be considered without the covering contribution of the bus bar, increasing the overall efficiency of the receiver.

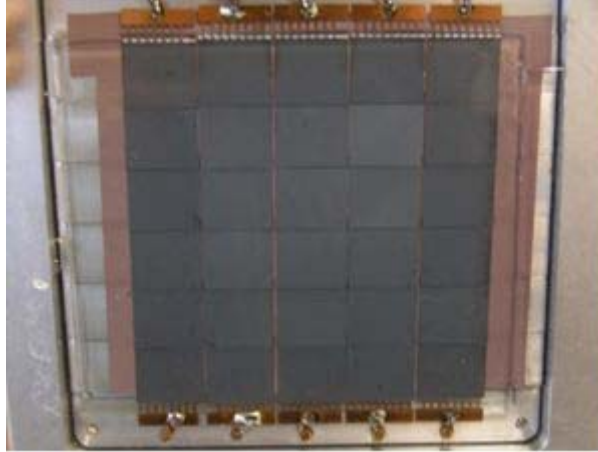
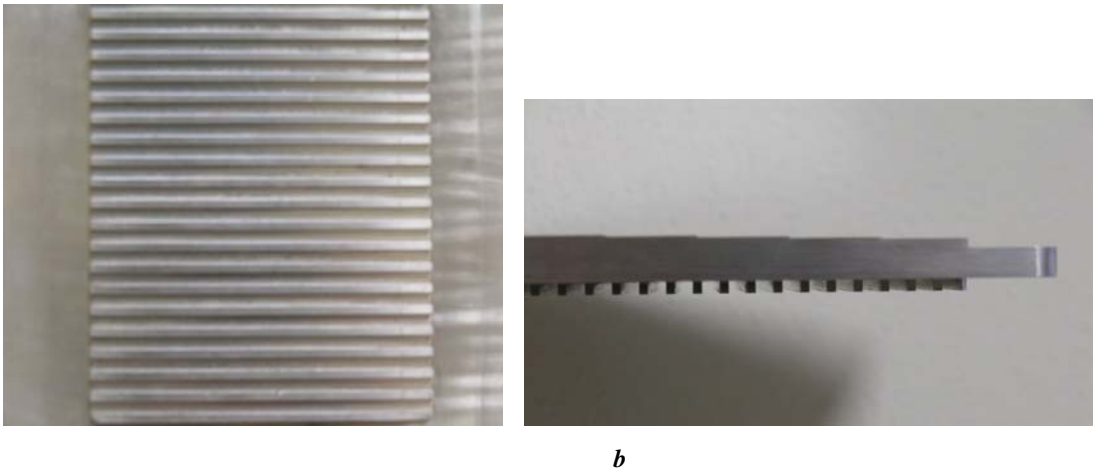


Figure 4-22 – Module of 5 encapsulated strings of cells series connected, placed on the stepped substrate and with the Keratherm foil as thermal conductive layer

The heat exchanger is fabricated on the same stepped plate, on the rear side. It's for water cooling and has the structure shown in fig.(4-23).



a

b

Figure 4-23 –Backside of the substrate, acting as heat exchanger

Both the PV receivers are encapsulated in transparent silicone (mod. Wacker Silgel 612) and closed with a highly transparent glass.

4.3 Dichroic approach

The solar cells power conversion has not the same efficiency for all the wavelength of the light; this because, as comes out from (2-17, 2-19), the cell output voltage is proportional at the energy gap of the semiconductor. The energy excess respect to the E_g of the electron exited from radiation with $E > E_g$ is dissipated through rapid thermalization toward the bottom of the conduction band, as graphically sketched in fig.(4-24); this energy excess can not be converted. As for the MJ solar cell, to improve the PV conversion efficiency is possible to dedicate different semiconductors for different wavelengths; an alternative approach at the MJ is the spatial splitting of different spectral portions of the solar radiation. This concept has been widely investigated in the past [71] and appears especially adapt for the concentration.

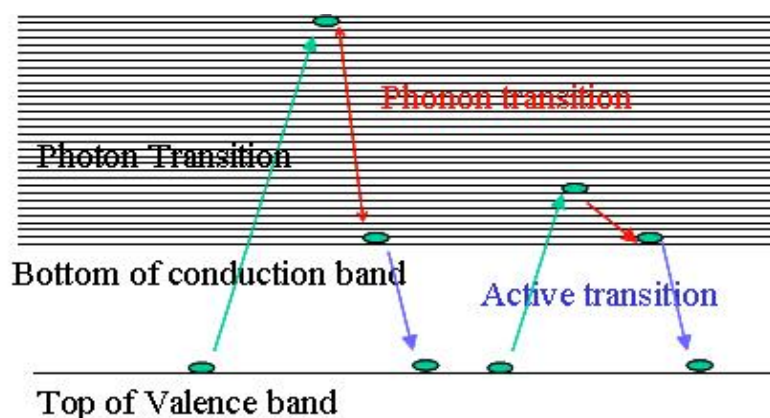
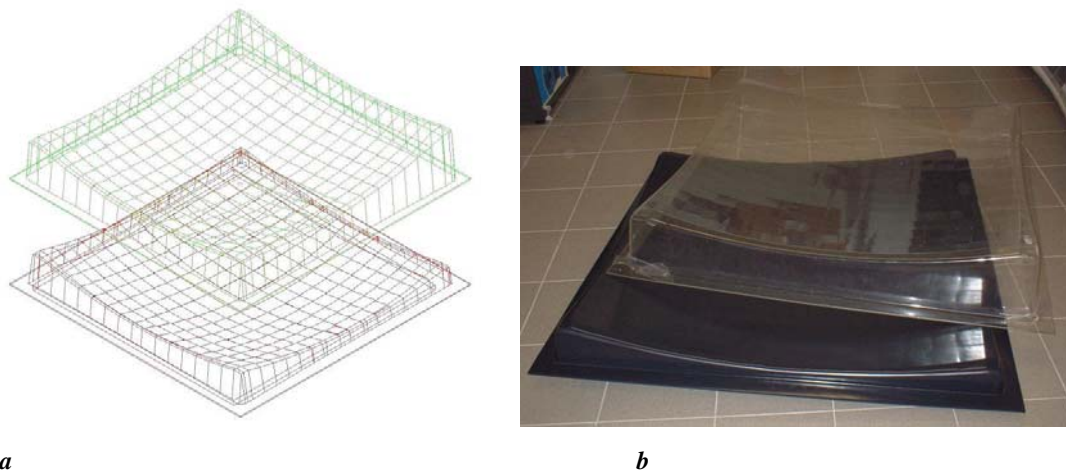


Figure 4-24 – Diagram of the excitation and de-excitation for electrons ionised in a semiconductor, for two different incident radiation

Our investigated solution for apply this concept is an evolution of the described flat faceted collector. With the same computational procedure previously illustrated, two dishes covered with properly designed dichroic reflectors have been projected for sending the different parts of the spectrum on different modules. These dishes are stacked together. While the structural material for the back, total reflective dish is ABS, the selected material for the material for the front shell is the PMMA, for its properties of transparency and manufacturability. The CAD of the two shell is depicted in fig.(4-25a) with the corresponding real structures in fig.(4-25b)



a *b*
Figure 4-25 – (a) CAD design of the two shell for the dichroic concentrator; (b) real shells in ABS and PMMA

The two shells are slightly different and are designed in order to obtain a tilt angle between corresponding flat surfaces; for an incident beam, the deflected radiations have angles dependent on the inclinations of the reflective surfaces for each wavelength, as sketched in fig(4-25) for three different reflective layers [72,73].

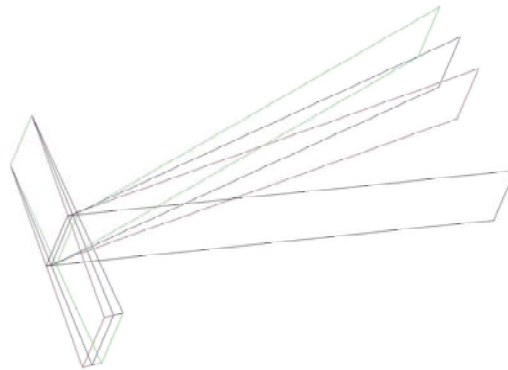


Figure 4-26 – Schematic spatial beamsplittig in different (3) light spectral portions of an incident ray (the bottom one)

This approach produces different target zones with quite good light flux uniformity as demonstrated by the simulated flux distribution in fig.(4-27); the grain size of the flux map is of 2.5mm×2.5 mm, i.e. in the order of 1/20 of the cells size. The fluctuations in the less homogeneous spot can be recovered with a secondary collector appositely design; in particular, a diffusive window as in the Solar System approach of fig.(3-8) can be here very useful; moreover, the random errors produced in the dishes fabrication contribute at a smoothing of the peaks, as observed for the single reflector, flat faceted concentrator [66].

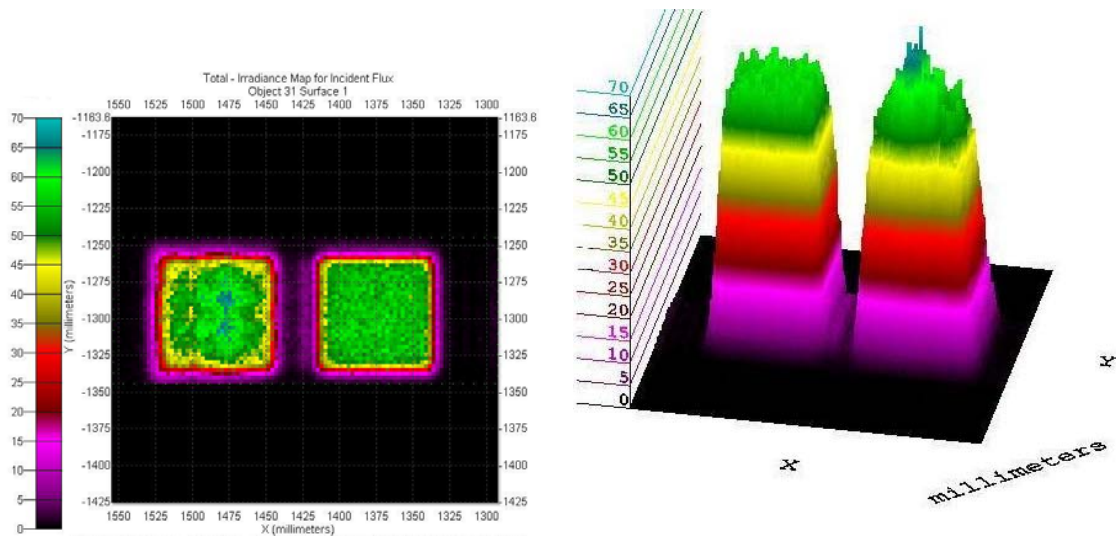


Figure 4-27 Illumination flux profile from the two shells of fig.(4-25a) in arbitrary units

The dichroic reflective surface is obtained by attaching an adhesive, dichroic layer on the rear side of the PMMA shell; in such a way, the plastic protects the film from the external agents. The optical reflectance characteristics of the dichroic layer is function of the kind of cells employed. The proposed configuration has two different modules, one with silicon cells, one with InGaP cells. With these materials and appropriate dichroic reflectors, the conversion efficiency can reach and overtake the 30%; the fraction of converted solar light power is represented by the union of the two regions coloured in fig.(4-28), one corresponding at the power fraction produced by Si and the other from InGaP high efficiency solar cells.

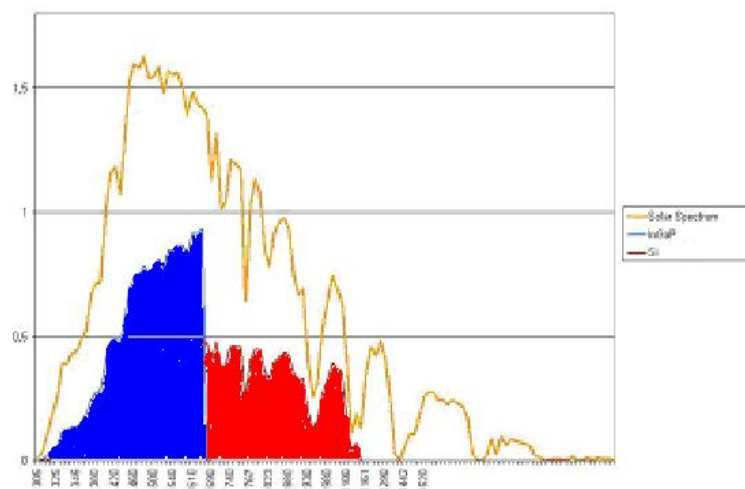


Figure 4-28 – Fractions of the incident solar power converted in electrical energy from InGaP cells (blu) and silicon cells (red) with a dichroic concentrator

In our prototype, 3M products are used as reflectors; the mirror on the rear shell is the commercial 3M radiant mirror film VM2002, while the dichroic on the PMMA shell is, at the moment, an experimental product; their reflectance characteristics measured with a spectrophotometer are respectively in fig.(4-29, 4-30). The light reflected from the first dichroic reflector is sent to the silicon receiver; part of the light with wavelengths suitable for the InGaP (20-25%) is reflected from this layer, but it isn't lost radiation, because it's converted by the silicon cells. Unfortunately, the product doesn't match the ideal optical requirements; in particular, the wavelengths in the range $600\text{nm} < \lambda < 650\text{nm}$ are directed to the Si instead of on the InGaP, and those in the range of $350\text{nm} < \lambda < 400\text{nm}$ are lost. Moreover, the partial dichroism, i.e. the non 100% transmittance in the range of $400\text{nm} < \lambda < 600\text{nm}$, gives a fraction of light definitively lost; indeed, while the portion of light reflected at the first encountered interface is reflected to the silicon, the portion of light from the mirror to the receiver which is reflected back at the dichroic shell, again toward the mirror, is lost. If $R\% \cong 25\%$, then 25% of 75% (=18.75%) of light with these wavelengths doesn't reach the module. This effect can be clearly recovered using a dichroic layer with better optical properties. However, the weight of these detrimental effects can be quantitatively evaluated, and the prototype can work effectively as a good proof of concept.

Both the layers, also the mirror one, present dichroic behaviour; this fact produces the elimination of part of unconverted radiation (UV and $\lambda > 1100\text{nm}$), with consequent reduction of thermal budget of the module.

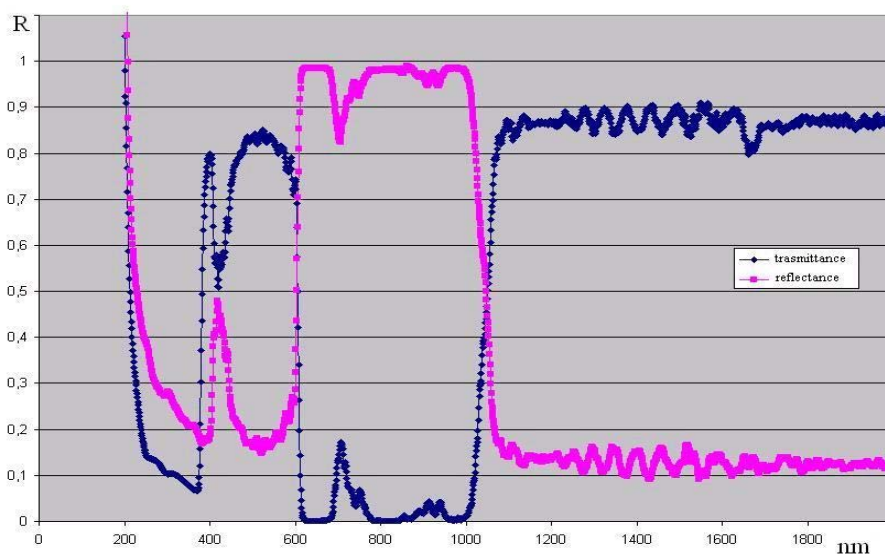


Figure 4-29 - Dichroic reflectance and transmittance characteristics for the adhesive film employed

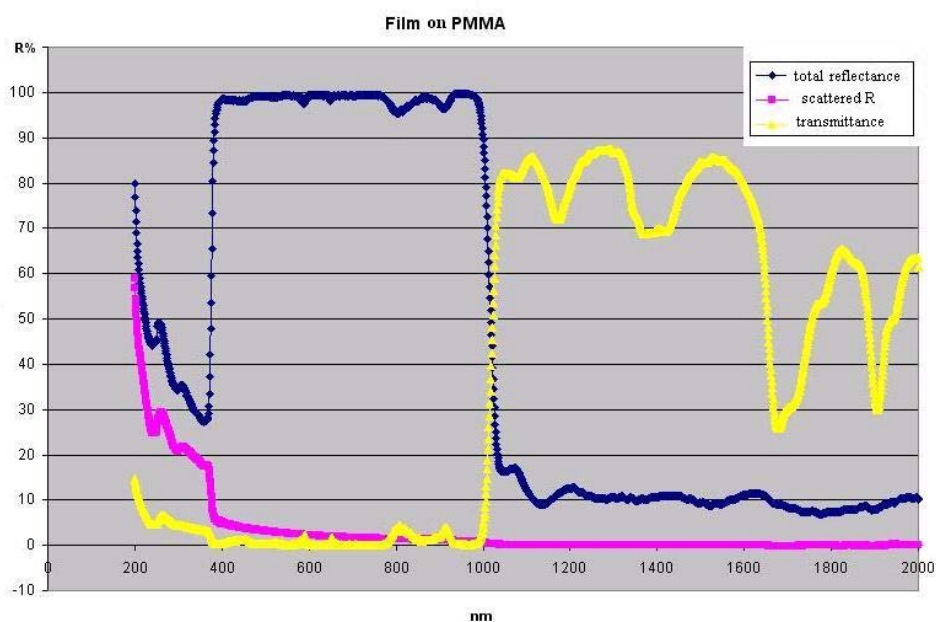


Figure 4-30 - Reflectance and transmittance characteristics for the mirror adhesive film employed

The thermal budget reduction is the second main advantage of the dichroic approach. For the InGaP receiver, except done in our case for the light portion reflected on silicon due to the not optimised dichroic, the concentration flux is exactly the concentration factor of the dish, i.e. about $200\times$. All the light of the global spectrum which, without the dichroic approach, should be transmitted by the InGaP thin layer and absorbed by its substrate (usually Ge) is aimed to the Si, avoiding the overheating of the devices. The heating is only due to the energy dissipation of the electrons promoted at high energy level in the CB. Moreover, the temperature coefficient which gives a decreasing output voltage for these solar cell is low, compared with other semiconductors, because of the low density of state effective electron and hole masses ($0.088m_0$ and $0,7m_0$ respectively) and the consequently low effective density of states. For the silicon receiver, the light flux is reduced respect to the nominal, and the portion of the radiation cut down is the most detrimental, from a thermal point of view.

In table (4-1) are summarized the calculated data regarding the dichroic system, supposing the ideal condition of negligible geometrical optical losses; only the optical losses due to the reflectivity characteristics of the coatings are taken into account. Depending on the efficiency of the mounted cells and on the characteristics of the reflective layers, the conversion efficiency varies significantly. The cells considered are

realistic devices; the efficiencies here supposed are for the equivalent concentration level at full light solar spectrum which gives the equivalent current on the cells. While in the configuration with the ideal dichroic the InGaP cells are reached from the same useful flux radiation as in the total spectrum, for the silicon cell the amount of photo-convertible light is shorted at about the 64%; so, the current production for a flux of 200× split beam is equivalent at that under 130× full spectrum beam. This feature permits less problems in the technological fabrication of the devices. The system efficiency is considered as the fraction of electrical power generate respect to the direct flux illumination energy on the collector; the direct flux is about the 90% of the global radiation. Diversely, the receiver efficiency is the fraction between the electrical power produced and the energy flux impinging on it.

The heat fluxes to sink out from both the receivers are fairly low in any cases, compared to conventional non dichroic approaches, permitting higher efficiency in working conditions.

dichroic characteristics	cell material	optical concentration	eff. Si cell @ 130x and InGaP @ 200x on full spectrum	Incident power density (W/cm ²)	Converted power density (W/cm ²)	Reflected power density (W/cm ²)	Heat flux (W/cm ²)	System efficiency on direct flux	Receiver efficiency
on prototype	Si	200	16,3%	8,1	2,2	15,0%	4,7		
	InGaP	200	13,3%	2,9	1,2	15,0%	1,3		
								18,6%	0,30508108
ideal	Si	200	16,3%	7,4	1,9	15,0%	4,4		
	InGaP	200	13,3%	5,7	2,4	15,0%	2,4		
								23,8%	0,32681178
on prototype	Si	200	21,8%	8,1	2,7	15,0%	4,2		
	InGaP	200	16,0%	2,9	1,4	15,0%	1,1		
								22,7%	0,37270369
ideal	Si	200	21,8%	7,4	2,5	15,0%	3,8		
	InGaP	200	16,0%	5,7	2,9	15,0%	1,9		
								30,0%	0,41259207

Table 4-1

The first prototypes produced are shown in fig.(4-31)



Figure 4-31 – Dichroic flat faceted concentrator with the two shells with films

The receiver for this double concentrator is obviously different at those already described for the global reflector dish; two panels are oppositely designed, one made with Si solar cells and the other one with InGaP cells; the technology adopted in this case is that without the stepped substrate. The two PV panels are separated each other of 1.7 cm, as result from the ray-tracing. The two PV tiles are attached at the commercial heat exchanger for water cooling (Lytron, Mod. cp-15) with the specifics reported in fig.(4-32)

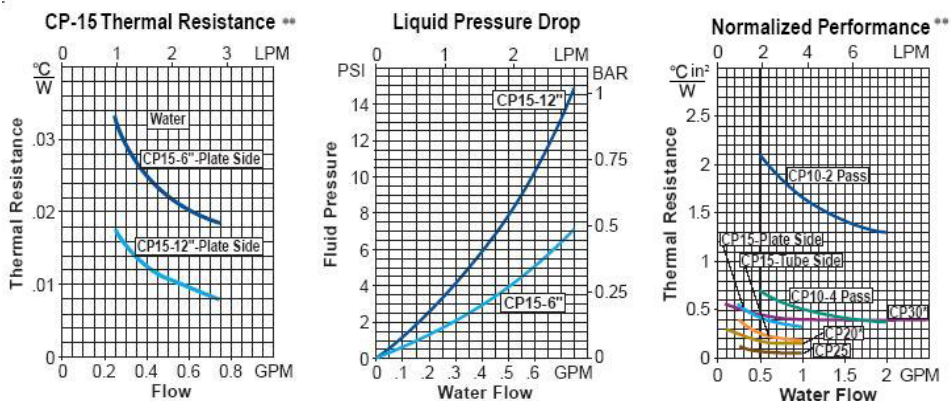


Figure 4-32

The receiver block is shown in fig.(4-33); the left side module is made of Si solar cells, while the right side of InGaP solar cells.

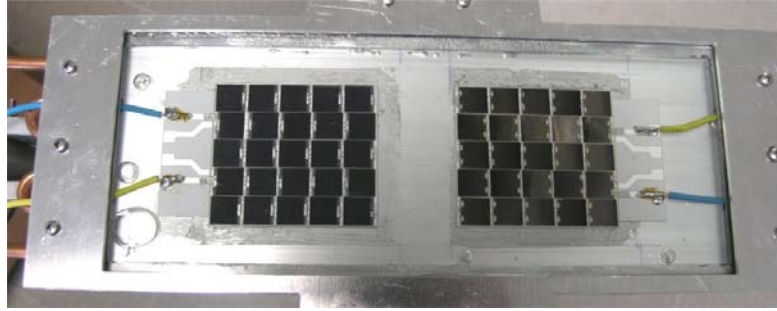
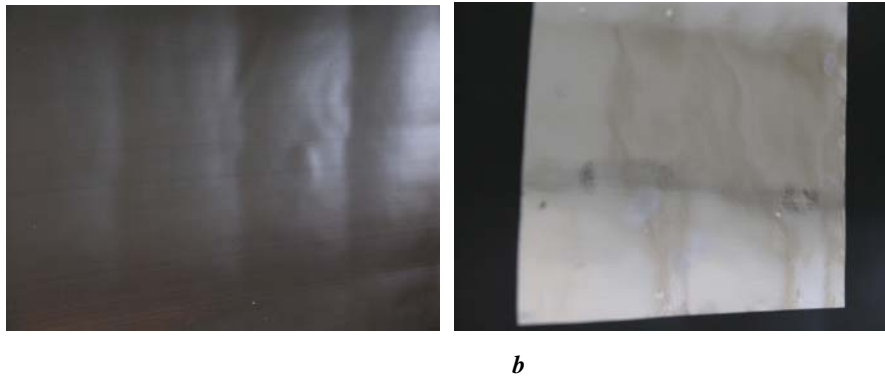


Figure 4-33 – Receiver for the dichroic dish, with a module with silicon Saturn cells (left) and a module with InGaP solar cells from CESI (right)

Also in this case, a secondary collector has been projected to recover at the errors in the fabrication of the primary concentrators; indeed, especially for the back dish made of ABS, the surface appears with imperfections: deformations are present on the flat surfaces and the interconnections between the flat surfaces are quite smooth, as sketched in fig.(4-34). On the other side, the PMMA dish appears accurate, as in fig.(4-35); this difference is due to the different stamps in the fabrication processes.



a

b

Figure 4-34 – Optical inspection of the ABS shell without (a) and with (b) a reflective film

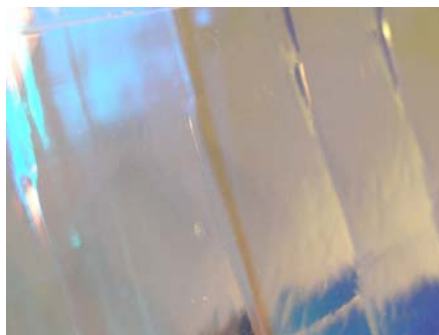


Figure 4-35 – Optical inspection of the PMMA dish covered with dichroic reflector

The two spots of light with different spectral region produced from the dishes are shown in fig.(4-36), while the mounted, complete concentrator and the illuminated receiver are in fig.(4-37) and in fig.(4-38).



Figure 4-36 – Two light spots of different wavelengths separated with the dichroic concentrator

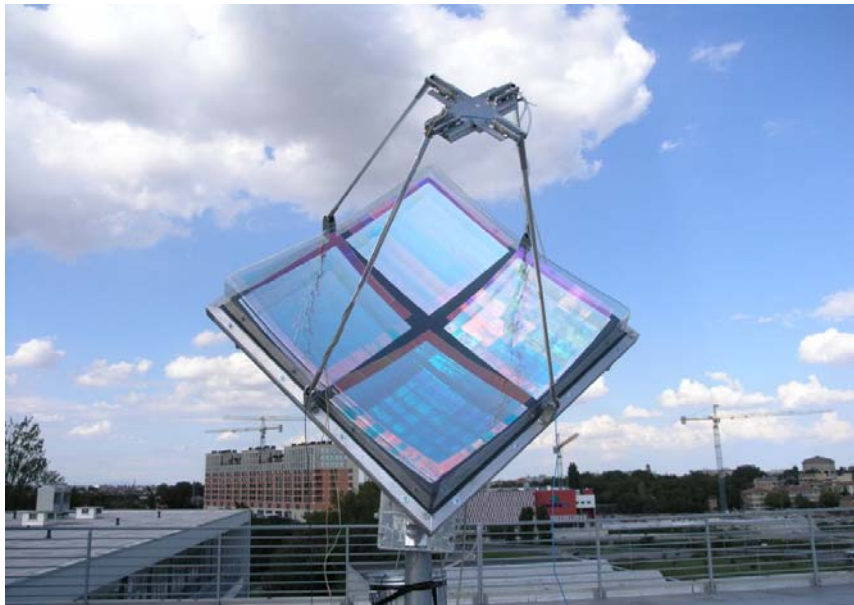


Figure 4-37 – Dichroic concentrator mounted on its tracker system



Figure 4-38 – Illuminated receiver in working conditions

CHAPTER 5 FABRICATION OF SILICON SOLAR CELLS FOR CONCENTRATION

5.1 General description and state of art

Currently, the PV world is dominated by the silicon solar cells technology; the solutions for their fabrication are largely treated in a number of books and papers [74,75]. Otherwise, silicon solar cells for concentration are not so largely diffused, because concentrator PV systems are not yet common. Although part of the fabrication procedure can be derived directly from the “traditional” processes for the solar cell production, the peculiarities of the working conditions for concentrator PV cells constrain some aspects of these cells to be fabricated in different ways.

Currently, only one commercial company sales concentrator Si solar cells [20]; its devices are IBC solar cells. The very high purity material required and the complexity of the fabrication process make these devices quite expensive, even for concentrating solar application, if the concentrator factor is not very high; in this last case, however, these cells have to compete with the MJ solar cells. Sunpower Corporation [76] produced and commercialised high efficiency IBC solar cells for concentration until some time ago; they have currently dismissed this product line.

Diversely, at the moment, only research centres and universities (ANU, NaREC, Univ. of Madrid, ENEA) are fabricating front contact solar cells for concentration; high performances devices was produced even in the '80 [21]. In general, for these cells some problems arise working under concentration level over 120 suns for effect of ohmic losses; besides, for the fabrication of these devices, non standard procedures are required with consequent cost increasing.

The investigated solutions at the University of Ferrara are here presented, revealing their problems and the selected way to follow for the concentrator silicon solar cells production.

The most common processes [77] for the concentrator solar cells fabrication doesn't move far from the procedures for one sun, high efficiency solar cells. There are different possible processes to achieve good results; aside at the device performances is important the simplicity, and consequently the cost-effectiveness, of the fabrication process.

In general, the lifetime material is a little less important issue than in high efficiency solar cell for one sun applications, because of the SRH recombination process reduces its importance as the injection level increases. However, the small amount of silicon necessary for this kind of cell permits us to use good quality material, finding the right trade off between low costs and material purity. Particular care regards the contacts; they have to introduce less series resistance as possible, from the metal layout component as well as at the silicon metal interface. Another important issue is the resistance of the emitter layer which can be reduced with two methods: shortening the current path in this region using a more capillare contact layout and decreasing the sheet layer resistivity. Both these solutions can be applied under some limitations; the first, because it produce an higher shadowing of the cell, the second because the reduction of the sheet resistivity increases the recombinations.

5.2 Silicon solar cell for concentration - 1

In order to find a correct procedure, cells with a contact pattern adapt for low illumination level (one sun) are initially produced with the follow list of steps:

- RCA1 and RCA2
- doping the wafers surfaces with phosphorous through the diffusion of P atoms in the silicon; a PSG (phosphorous silicon glass) is created on the silicon wafer surfaces with the chemical reactions (5-1, 5-2) in POCl_3 vapour rich atmosphere, at temperature of 860°C ; this step process takes 20'. The wafer are inserted and taken out the furnace at the temperature of 600°C .
- Photolithographic process for patterning the PSG, using a mask for regular texturing
- Anisotropic silicon etch, dipping the wafers in TMAH at 90°C for 8'.
- Phosphorous diffusion step analogous at the previous one
- Remotion of the PSG by chemical etching (short dip in diluted HF)
- blanket etch obtained dipping the wafer in a solution of HF and HNO_3 ; a very thin layer closed to the wafer surface is removed.
- creation of about 10nm of thermal SiO_2 at temperature of 860°C for 15'.

- Chemical etching of the back diffused layer, through brief dip in TMAH at 90°C, after remotion of the back thermal oxide layer.
- Back aluminium contact formation by screen printing and rapid sintering at 850°C
- Patterning the SiO₂ in the front surface with photolithographic process and chemical etching
- Evaporation of the metal contacts (Ti/Pd/Ag)
- Photoresist lift-off process
- Annealing of the front contact metals at 400°C
- Copper electroplating for thickening the front contacts
- Evaporation of antireflection coatings
- Cutting of the cells in the wafer

As a general rule, it is done particular care in avoiding prolonged high temperature steps, and steps at temperature higher than 870°C have been eliminated. These attentions are taken to reduce the diffusion of detrimental impurities in the material; moreover, every high temperature step has been carried out with the phosphorous doped layer, because of its gettering properties [78].

The first step in the process consists in the wafer cleaning; the standard procedures for silicon wafers are the RCA1 and RCA2. They are chemical treatments for the cleaning of the surfaces.

RCA 1 clean removes organic contaminations and dissolves particles by chemical oxidation of the silicon. It is important to remove any organic contamination in the beginning of the cleaning cycle, because some types of organic contamination cause incomplete oxidation of silicon and therefore lead to partial contamination. In a RCA 1 bath, hydrogen peroxide acts as an oxidizing agent and OH⁻ ions from NH₄OH leave a negative surface charge which repulses particles [79]. Some ion exchange processes between metals and ammonia can also take place during RCA 1. RCA 1 has been reported to remove copper contamination effectively [80]. The principle of the particle removal by chemical oxidation is presented in fig.(5-1)

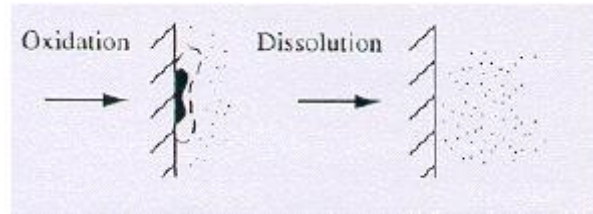


Figure 5-1 – Mechanism of removal of impurities from the silicon surface in RCA1 process

Next, chemical oxide formed during RCA 1 is removed by a short HF dip. After rinsing in DI water, the wafers are placed in RCA 2 bath. Cleaning mechanism of RCA 2 is based on Cl^- ions which form volatile metal chlorides that are desorbed from the wafer surface.

To improve the optical efficiency of the device the front surface has been texturized, as in fig.(5-2); it's a regular texturing obtained after the photolithographic patterning of the PSG layer, used as etch stopping layer.

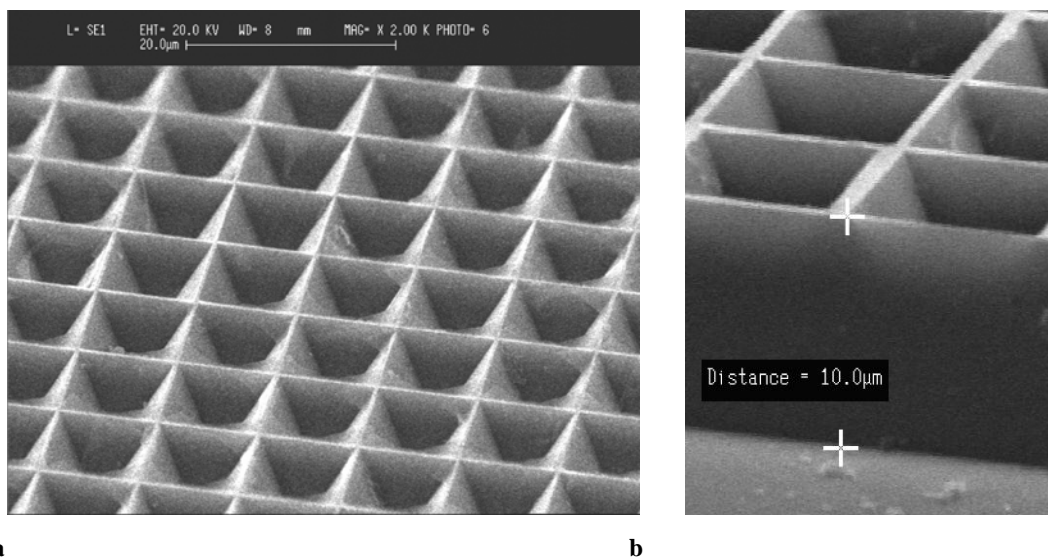


Figure 5-2 – Regular texturing; (a) top view; (b) edge of the etched region

This process can be done in [100] silicon surfaces, through the anisotropic etching given by the TMAH (but also KOH, NaOH are effective) on the different crystallographic Si planes [81]. With this micromachined surface the impinging light is “trapped”; the probability to absorb the light rises because of the first reflected radiation hits the silicon a second time; a regular texturing gives a global reflectance at the silicon surface of about 12%; the angular improvement in light collecting for this kind of structure respect to the

flat surface and the random texturing as reported in [82] can be useful in concentrated solar cell to absorb the high incident angle radiation directed toward the receiver from the secondary collector or to absorb some radiation reflected into the silicon from the cell contacts. Moreover, because of in concentration the incidence radiation has an impinging angle in general not perpendicular at the receiver, a not complete texturing with a cross section profile as in fig. (5-3) is good enough for the optical purposes; it gives advantages in the tolerance of this step process, which can be a quite sensible issue because of the etching time can vary in different wafer positions for effect of thin native oxide randomly grown or different hole apertures in the mask, as in fig.(5-4); moreover, as will be later described, there's the possibility to have less [111] silicon planes area, with consequent lower surface recombination rate.

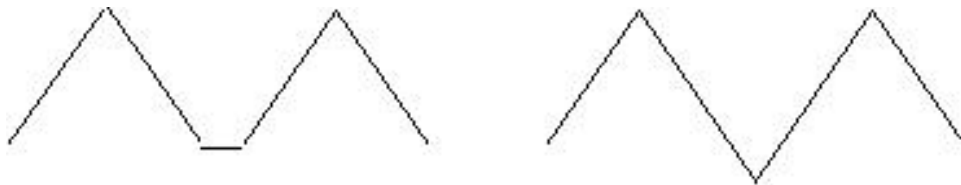


Figure 5-3 – Cross section profile of a non complete etching process and of a finite etching

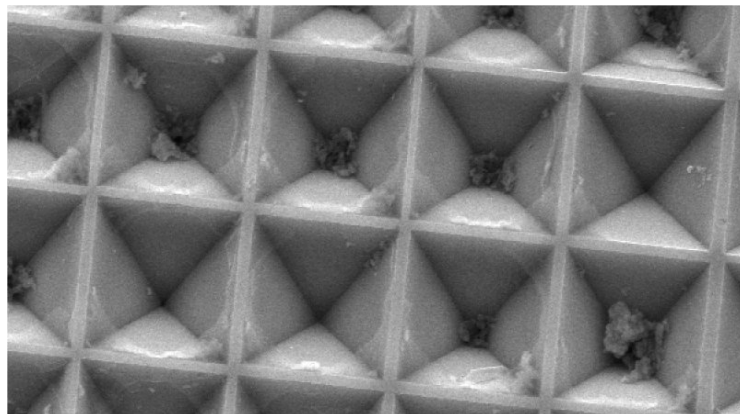


Figure 5-4 – Top view of some inverted pyramids, with different characteristics

Because of, as shown in fig.(5-2b), the deepness of the inverted pyramids is of about 10 microns, with the texturing production the diffusion layer is removed and a second diffusion step is necessary. Both the diffusion steps have been carried out with vapour of POCl_3 as phosphorous source; nitrogen is fluxed, bubbling in the liquid POCl_3 source kept at 23°C ; the vapours are carried to the reaction chamber heated at the selected temperature.

The scheme of the diffusion furnace and the connected gas lines is in fig.(5-5). A partial pressure of oxygen is necessary to allow the reaction (5-1) for the creation of the PSG layer on the wafers surfaces. The phosphorus is liberated in the silicon with the chemical reaction (5-2).

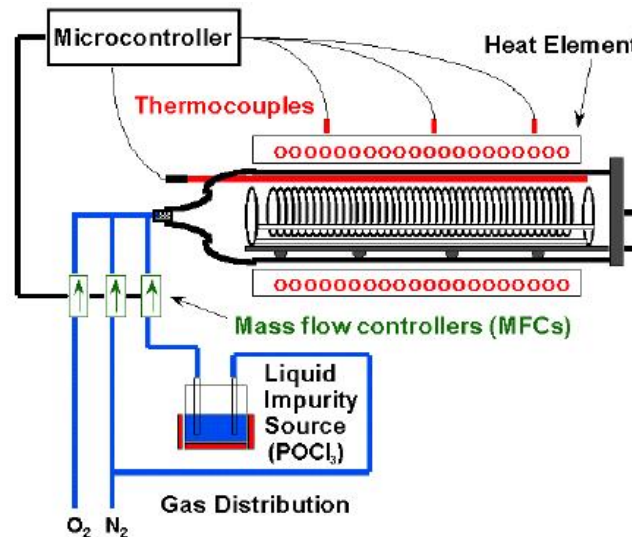


Figure 5-5 – Schematic diffusion furnace and gas lines

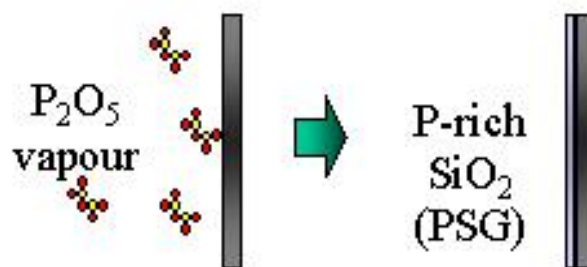
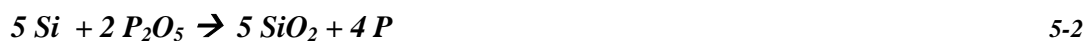


Figure 5-6 – Reaction at the wafer surface in the diffusion furnace

The P diffusion in silicon from a constant source of dopant (the PSG) is largely discussed and described in literature [83], because of its great importance for the electronic devices. In practical cases, phosphorous diffusion doesn't follow the simple diffusion model accurately [84]. With high phosphorous concentrations, the diffusion coefficient increases

rapidly; an extensive discussion of the diffusion phenomena in silicon is presented in [85]. A measured profile on a flat (100) surface after the described diffusion process is shown in fig.(5-7); it has been obtained with stripping-hall technique.

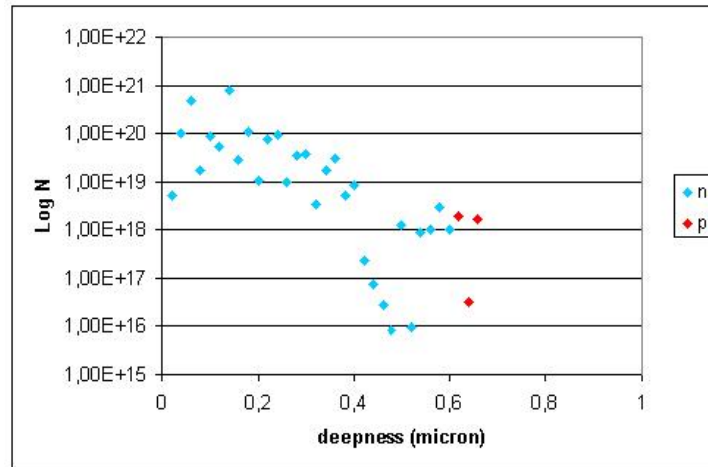


Figure 5-7 – Diffusion profile measured with stripping-hall technique for an as diffused wafer

After the second diffusion step a slight isotropic etching is carried out at the surface; this because the diffusion process with PSG as constant-surface dopant source produces a region with non-electrically active phosphorus impurities closed at the surface, as shown in fig.(5-8) from [86].

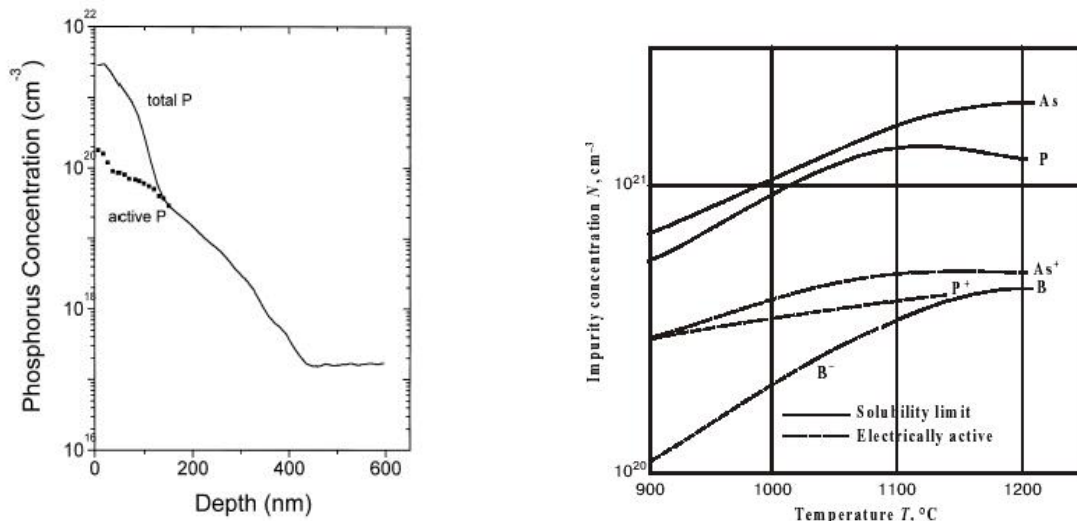


Figure 5-8 – Diffusion profiles and active phosphorous concentration in silicon [86]

These electrically inactive impurities don't contribute at increasing the layer conductivity and create an high recombination region at the front surface, the region with higher

electron-hole pairs generation, because of Auger and SRH processes. This dead layer [7] is partially removed with a very slow isotropic silicon etch based on HNO₃ and HF; the deepness of the etched layer is checked with four point measurements of the sheet resistance of the diffused layer. This step is terminated when the sheet resistance has achieved a value in the range of 40-60 ohm-square; after the diffusion step it's of about 20-25 ohm-square. The difference between the diffusion profile before and after the blanket chemical etch is clear in fig.(5-9); about 100 nm was removed.

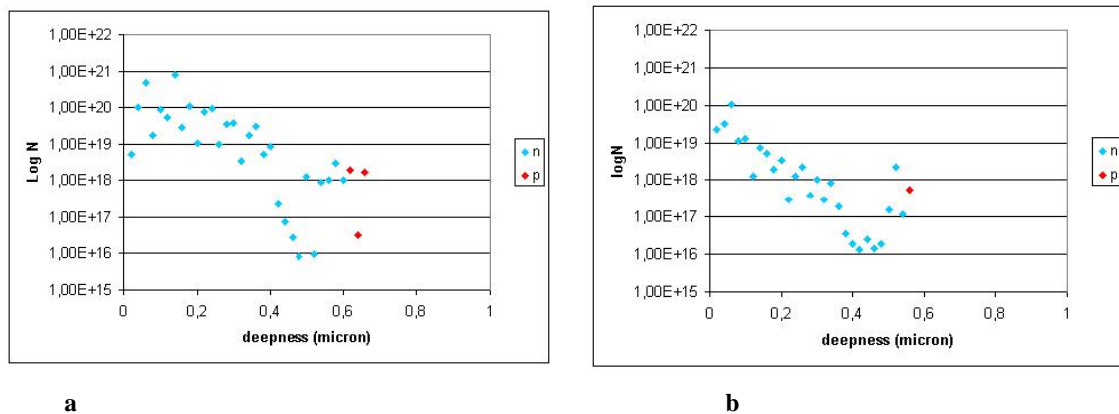


Figure 5-9 – Phosphorous concentration after diffusion, before and after the blanket etch step.

Next, a thermal silicon oxide is formed on the wafer surface to saturate the dangling bond and, consequently, to reduce the surface recombination velocity. The passivation properties of the thermal oxide have been largely studied [9]; it appears that the higher the formation temperature, the lower the recombination rate at the interface Si-SiO₂. However, to avoid the detrimental effects of the high temperature processes, this step has been carried out approximately at the diffusion temperature. The textured surface is more difficult passivated than the flat [100] surfaces [87] this because of the [111] bare silicon surfaces have an higher number of dangling bonds than [100] and because of the interface area in textured wafers is higher. Although the higher the SiO₂ thickness, the lower the recombination rate [9], the SiO₂ grown has a thickness of about 15 nm to obtain the best optical matching using the antireflection coatings, as will be later illustrated. This thermal step contributes at pushing into the silicon portion of the electrical inactive phosphorus not removed with the blanket etch, increasing the electrical properties of the layer.

The diffusion step in POCl₃ vapour environment gives a n-doped layer in both the wafer surfaces. The rear diffused layer is removed with TMAH chemical etching, protecting the front side of the wafer. After this, the back contact is deposited on the wafer, consisting in

a screen printed Al layer of about 15 micron of thickness, sintered at about 850°C in an infrared RTC belt furnace. The beneficial effects of Al on silicon are reported in a number of publications [88,89], creating a BSF and giving impurity gettering [90].

The front contact has been fabricated using photolithographic technique and metal evaporation; a negative photoresist has been used for the lift-off process. The process sequence is sketched in fig.(5-10)

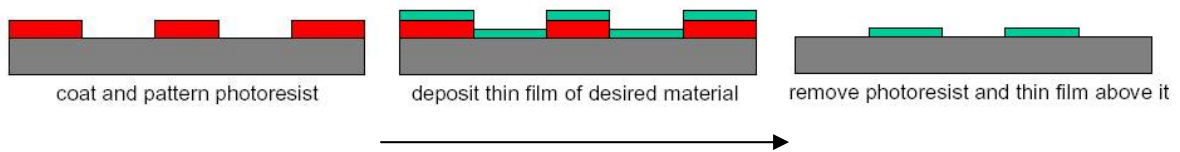


Figure 5-10 – Sequence of steps in lift-off photolithographic process

The used photoresist (NT-90) has enough viscosity to be deposited on the textured surface without suffer the non planarity, as shown in fig.(5-11)

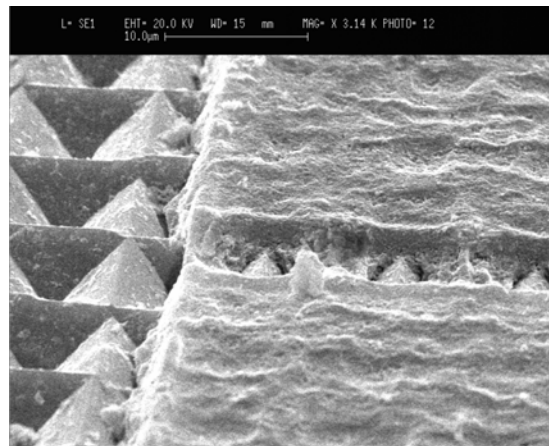


Figure 5-11 – SEM image of 3 μm photoresist deposited on textured surface

A stack of Ti/Pd/Ag (30/30/300nm) has been deposited on the patterned wafer. This particular stack of metals is usually selected for these reasons:

Ti has good ohmic properties at the silicon surface; annealed at a temperature in the range of 400 -450°C, low resistivity titanium silicides are created [25]. Because of the fairly high resistivity of the titanium there’s the necessity to have other metals for the electrical conduction; the best conductor is the Ag, so it’s selected as conductive layer. The poor adhesion of Ag on Ti, especially in wet environment, leads to the necessity to introduce a layer in between; the material acting as adhesion layer is the Pd.

The metal contact after the lift-off follows the surface morphology as shown in fig.(5-12)

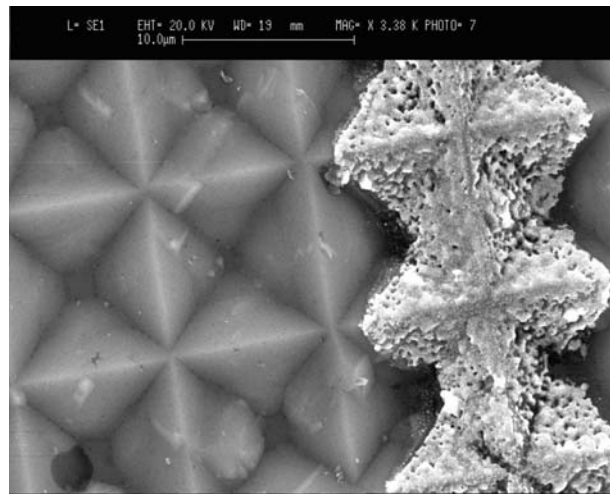


Figure 5-12 – Metal finger evaporated on textured surface

Because of the concentration PV cells require very low contacts resistance, the annealing step is followed by electroplating, for metal thickening. Due to the toxicity of the Ag electroplating bath, copper has been growth on the evaporated Ag top layer. The copper deposition happens with the chemical reaction (5-3) in the acid bath with the following components:

Copper Sulfate (CuSO₄·5H₂O) 188 g/l

Sulfuric Acid (H₂SO₄) 74 g/l

The operating current, with little agitation, has been limited to 3.7-5.4 A/dm²



The resulting metal layer presents sufficiently small grain size, as shown in fig.(5-13)

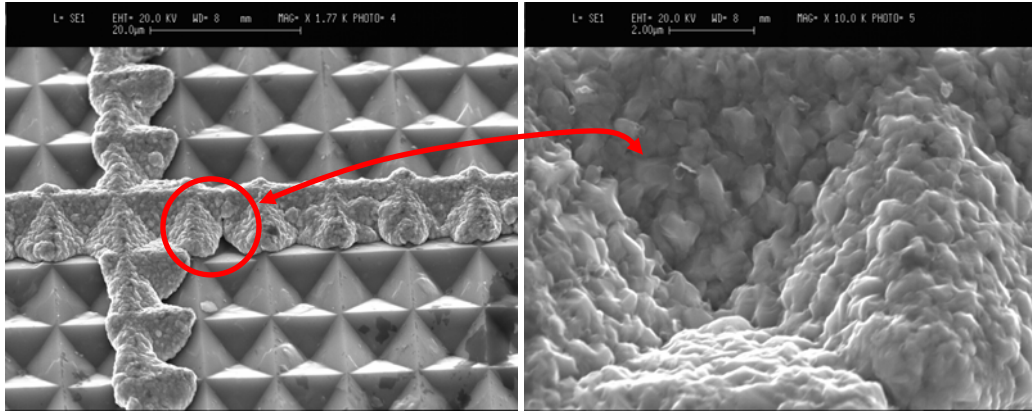


Figure 5-13 – Copper electroplated on evaporated metal fingers

Finally, a double antireflection coating (ARC) is deposited on the front surface. Even with a textured surface, there's a global reflectance of about 12%. To reduce it as low as possible, two transparent materials with appropriate refraction indexes have been chosen. These materials are ZnS ($n=2.35$) and MgF₂ ($n=1.38$) and have been deposited by evaporation. A proper coating of the textured surface is more difficult than for a flat surface, because of the different incident angle of the evaporated particle; moreover, the light reflectance is angular dependent, so the thickness layer couldn't be calculated as for a flat surface. From a practical point of view, however, to calculate the thickness of the coatings the approximation of considering the reflectance of the light at every angle as that for perpendicular radiation was used. The lost performances with this approximation are well recovered from the double reflections generated by the texturing. The thickness of these layers have been calculated using the matrix method as in [91].

The I-V characteristics of cells fabricated following the presented procedure is discussed in cap.6.

Some points have created problems or are not strictly necessary in this fabrication process:

- The PSG used as TMAH etch stop has shown anomalous and not uniform behaviour; strong differences have been observed for wafers which have followed very similar processes and even for closed points in the same wafer, as shown in fig.(5-14).
- The lift-off technique doesn't match very well with the process described; this because the copper doesn't grow only vertically on the evaporated metal. The copper spreading produces a direct contact between this metal and the silicon bare surface; indeed, the surface where the SiO₂ was etched for the metal contact is not completely covered with

Ti, because of shadowing of the photoresist walls in some substrate regions during the evaporation step and because the deposition of the resist on the textured surface doesn't fill the voids completely; in fig.(5-15) the edges of the SiO₂ after the metal evaporation are marked. The copper can consequently diffuse into the silicon producing the known [12,92] detrimental effects of this impurity. A way to recover this problem is to dedicate a two step photolithographic process at the front contacts fabrication: a first wider lines pattern for the evaporated metals followed by the deposition of a thick photoresist, realignment and creation of a new pattern with narrower lines; these could work as walls for the metal electroplating. However, this procedure doesn't appear cost-effective.

- The double antireflection coating gives the best result for the cell optical performance, but it loses its benefits in real operating conditions, where silicone potting is applied.

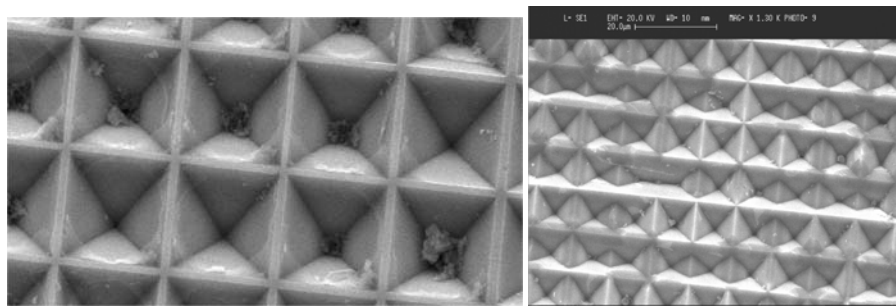


Figure 5-14 – Non-uniformity in chemical etching for the regular texturing, using PSG as masking material

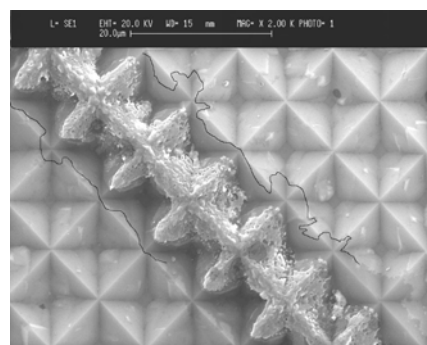


Figure 5-15 – Evaporated finger on textured surface; the black line delimits the region with etched SiO₂

Alternative processes have been carried out to recover these points.

5.3 Silicon solar cell for concentration – 2

To overtake the previous problems, a strong process change ment was done. The substantial differences consist in the utilization of LPCVD Si_3N_4 as ARC and electroplated Ni as adhesion metal layer. The main advantages given by the silicon nitride are the suppression of an evaporation step, substituted with a furnace passage where a great number of wafer can be processed simultaneously, and it's high masking resistance at various Si chemical etchings. The introduction of this point changes largely the process sequence.

The nickel has been chosen as adhesion metal layer for some very useful peculiarities: it forms low temperature (400°C) silicides with the lowest resistivity [93] and it grows on silicon bare surface by electroplating without any particular activation step or other metal adhesion layers. It's already used in the LBCSCs (Laser Buried Contact Solar Cells) and has given good results in high efficient solar cells [94], although it's not yet extensively used in processes for high efficiency or concentrated solar cells.

The list of process steps becomes as follow:

- RCA1 and RCA2
- Thin layer (10nm) of Si_3N_4 deposition using LPCVD technique
- Photolithographic process, patterning the Si_3N_4 with BHF and a mask for regular texturing
- Anisotropic silicon etching dipping the wafers in TMAH at 90°C for 10'.
- Remotion of the Si_3N_4 by chemical etching (dip in diluted HF)
- doping the wafers surfaces with phosphorous, analogously at the previous described process
- Remotion of the back PSG by chemical etching (short dip in diluted HF)
- Chemical etching of the back diffused layer, through brief (1 minute) dip in TMAH at 90°
- blanket etch
- creation of about 15nm of thermal SiO_2 at temperature of 860°C for 20'.
- ARC layer (75nm) of Si_3N_4 deposition using LPCVD technique
- Pattern the Si_3N_4 and SiO_2 layers in the front and back surfaces with photolithographic process and chemical etch of these layers in the contacts layout (dip in BHF), using thick photoresist as protective mask for the rest of the surface
- Back aluminium contact formation by screen printing and rapid sintering at 850°C

- Ni electroplating
- Copper electroplating for thickening the front contacts
- Annealing of the front contact metals at 300°C
- Ni electroplating to cover the copper
- Cutting of the cells in the wafer

A thin layer of Si_3N_4 has been used as masking layer for the regular texturing creation. Indeed the very low TMAH etch rate on this material allow us to leave the samples in the chemical solution without problems of non-uniform etching. Although the LPCVD process has to be carried out at higher temperature respect to the LECVD largely used for PV applications [95], the required temperature (750°C) is fairly lower than the other high temperature steps in the process. Before of the diffusion step, the Si_3N_4 thin layer was removed in order to permit a good phosphorus diffusion in all the topper surface region.

An ARC layer of Si_3N_4 has been deposited on the passivating thermal oxide. Having a refractive index $n = 2$, it works as an effective antireflection layer; considering a flat surface, it reduces the average reflectance in the interested wavelengths range at less than 10% instead of the 33% of a bare surface. The reflectance vs. wavelength graphs for a flat silicon surface with 15nm of SiO_2 and 75nm of Si_3N_4 in air and potted with a silicone of refraction index $n = 1.5$ are shown in fig.(5-16, 5-17). Considering the reflectance reduction given from the texturing, optical losses for reflection on the active material lower than 4% can be assumed.

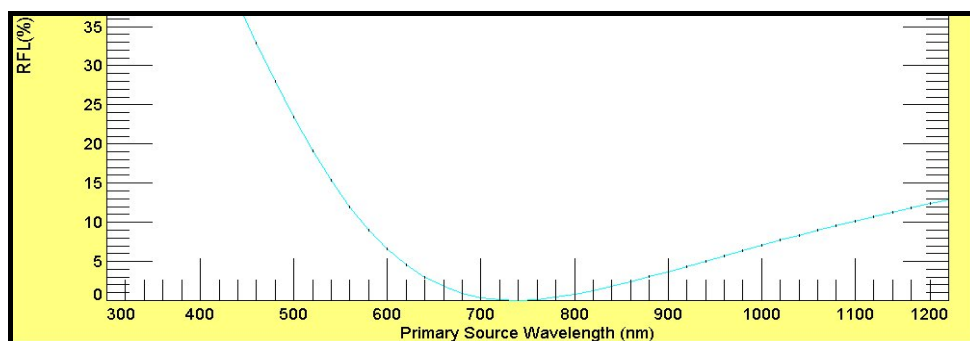


Figure 5-16 – Reflectance vs. wavelength for silicon with 75nm of Si_3N_4 on 15nm of SiO_2 on the front surface

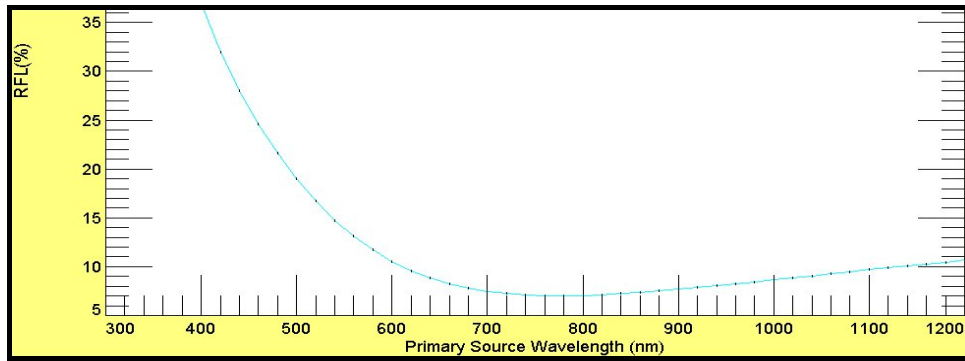


Figure 5-17 - Reflectance vs. wavelength for encapsulated silicon with 75nm of Si_3N_4 on 15nm of SiO_2 on the front surface

A thick photoresist (Microresist ma-100) was used as protective mask during the Si_3N_4 and SiO_2 etching from the contacts pattern. The layers on the back surface wasn't completely removed to improve the rear surface passivation [22]. About the 20% of the back surface has been directly contacted with screen printing Al paste.

The front metal has been grown with electroplating; the galvanostatic bath is the Watts electroplating solution, and is composed of:

$\text{NiCl}_2 \cdot 6\text{H}_2\text{O}$	~ 33g/L
$\text{NiSO}_4 \cdot 6\text{H}_2\text{O}$	~ 165 g/L
CH_3COOH	~ 40g/L
H_2O	until $\text{PH} = 4.7$

The operating current, with little agitation, was limited at about 1 A/dm^2 .

The electroplating procedure has been preferred to the electroless, because the latter can happen only in the case of current flowing through the metal-silicon interface; so, a not complete etch process of the insulator layers is revealed, while electroless deposition can happen if the surface is electrically activated, even without current flowing. After the deposition of approximately $1\mu\text{m}$ of Ni, Cu electroplating follows, to ensure low resistance contact.

The photoresist was removed in acetone bath and the metal contact was annealed in an atmospheric furnace at 300°C for 3 minutes to form low resistance Ni silicides [96].

A final cap of Ni was grown on the copper to increase the contacts reflectivity.

A portion of a resulting contact finger, not yet thickened as needed for concentration purposes, is shown in fig.(5-18)

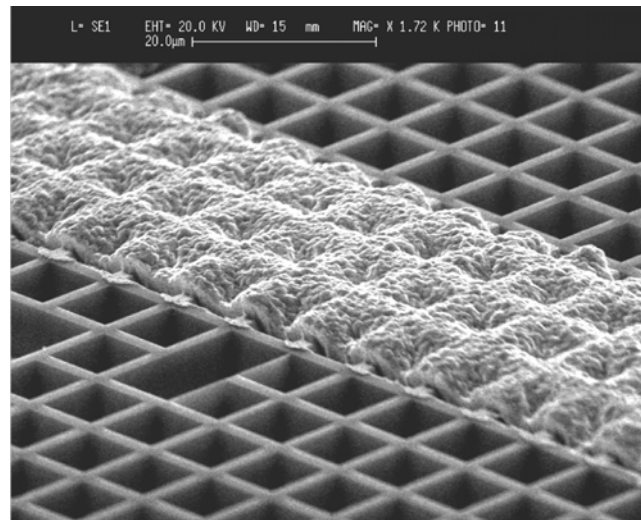


Figure 5-18 – Nickel electroplated directly on textured silicon surface

This process seems more effective than the previous, even if the results have been not so good. Some new problems raised in this procedure:

- The series resistance appears to be too high, in the order of 1 ohm/cm^2 ; the annealing step doesn't show benefits, but even damage the devices. This fact can be attributed to the not controlled atmosphere in the annealing furnace. Lower temperature annealing damages less the cells, but the low resistance silicides are not formed. The dominant resistance component is individualized in the metal-semiconductor contact interface, because the device resistance doesn't vary significantly, changing the contact layout from the configuration in fig.(5-19a) to that of fig.(5-19b), or thickening the metal contacts.

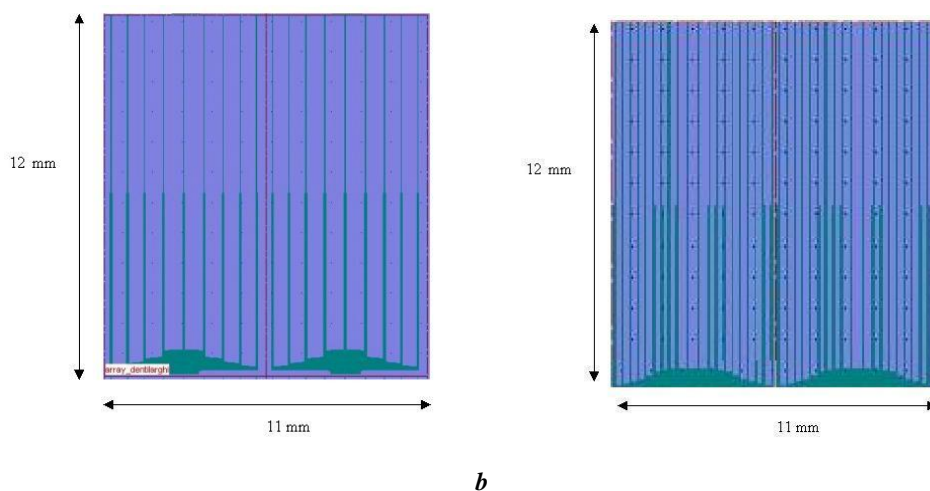


Figure 5-19 – Contact layout for the concentrator solar cells produced

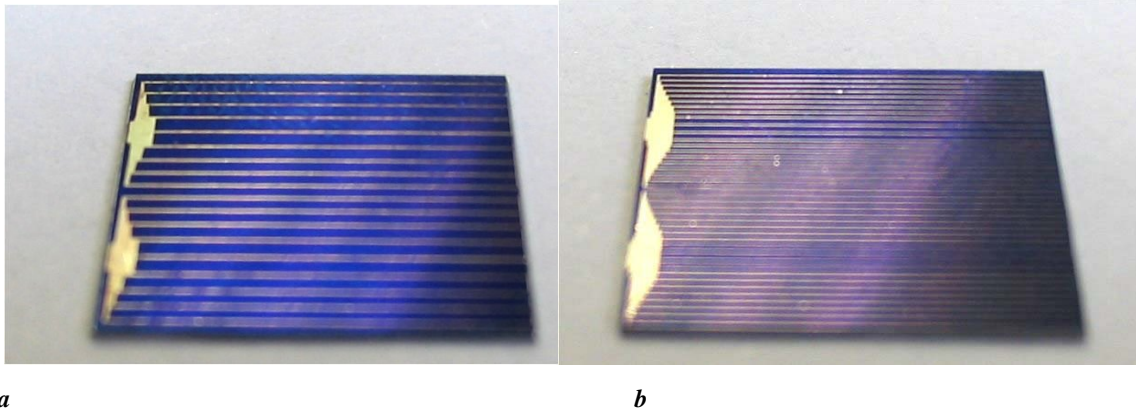
*a**b*

Figure 5-20 – Solar cells of 1.32 cm² fabricated at University of Ferrara, with Nickel front metal

- Low adhesion contact is present; this fact is clearly connected at the resistance problem. This phenomena appears not uniformly among the processed wafers and even inside single wafers. An example of contact peeling is shown in fig.(5-21). The observed non-uniformity is attributed at the chemical etch steps; in particular, for the remotion of Si_3N_4 from the contact pattern a long taking etch ($\sim 1\text{h}30'$) is required. The BHF solution has a very low silicon etch rate, but it is not negligible for the heavy doped Si, as the front surface is. Because of the Si_3N_4 etch rate is in the order of 1nm/minute, a small non uniformity in the silicon nitride deposition on the wafers leads to an additional, spatial non uniform etch for the heavily doped silicon contacting the Ni; reducing the etching time there's the possibility of obtaining areas where the insulator layer is not completely removed. As explained in cap.2, a low doped surface contributes at an higher contact resistance because the Schottky barrier is wider.

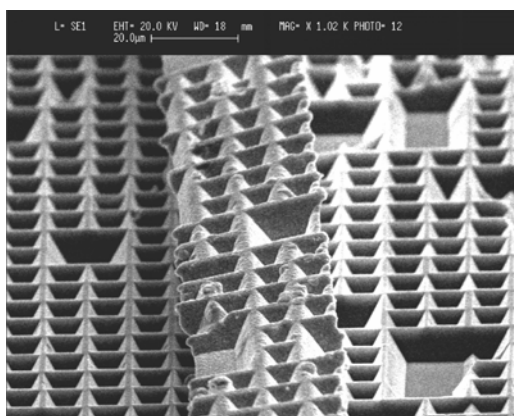
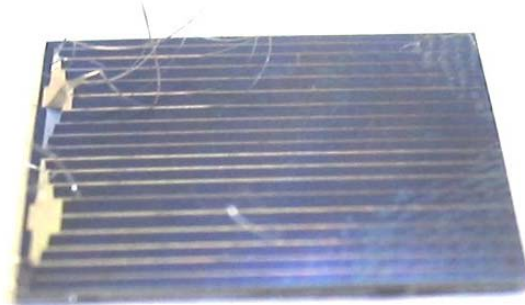
*a**b*

Figure 5-21 – Peeling of metal contact; (a) SEM view; (b) complete device

5.4 Silicon solar cell for concentration – 3

Although the faced problems, the way with Si_3N_4 and electroplated Ni appears to be the more effective. Changes in this last process has been carried out to recover the contacts problems; in particular, chemical grooved contacts have been manufactured to achieve the desired result. The followed process is here presented:

- RCA1 and RCA2
- Thin layer (10nm) of Si_3N_4 deposition using LPCVD technique
- Photolithographic process, patterning the Si_3N_4 with BHF, using a mask for regular texturing
- Anisotropic silicon etching dipping the wafers in TMAH at 90°C for 10'.
- Remotion of the Si_3N_4 by chemical etching (dip in diluted HF)
- doping the wafers surfaces with phosphorous analogously at the previous described processes
- blanket etch
- creation of about 15nm of thermal SiO_2 at temperature of 860°C for 20'.
- ARC layer (75nm) of Si_3N_4 deposition using LPCVD technique
- Patterning the Si_3N_4 and SiO_2 layers in the front and back surfaces with photolithographic process and chemical etching of these layers from the contacts layout (dip in BHF), using thick photoresist as protective mask
- Anisotropic silicon etch, dipping the wafers in TMAH at 90°C for 10'.
- Doping the grooved pattern with phosphorous by diffusion
- Remotion of the back PSG by chemical etching (short dip in diluted HF)
- Chemical etching of the back diffused layer, through brief (1 minute) dip in TMAH at 90°
- Back aluminium contact formation by screen printing and rapid sintering at 850°C
- Ni electroplating
- Annealing of the front contact metals at 300°C in nitrogen atmosphere
- Copper electroplating for thickening the front contacts
- Ni electroplating to cover the copper
- Cutting of the cells in the wafer

The principal change respect to the previous process is the digging in the silicon in correspondence of the contact layout, using the Si_3N_4 as etching mask, after the phosphorus diffusion of the front surface. The grooves are deep up to $20\ \mu\text{m}$, and appear as shown in fig.(5-22)

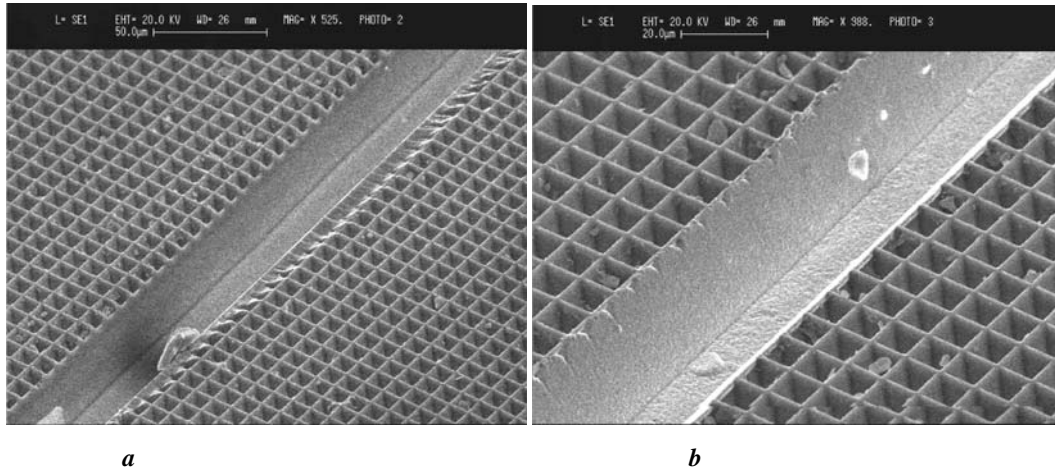


Figure 5-22 – (a) Chemical grooved channel on textured silicon; (b) grooves with $1\ \mu\text{m}$ of Ni electroplated

If the lateral groove size is in the order of $10\ \mu\text{m}$ or less, has been experimentally observed that the etch rate decrease, probably because of the low effect of agitation in these cavities; the bubbles of H_2 created with the etching chemical reaction are not removed efficiently, with consequently slowing of the etch rate. The two contact layouts of fig.(5-19, 5-20) have fingers of width decreasing from $40\ \mu\text{m}$ near the pad region to about $10\ \mu\text{m}$ at the opposite end. The different deepness along the finger isn't a problem, because the metal thickness increases with the carried current, i.e. moving toward the pads, so there isn't significant voltage drops.

A cross section of a grooved contact with about one micron of metal grown is shown in fig.(5-23a)

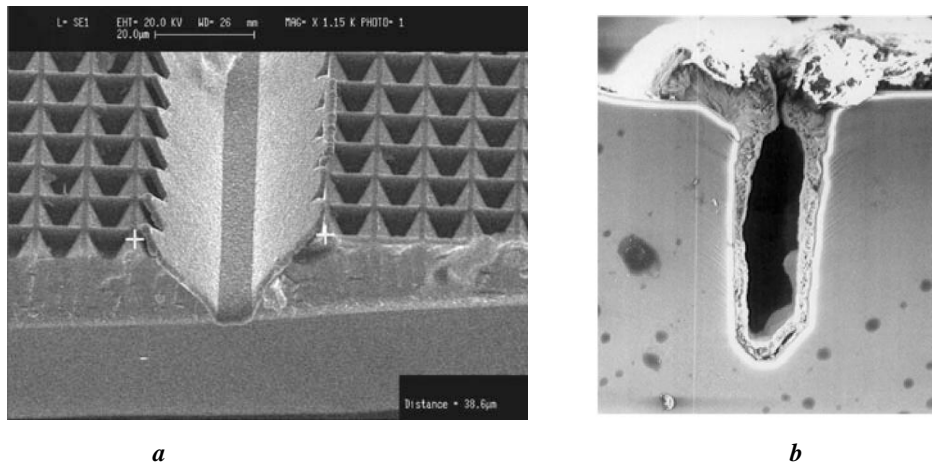


Figure 5-23 – Cross section of the metal contact grown in a groove

The metal adhesion is good, because of the second diffusion step and the higher contacted area. The V-shape given by the crystallographic [111] planes reduces the risk of void formation during the metal electroplating caused from junction of the metal at the two sides of the grooves as happen in LGBC (laser grooved buried contact) solar cells as in fig. (5-23b) from [95].

Some problems have been encountered even in this process:

- strong reduction of the material lifetimes, as revealed from the lifetime measurements using the OCVD technique on ultimate devices, as shown in cap.6; it was probably due to impurities introduced in the wafers from a contaminated chemical solution. The second phosphorous diffusion or the silicon nitride deposition have contributed in the diffusion of the contaminants. This problem can be corrected with the cleaning of the used facilities and products.
- The higher contact area has led to an error in the determination of the thickness of the final electroplated metal; as shown in fig.(5-23), only a thin metal layer thick about $1\mu\text{m}$ has been grown. This error is easily corrected with a recalibration of the electroplating parameters.
- An high series resistance has been found in many devices. The reason of this effect are attributed at the very high fluctuation in the PSG properties; indeed, during the etching of the diffused rear wafers surfaces, PSG has been used as protective mask, but an etching chemical reaction seemed to be happened also at the front surface. This conjecture finds an additional proof in the non uniform metal growth on the contact region: in the larger flat area for the pads, the metal didn't grow as well as in the finger grooves, as shown in fig.(5-24); a slight etching of the top layer, highest doped silicon layer in the larger zone where the

TMAH as worked faster, has probably changed the uniformity of electrical properties in the contact layout. Protect the front region during the etching of the rear wafers sides should recover this issue.

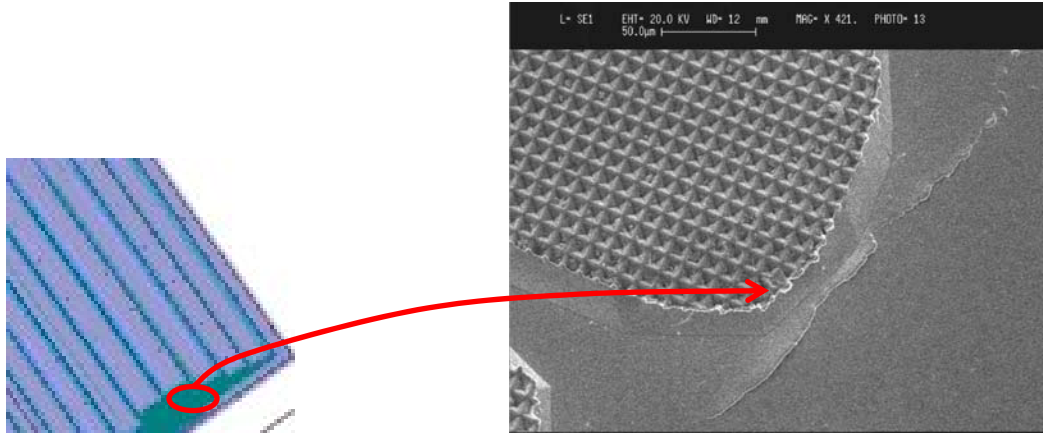


Figure 5-24 - SEM image of portion of cell near the pad; the metal hasn't grown homogeneously

Although these problems, better results respect to the previous cases for the fabrication of concentrator solar cells have been achieved, as described in cap.6.

CHAPTER 6 RESULTS

6.1 PV cells measurements under concentrated light flux

The measurements of solar cells under concentrated light beams need methodologies only partially coincident with those for tests under one Sun. First of all, an optical set up configuration able to produce the necessary concentration level with a sufficient illumination uniformity grade on the target area is required; the tolerance in the flux uniformity is dependent on the receiver: while for the series string connected cells the tolerated fluctuation is fairly small, for single solar cells weaker constraints are imposed, depending on the device peculiarities [21,97]. Moreover, it's important to have a radiation source with the solar spectrum properties.

The physical support for the cell has to satisfy some fundamental requests:

- ensure a good cooling
- permit a good electrical contact
- don't create shadowing on the cell

An outdoor experimental set up has been prepared; in this way the light source is the Sun and the spectral properties required are automatically satisfied. Problems related at this approach are the dependence on the meteorological conditions and the measurement reproducibility. To do direct comparison of measurements taken in different irradiation conditions, a piranometer and a pyrheliometer are used to identify the illumination level, both the global and the direct. For tests of single cells, supposing for good PV cell the linear response of the short circuit current at the illumination level from 1 sun up to high illumination level ($\sim 200\times$), the concentrated illumination flux can be derived directly from the I_{sc} . In this case it's important to have the cell working in short circuit condition, without suffer the effect of the series resistance of the device.

Single PV cells have been tested under concentration using the 30cm \times 30cm flat faceted 190 \times concentrator dish of fig.(6-1)

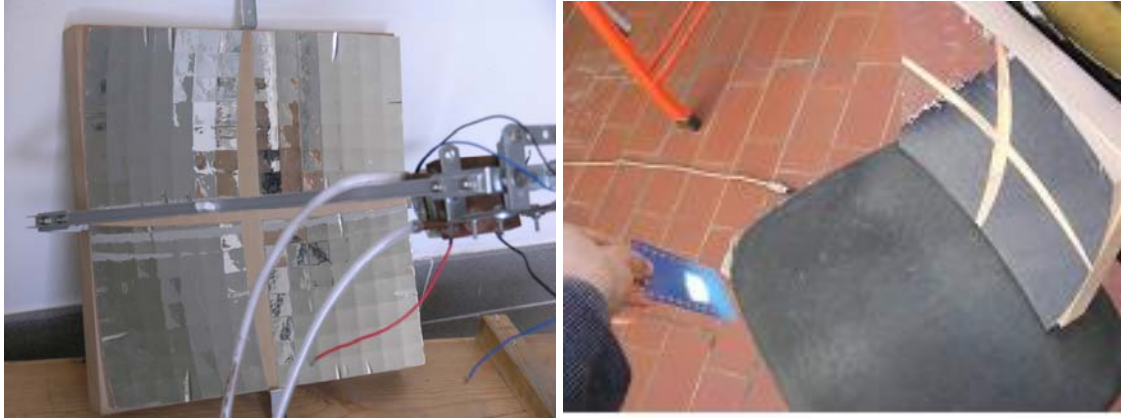


Figure 6-1 – Small flat faceted concentrator dish used for outdoor test of cells under concentration

Different cells have been tested; the supporting structure for the devices can vary, depending if the cell has a front contact grid or if it's an IBC cell. In both the cases, the device is mounted on a Peltier heat pump with its hot side in contact with a water heat exchanger, with a water flux of about 3 L/min; to ensure a good thermal contact, thin layers of thermal grease have been laid down at the interface between the water cooler and the hot Peltier side and at the interface between the refrigerated Peltier side and the cell substrate. A micro thermocouple has been thermally connected at the cell substrate, closed at the cell and covered with white grease, to avoid the heating of this element for the light flux on it.

For the measurement of back side concentrator solar cells HECO 252 produced by SunPower Corporation, a contact structure made of two thick, tin rigid wires pressured on the two golden cell contacts has been manufactured, as shown in fig.(6-2). The cells have been lodged directly on the Peltier heat pump.

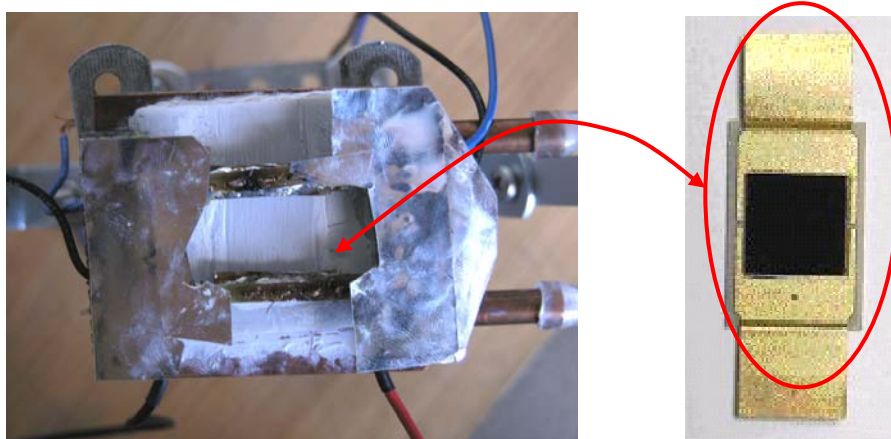


Figure 6-2 – Arrangement for test under concentration the SunPower HECO 252

At each contact, two wires are connected. They allow a 4 wire measurements, necessary in this cases to obtain results without the series resistance effect of the wires.

For the test of front contact solar cells the support is partially different; the cell is mounted on a Thermalclad thermoconductive ceramic substrate for power electronics, as in fig.(6-3). The electrical connection at the front contact is obtained using two golden springs, while for the rear side is ensured from the pressure of the front springs or, if it doesn't give a low enough resistance, soldering the cell at the substrate. Two copper foils are soldered at the substrate, and 2 wires for each of these foils are connected. The measured parasitic resistance introduced with this set-up is lower than 2 mOhm.

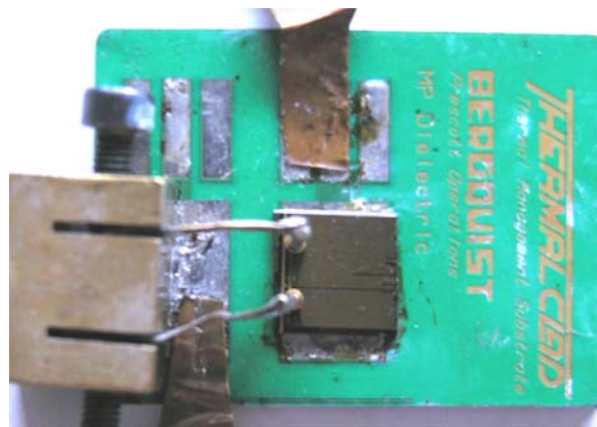


Figure 6-3 – Front contact solar cell on thermoconductive substrate

The 4 wire measurements is necessary in the test of single solar cell, because the voltage drop on the wire resistance is not negligible; this fact becomes even more crucial for testing single cell under concentration, because, while the voltage slightly increase with the light flux, the current rises proportionally. By using a four-points contact, it is possible to greatly reduce the effect of the wires resistance. As schematised in fig (6-4), two wires carry the main cell current, and the other two measure the cell voltage. In general, care has to be taken in the placement of the probes. If the current and voltage contacts are far apart on the cell, the FF can be exaggerated. Series resistance in the cell causes different parts of the cell to be operating at different I-V points. When there is a substantial current flowing, the ohmic voltage drop will cause points further from the current probe to be at a higher voltage. If the current probe is extracting current from a part of the cell that is near I_{sc} while the voltage probe is measuring voltage on a part that is near V_{oc} , the output power

will be badly over-estimated. In our configuration the two wires are connected out of the solar cell, so this fact cannot influence the measurement.

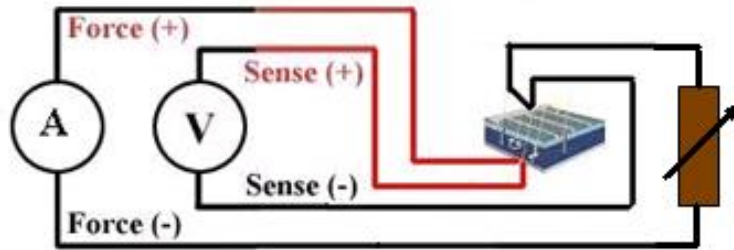


Figure 6-4 – Four wires diagram for the measurement of the I-V characteristics of solar cells

For testing cells producing currents up to some amperes, the use of a variable rheostat as external load has some disadvantages: first of all, the parasitic resistance in the circuit prevents the cell measurement in short circuit conditions; beside, the creeping contacts could create fluctuations in the results. One method to solve these problems is using a variable current source as external load; this device sinks the current produced by the cell and can polarized the device in inverse, if its current furnished is higher than the cell I_{sc} . An alternative way is to use a capacitor as external, variable load; the voltage varies at its terminals following the (6-1) with the current from the cell, if it starts from a initial discharged state. The equivalent circuit for this possibility is shown in fig.(6-5), where the dashed line encloses the cell electrical equivalent circuit.

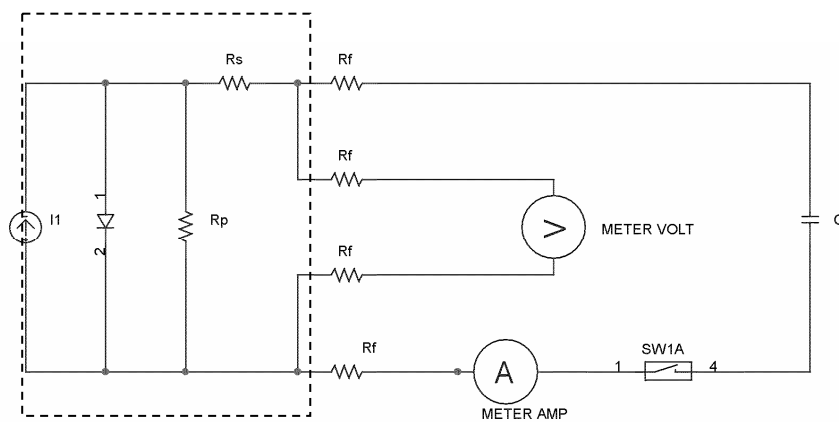


Figure 6-5 – Simplified electrical circuit of the 4 wires measurement using a capacitor as variable load; the circuit in the dashed line is the equivalent electrical circuit of the solar cell

$$V(t) = \frac{1}{C} \int_0^t i(t) dt = \frac{1}{C} \int_0^t i_0 \left(e^{\frac{qv(t)}{kT}} - 1 \right) dt \tag{6-1}$$

Both these two last methods have been used to test PV cells under concentration; because of the programmable current source employed could deliver a maximal current of 4.5A, the method using the capacitor as variable load is usually preferred and must be selected for the cases where the produced current is higher than the 4.5 Amperes.

6.2 Single cell measurement results under concentration

First, the currents and the absolute spectral responses of the different kind of solar cells were measured under 1 sun standard condition. Three kind of solar cells have been extensively tested under concentrated light beams: SunPower HECO 252, BP Saturn and InGaP solar cell produced at the ISE Fraunhofer Institute.

The Sunpower Heco 252 solar cells have an active area of 1.21cm², and produce a current of about 44.5 mA under 1 sun standard condition (0.1 W/cm²) with the spectral response as in fig.(6-6).

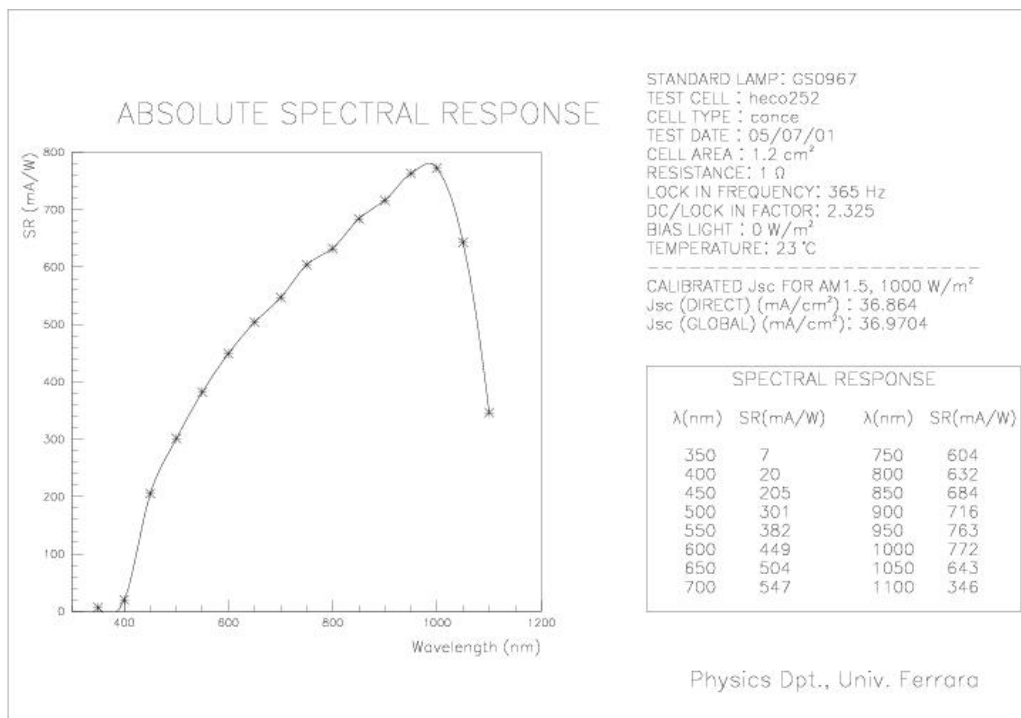


Figure 6-6 – Absolute spectral response of the concentrator Si cell Sunpower HECO 252

For these cells a linear increasing of the current with the illumination level has been demonstrated up to an incident flux of $20\text{W}/\text{cm}^2$ [98]. A comparison between the results obtained using the current source and the capacitor as external loads was done at the same illumination level ($8.65\text{ W}/\text{cm}^2$), to ensure the reliability of the measurements. A good agreement has been obtained, as shown in the graphs of fig.(6-7); a slight difference is due to a variation in the working temperature.

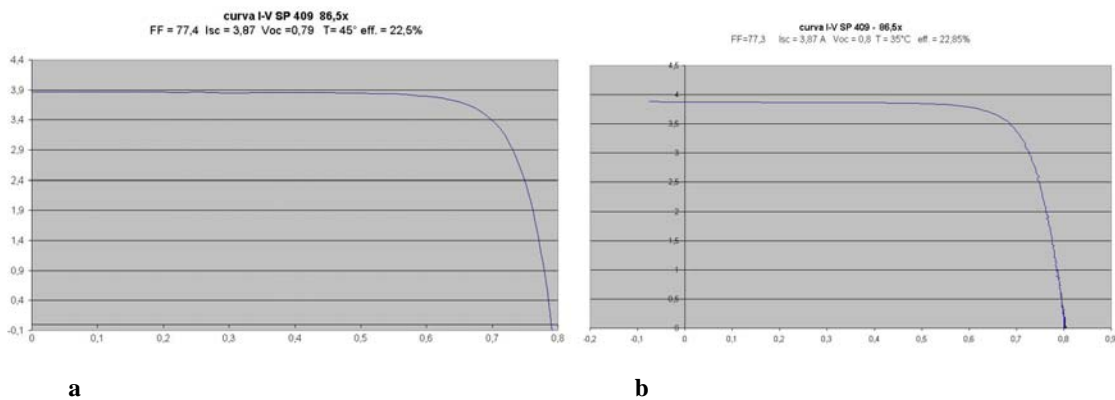


Figure 6-7 – I-V characteristics of the same SunPower HECO 252 cell, measured using as load an external variable current source (a) and a capacitor (b)

The higher illumination flux achieved is $14,6\text{ W}/\text{cm}^2$. The correspondent I-V characteristics of the HECO 252 solar cell is in fig.(6-8). Despite to the forecasted efficiency improvement with the increased concentration, the cell performances slightly decrease because of the higher operative temperature; indeed, the advantages given by the concentration are balanced from the temperature effect.

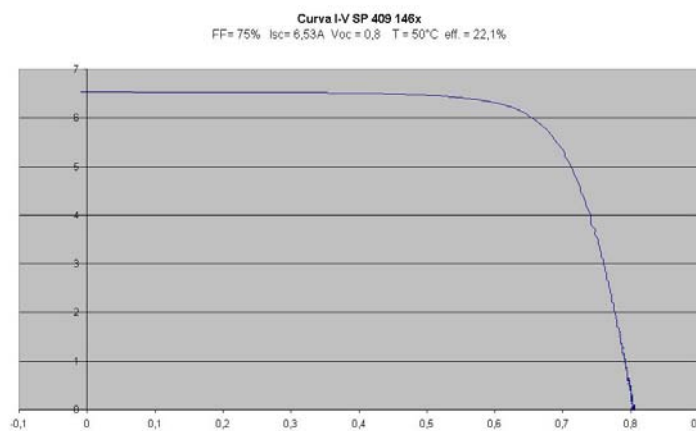


Figure 6-8 - I-V characteristics of a SunPower HECO 252 under $14.6\text{W}/\text{cm}^2$ light flux

In general the temperature determination has been not very precise; indeed the thermocouple contact on the cell substrate has not been characterized.

The average FF and Voc measured values for some HECO252 cells show a slight performances decrease passing from an illumination of about $12\text{W}/\text{cm}^2$ to $14\text{W}/\text{cm}^2$ as reported in table 6-1.

$12\text{W}/\text{cm}^2$			$14\text{W}/\text{cm}^2$		
n°	FF (%)	Voc (V)	n°	FF (%)	Voc (V)
1	77	0,8	1	75,7	0,76
2	77,3	0,79	2	76,8	0,79
3	78,7	0,81	3	74,1	0,78
4	78,6	0,8	4	75	0,8
5	77	0,79			
6	74	0,795			
average	77,1	0,7975	average	75,4	0,7825

Table 6-1 – Voltage and FF parameters of HECO 252 tested under different illumination fluxes

The other kind of silicon solar cells tested under concentration are the BP Saturn cells; these cells are analogue at those mounted on the linear concentrators of the Euclides project [99], designed for working under illumination flux of about $30\text{-}40\times$. The measured devices have an active area of $1.1\text{cm} \times 1.3\text{cm}$, including the bus-bar. The current density produced at 1 sun is about $30.3\text{mA}/\text{cm}^2$, as comes out from figure (6-9).

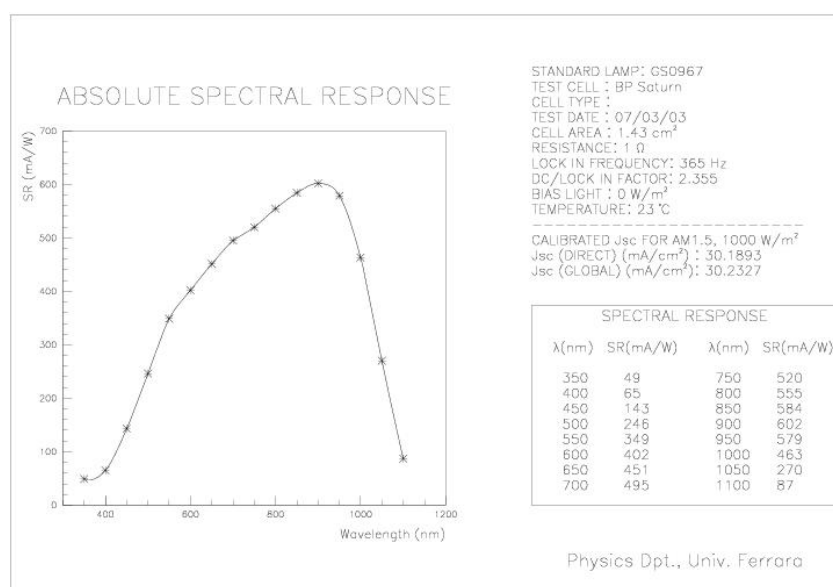
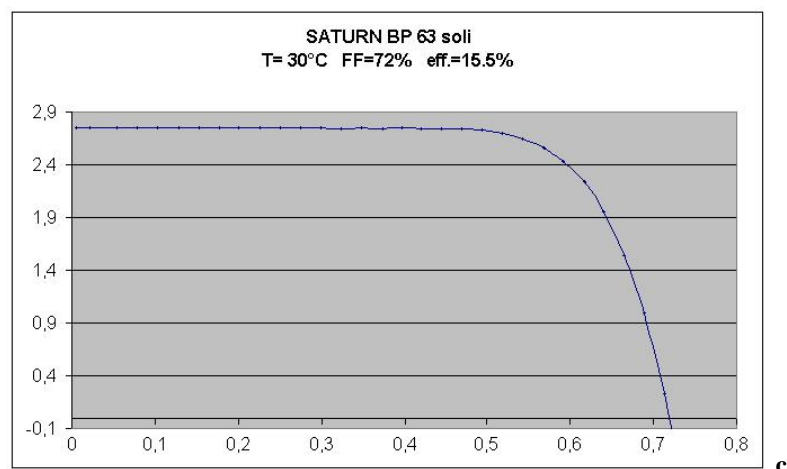
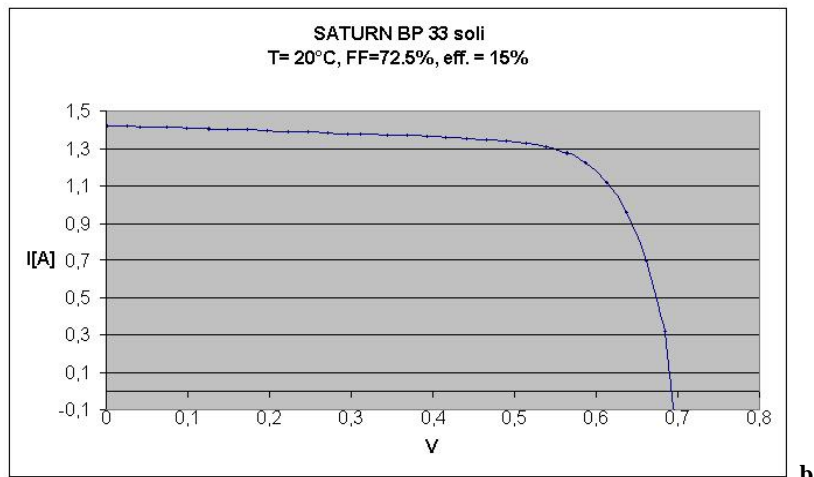
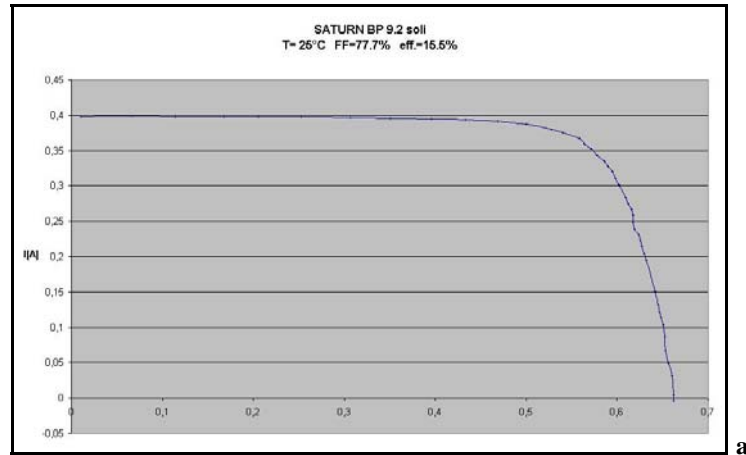


Figure 6-9 - Absolute spectral response of the BP Saturn Si solar cell

The tests under concentration show the effect of the series resistance as ohmic loss lowering the FF with the increasing illumination flux (fig.6-10). The effect of the series resistance decreases the slope of the I-V characteristics near the OC condition.



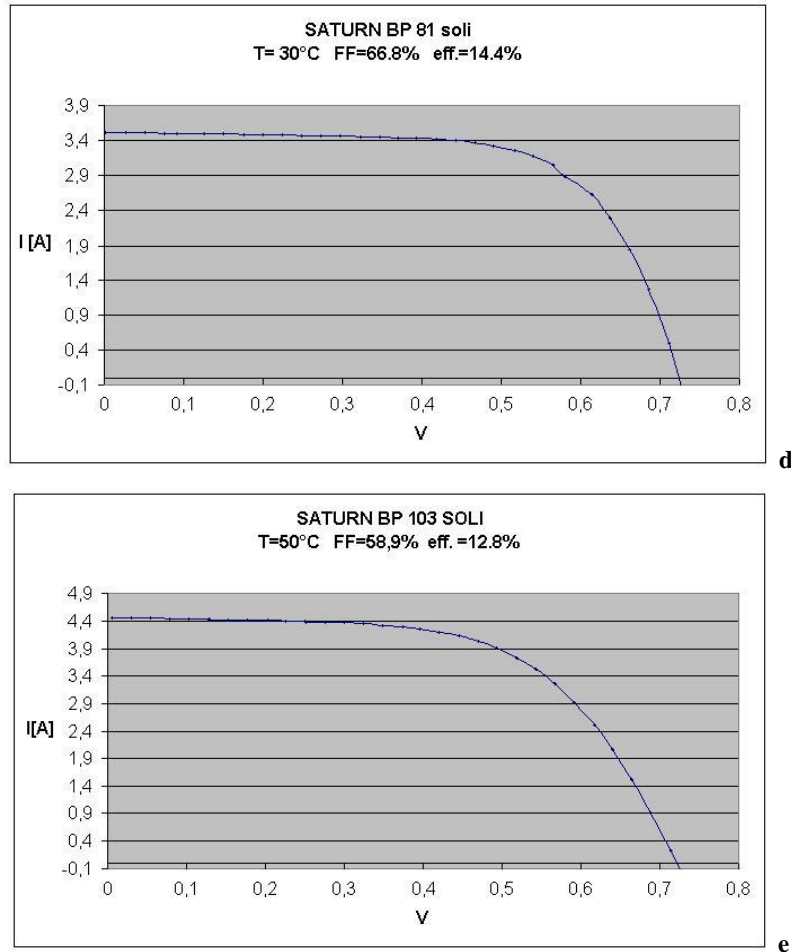


Figure 6-10 I-V characteristics of Saturn BP under different light fluxes

To account the losses due to the resistance introduced from the connections before the 4-wires, the characteristics of the BP cell under the higher light flux has been corrected; the 2 mOhm doesn't change significantly the measurement, as appear in fig.(6-11)

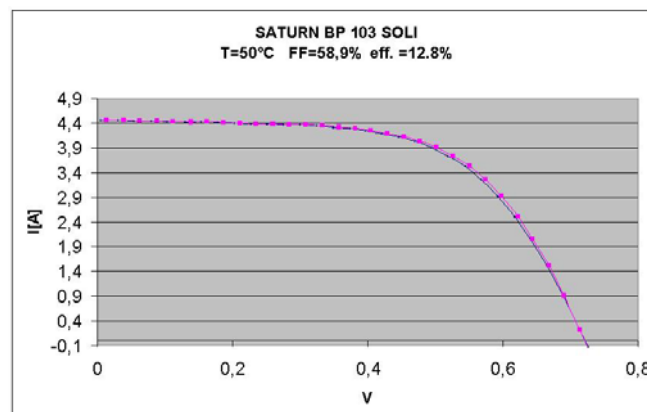


Figure 6-11 - I-V characteristics of Saturn BP solar cell without (blu line) and with (red line) the correction for the resistance introduced from the electrical connection from the contacts to the 4 wires.

The cell measured at 33 suns presents a shunt effect which reduces the device efficiency; the efficiency obtainable without this parasitic effect can be easily calculated assuming a FF of 77% under this illumination flux, as well as obtained under the $9.2\times$ concentration. This assumption can be done because of the series effect doesn't influence this measurement at this flux level. Conversion efficiency higher than 15% are obtained with these cells up to $6-7 \text{ W/cm}^2$.

The first InGaP devices tested under concentration have been produced at the ISE Fraunhofer Institute. They have a thick ($700\mu\text{m}$) substrate of p-type GaAs and a close spaced front contact grid. The EQE of two of these device are in fig.(6-12). Under one sun the parameters of the tested cell are:

A	V_{mp}	J_{mp}	V_{oc}	J_{sc}	FF	η
$[\text{cm}^2]$	$[\text{mV}]$	$[\text{mA/cm}^2]$	$[\text{mV}]$	$[\text{mA/cm}^2]$		$[\%]$
1,32	1208,7	9,34	1339,4	9,58	0,880	11,3

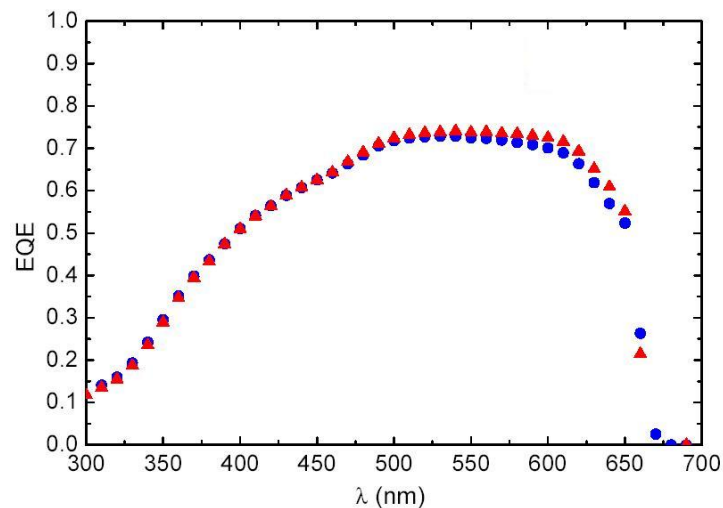


Figure 6-12 EQE of two InGaP solar cells delivered from ISE Fraunhofer Institute

As shown in fig.(6-13) they work well under concentration; the voltage decrease passing from the measurement at 33 suns from that at 82 is attributed at a thermal issue. As result from the test, the series resistance has not affected the measurement at 82 suns.

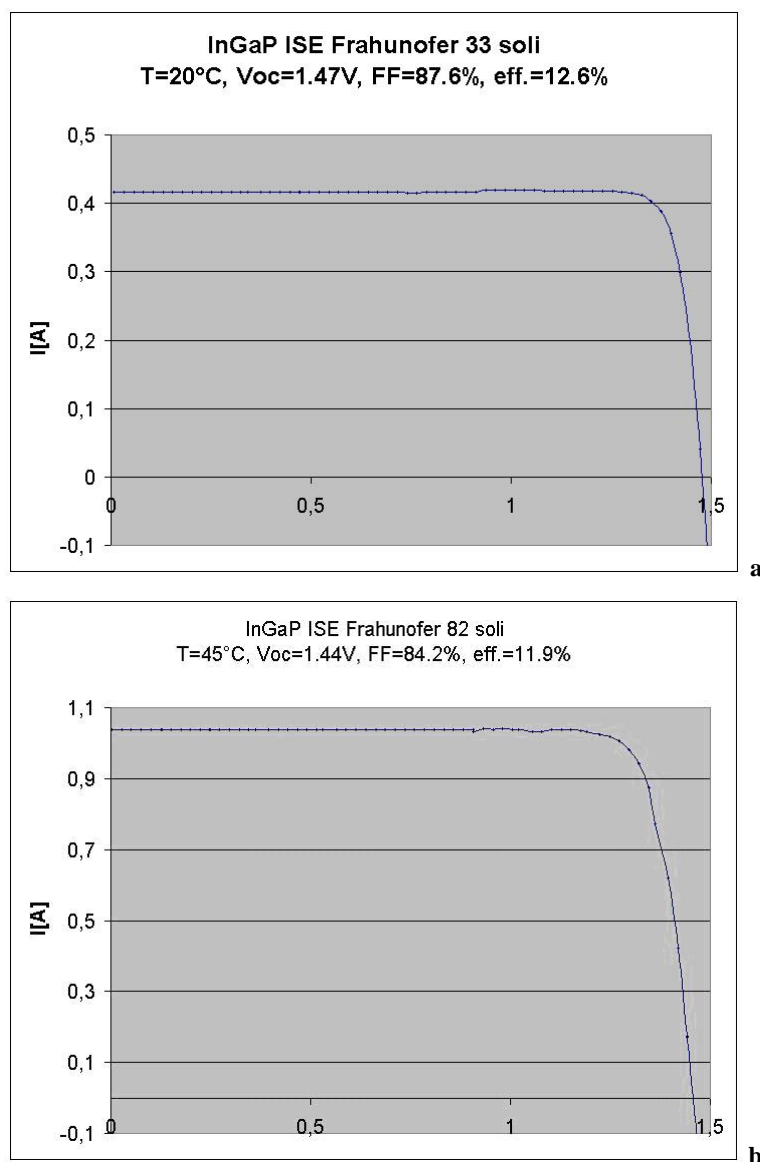


Figure 6-13 I-V characteristics of an InGaP solar cell delivered from ISE Fraunhofer Institute under different light fluxes

Because the very high cost of these devices, principally due to the high substrate cost, alternative InGaP cell structures have been considered for our application; in particular, for the fabrication of receivers of the dichroic concentrators, InGaP solar cells epitaxially grown on a germanium substrate manufactured at the Italian centre CESI are selected. Indeed, the performances of these devices are comparable with those of the cells fabricated on GaAs substrates even though the costs are significantly lower. Moreover the very expensive InGaP cells have shown a very critical adhesion problem at the contacts; for a large number of devices a peeling of the deposited contact is observed, even with very care handling. Pull-tests have been performed on soldered points at 45° on the front and on the

back metal layers; they have evidenced a force resistance $\cong 0$. Another pull test has been carried out using the adhesive tape (blue tape) by NITTO, model SPV 220P, usually used for the cut of chips; again the tested sample didn't pass the procedure.

6.3 Si PV panel under concentration

The PV receiver of fig. (6-14a) was tested on the concentrated light flux produced from the dish with flat squared mirror of fig.(6-14b), with the secondary. The module dimensions are smaller than the illuminated target zone; this fact ensures a good uniformity flux on the cells string.

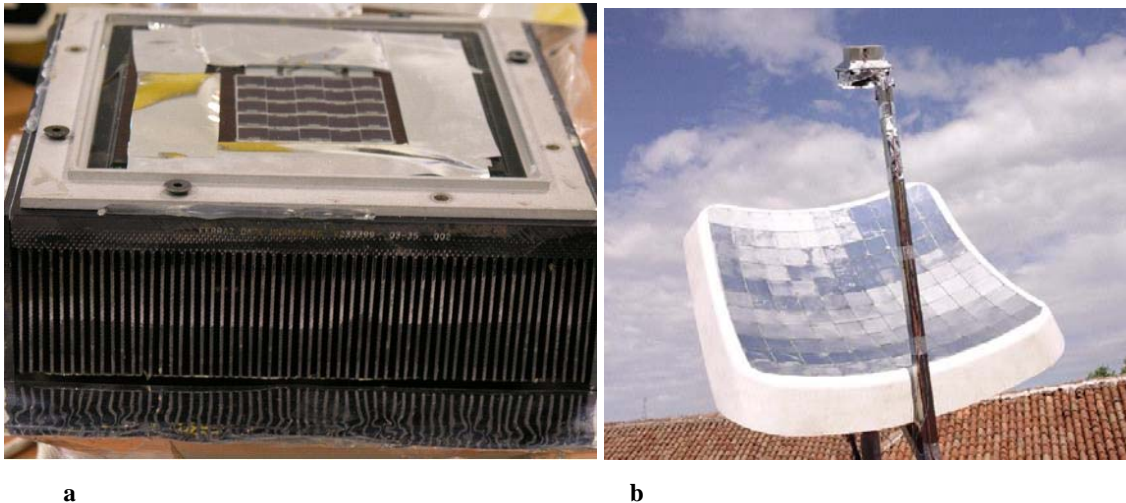


Figure 6-14 – Tested dense array module of Si Saturn solar cells (a) and concentrator used (b)

The tile with 25 cells covers an area of 57mm \times 65mm. The external, significant environmental conditions during the test are:

Air temperature: 28°C

Direct light flux: 900W/m²

The obtained I-V characteristics are in fig.(6-15)

The efficiency of this module is calculated considering the light flux impinging the PV tile. This value has to be compared with that of the single BP Saturn cells at similar illumination levels. First, from the voltage, appears evident the not optimal cooling of the cells; indeed, the average open circuit voltage of every device is 0.6V, significantly lower than the about 0.7V previously obtained. Considering a temperature coefficient of -2.2mV/°C, the cells was working at about 75°C, i.e. 35-40°C higher than the external air.

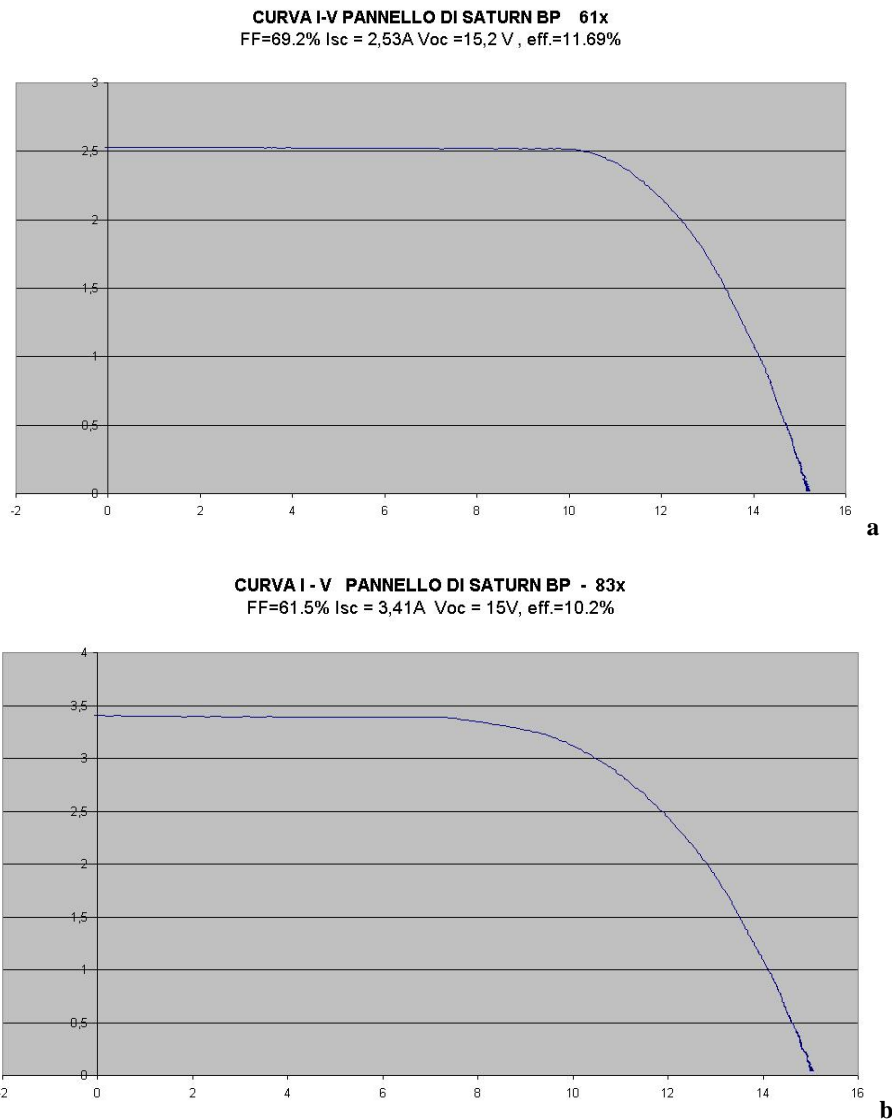


Figure 6-15 I-V characteristics from the small panel of fig.(6-14a) with air cooling, under different light fluxes

The FF is lower than for the single tested cells; this fact can be attributed partially at the higher temperature working conditions, partially at the variability of the FF of the series connected solar cells, considering that the values of the panel and of the single cell for analogue concentration levels don't differ for more than 3 percentage points at 63 suns and of 5 points at 82 suns.

The uniformity of the flux is good enough in this region, confirming the optical characterization of cap.4. Indeed, a fluctuation in the illumination should introduce kinks at the I-V curve as reported in [31].

6.4 Si cells for concentration fabricated at the SSL of the University of Ferrara

As presented in the previous chapter, different processes have been pursued in order to find the most feasible for mass production of high efficiently, low cost, Si concentration solar cells. Following, the results obtained from each of these process approaches are presented.

Process 1

The cell contact layout in this process wasn't for concentration solar cell; the problematic related at this procedure have aimed the develop of the devices toward the other two approaches. However, results have been obtained at 1 sun, and important pieces of information regarding some aspects of the fabrication parameters have been achieved. The best results obtained are on a FZ wafer (100) 0.3 ohm-cm, boron doped with a front contact grid covering about the 10% of the surface. The absolute spectral response is in fig.(6-16). In fig. (6-17) are represented the power of the electrons produced from the photoelectrical process and the power of the photon converted with this cell and with a Sunpower HECO 252.

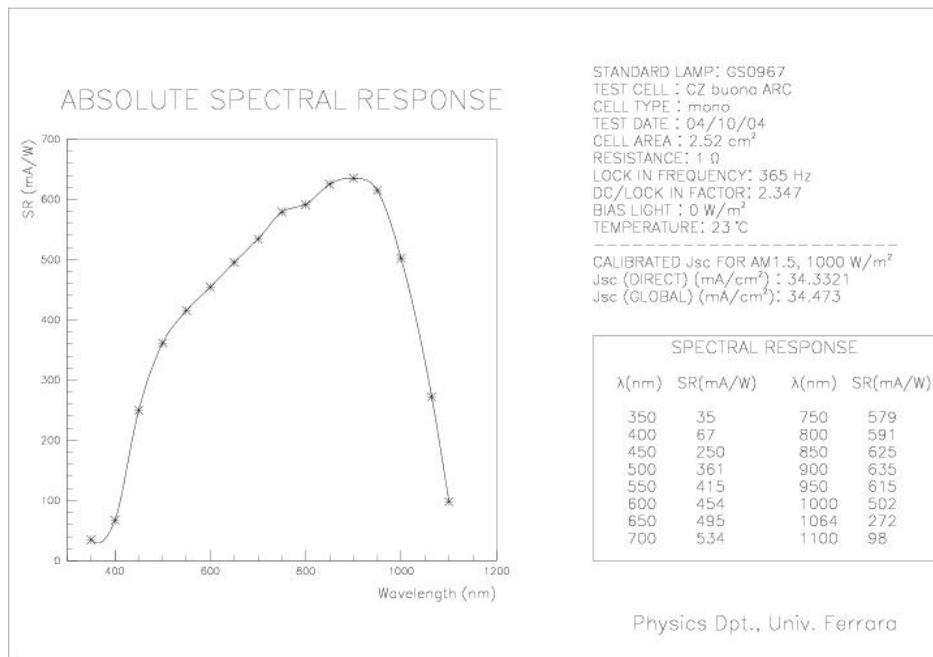


Figure 6-16 - Absolute spectral response of a Si solar cell manufactured at the Unife following the process 1 described, on an FZ wafer

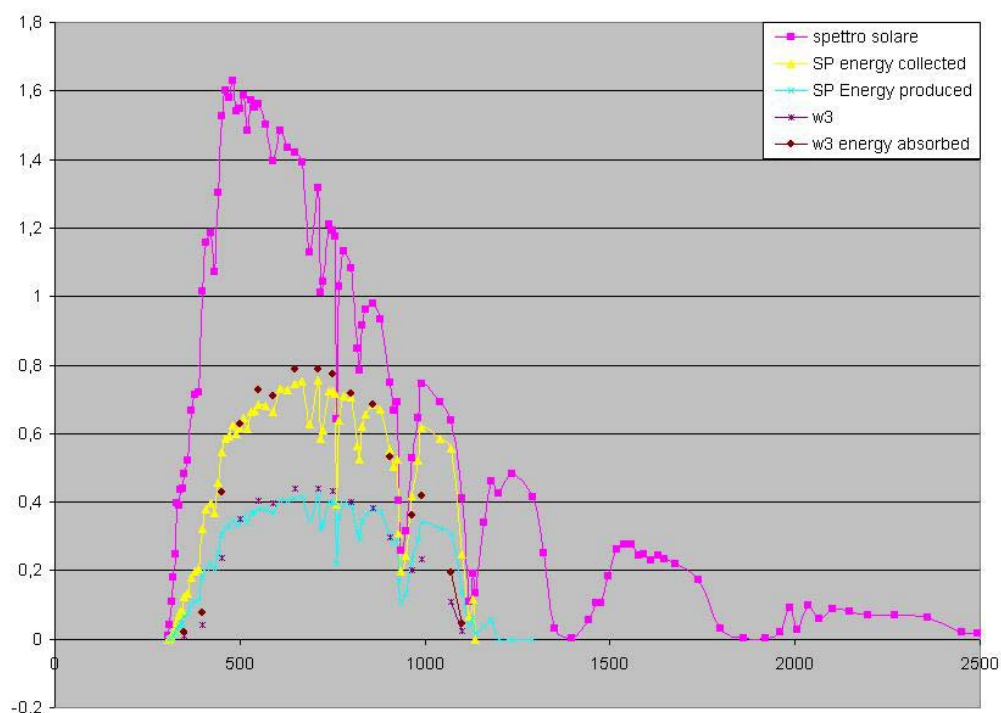


Figure 6-17 – Fraction of power of the solar spectrum absorbed and electrically converted for the HECO SC and for a cell produced at Unife (dots)

Unfortunately, a low shunt resistance has reduced the FF of the device at 71% as shown in the I-V characteristics of fig.(6-18). Although this inconvenient, the efficiency of the cell is of 15.5% under 1 sun; without the shunt the efficiency should be of about the 17%, including the bus bar area.

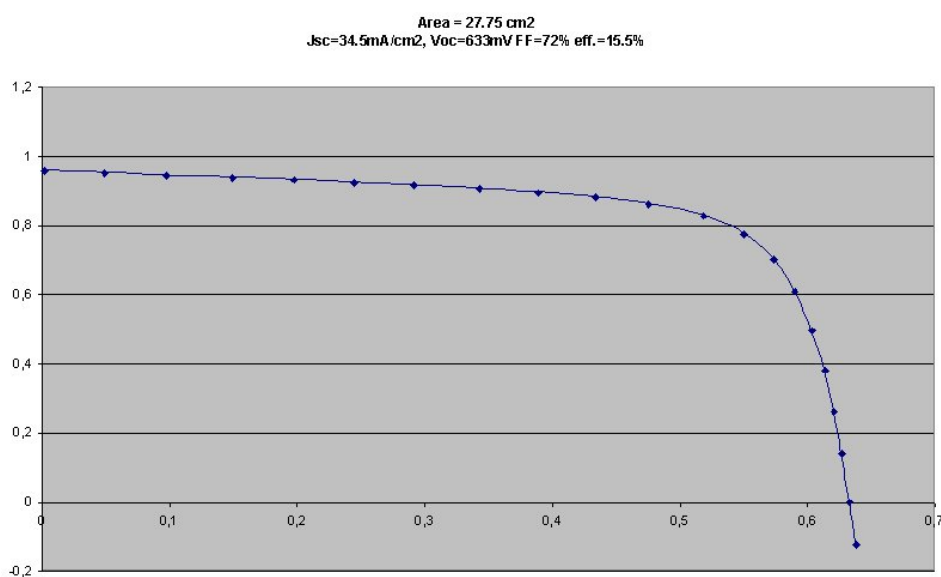


Figure 6-18 - I-V characteristics of a cell manufactured at Unife with process 1 on FZ material, under 1 sun.

The measurement of the main physical parameters of the material was carried out after the fabrication process using the open circuit voltage decay (OCVD) technique in quasi-steady-state (QSS) illumination conditions [100]; the results are summarized in fig.(6-19). They reveal the shunt resistance observed in the I-V characteristics and indicate a material effective lifetime of some microseconds, dependent on the injection level of minority carriers.

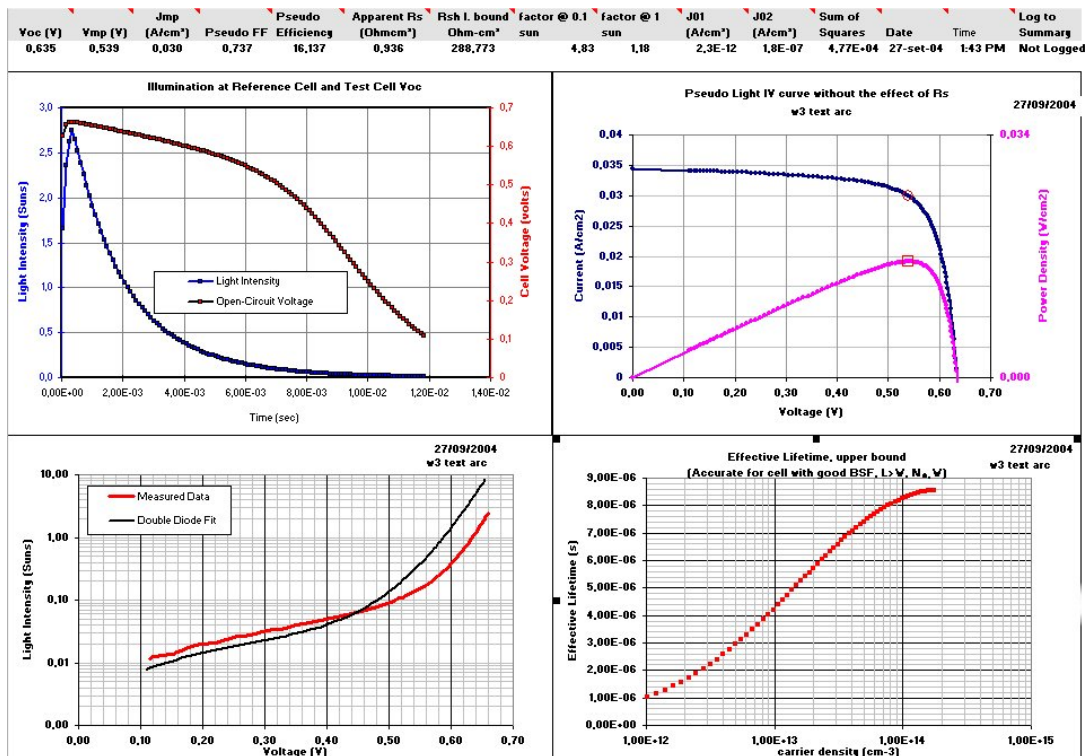


Figure 6-19 – OCVD analysis of the material properties on the ultimate cell with the results of fig.(6-18, 6-16)

The same process has been carried out also with commercial CZ silicon wafers (100), 1 ohm-cm boron doped. The best result obtained has the I-V curve in fig.(6-20), while the photo-voltage decay analysis for this cell is given in fig.(6-21). Here the FF is of the 78.5% and there isn't shunt effect; the poorer properties of the CZ bulk material respect to the FZ have reduced the voltage and current of the cells; the amount of these loss in performances is generally evaluated in about 1-2% of efficiency, according with.

The lifetime of these CZ wafers have been measured in the final devices, like for the previous cell; the graphs obtained are reported in fig.(6-21).

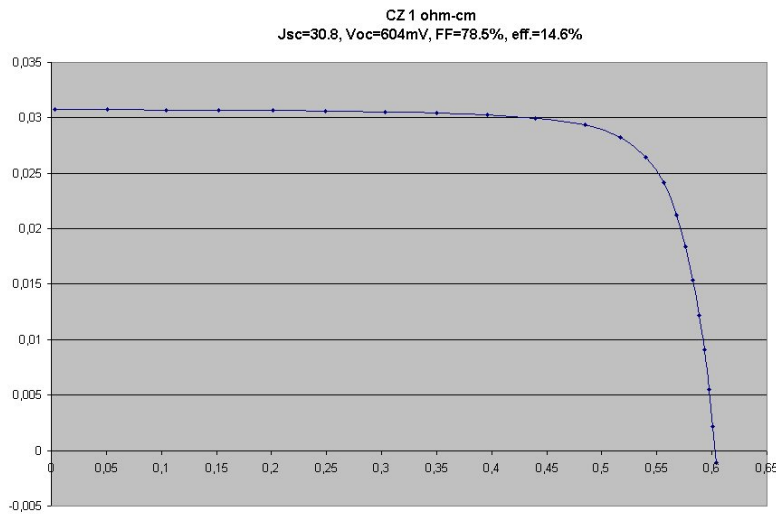


Figure 6-20 - I-V characteristics of a cell manufactured at Unife with process 1 on CZ material, under 1 sun.

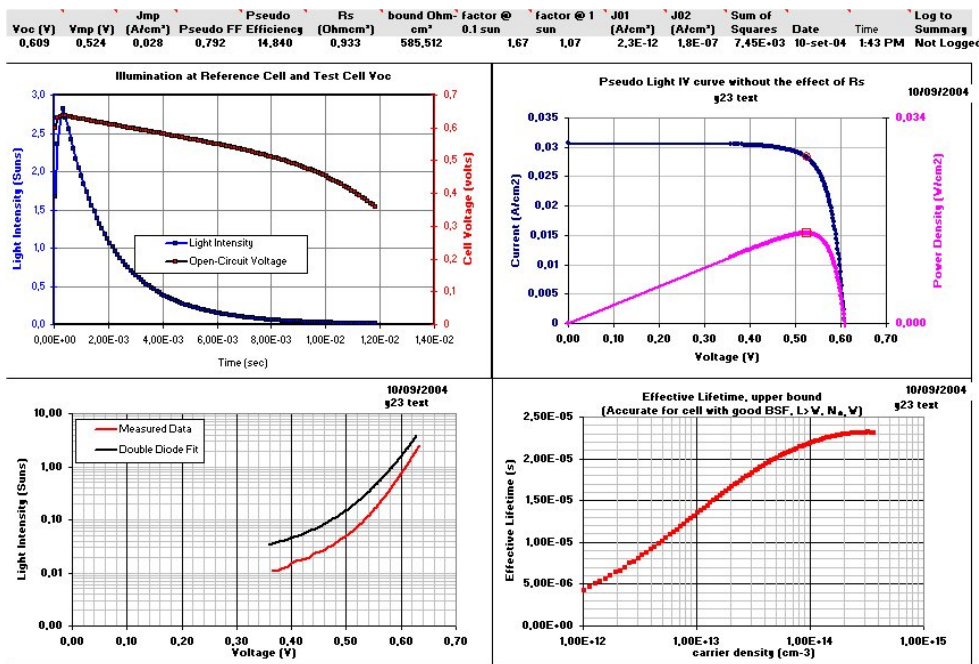


Figure 6-21 - OCVD analysis of the material properties on the ultimate cell with the results of fig.(6-20)

Process 2

The results of this procedure show an high series resistance and consequent low FF, even if the other electrical parameters of the devices are fairly good, as in fig.(6-23). Moreover, the high fluctuations of the obtained results for similar manufactured materials have evidenced some problems which have led at the process 3. However, interesting results have been obtained with this approach; in fig.(6-22) there's the spectral response of a cell

made on a FZ Si (100) 0.1 ohm-cm, boron doped. Considering the contact cover of about the 10%, the current density is the higher obtained.

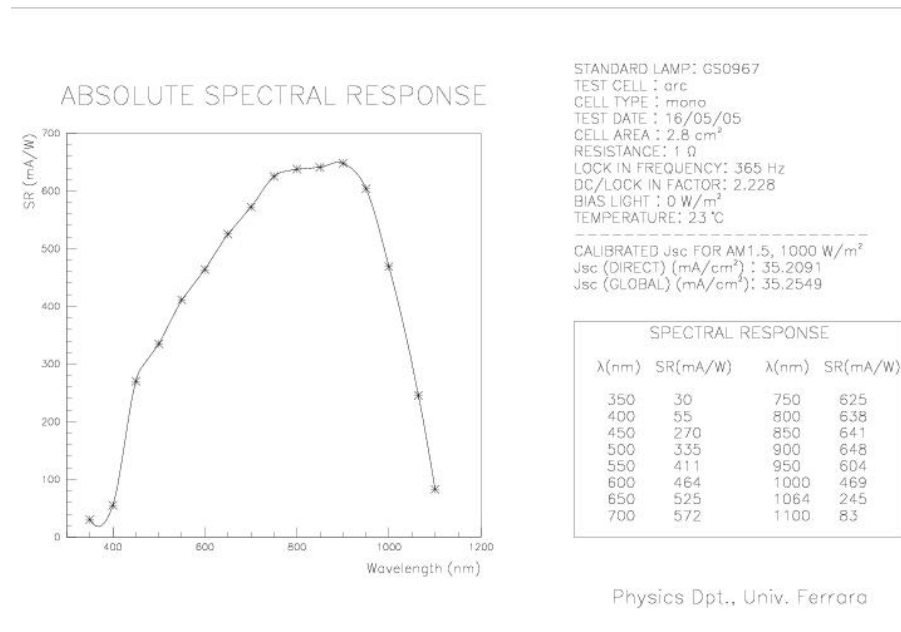


Figure 6-22 - Absolute spectral response of a Si solar cell manufactured at the Unife following the process 2 described, on an FZ wafer

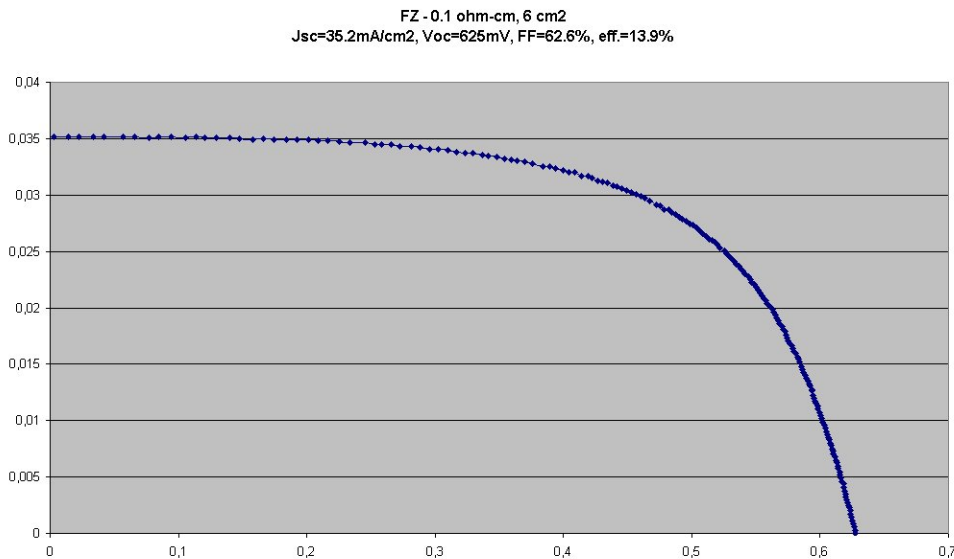


Figure 6-23 - I-V characteristics of a cell manufactured at Unife with process 2 on FZ material, under 1 sun.

The OCVD analysis has given the results in fig.(6-24); the non agreement of the pseudo FF here forecasted and that obtained in the real I-V characteristics makes suppose a non-uniformity in the contact resistance.

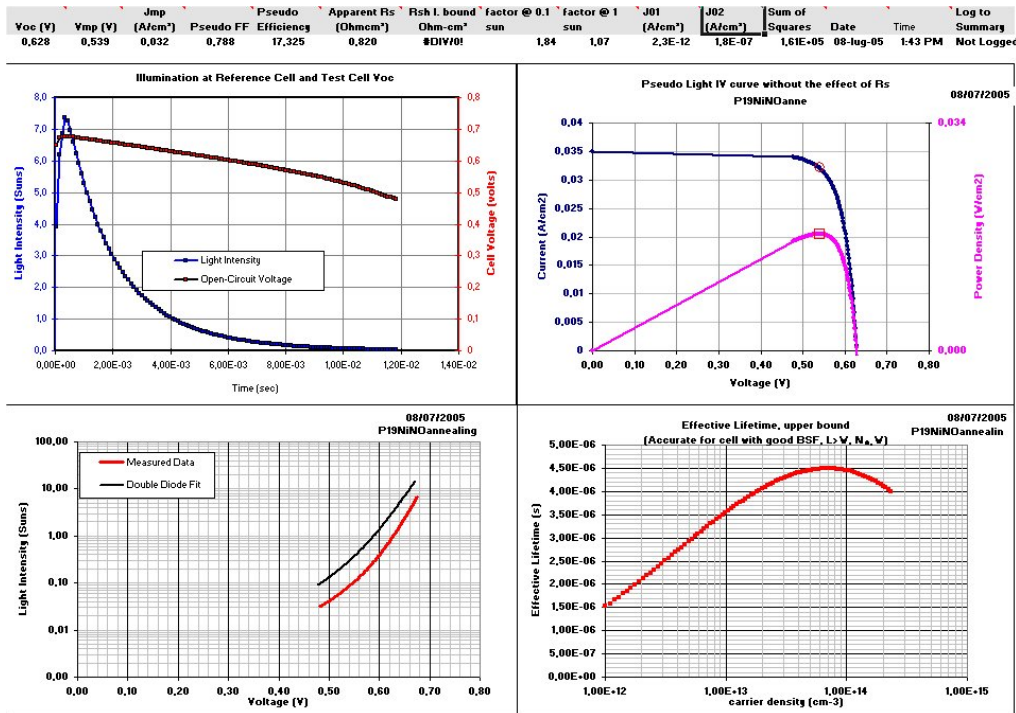


Figure 6-24 - OCVD analysis of the material properties on the ultimate cell with the results of fig.(6-23)

Analogue characteristics have been obtained for cells with the contact layout for concentration of fig.(5-19, 5-20); they are in fig.(6-25, 6,27), with the PCD analysis in fig(6-26). Fig.(6-27) reveals the series resistance detrimental effect under a concentration flux of about 0,43W/cm². This fact can be motivated considering a non-uniformity in the contact resistance at the metal-silicon interface.

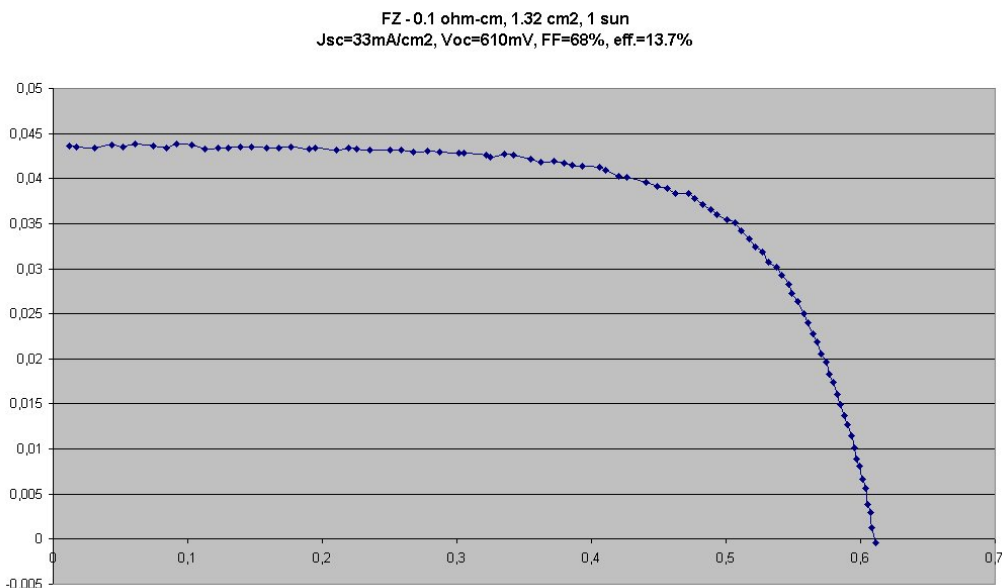


Figure 6-25 - I-V characteristics of a cell with contact layout and size for concentration manufactured at Unife with process 2 on FZ material, under 1 sun.

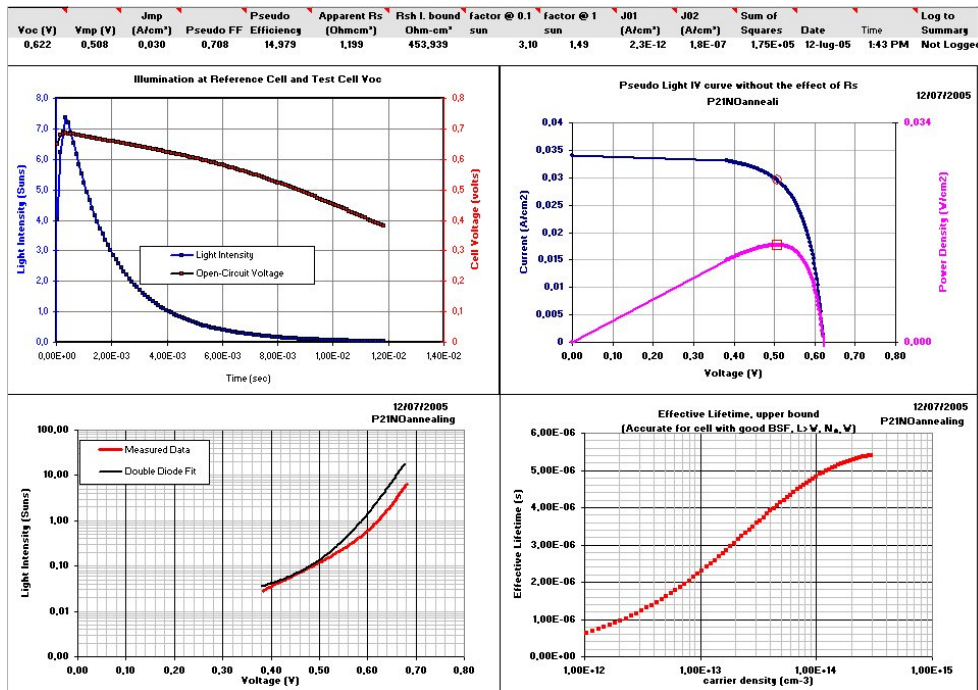


Figure 6-26 - OCVD analysis of the material properties on the ultimate cell with the results of fig.(6-25)

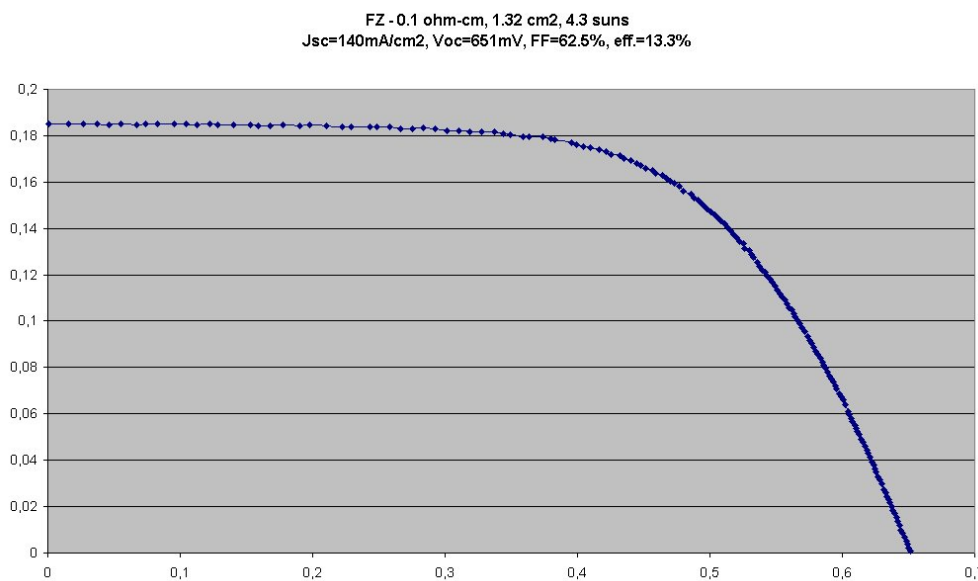


Figure 6-27 I-V characteristics of a cell with contact layout and size for concentration manufactured at Unife with process 2 on FZ material, under 4.3 suns.

The results on CZ material are summarized with the curves in fig.(6-28, 6-29, 6-30). Also in this case, the cells have the size and contact layout adapt for concentration have been produced; the spectral answer is in fig.(6-28), while fig.(6-29) is the I-V curve under 1 sun and fig.(6-30) under 5.2 suns.

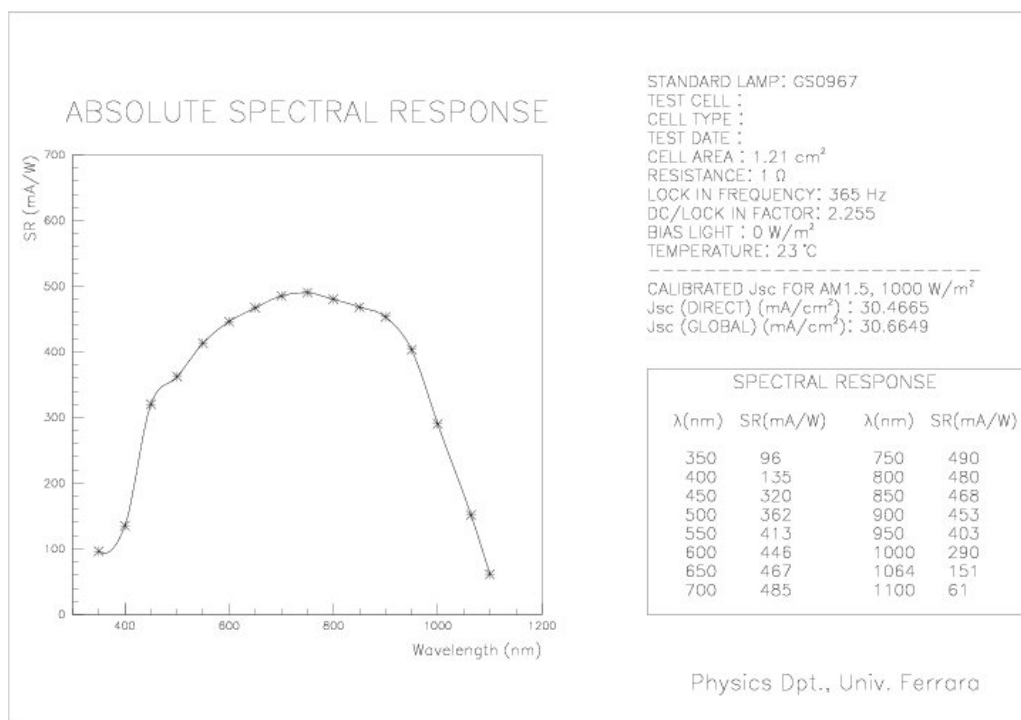


Figure 6-28 - Absolute spectral response of a Si solar cell manufactured at the Unife following the process 2 described, on a CZ wafer

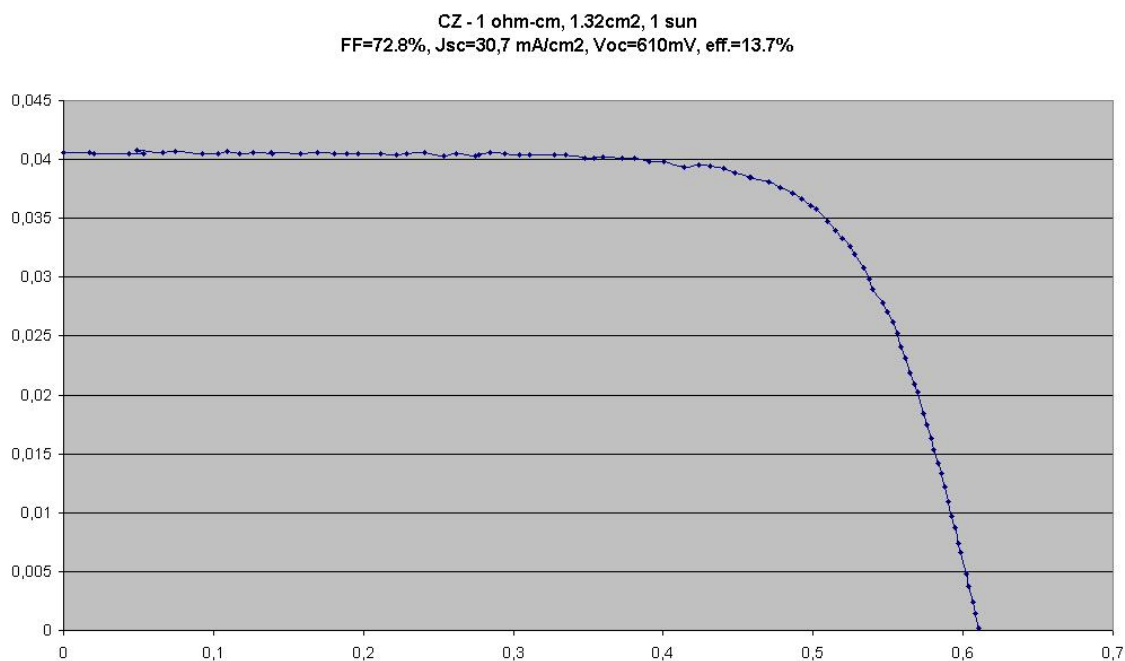


Figure 6-29 - I-V characteristics of a cell with contact layout and size for concentration manufactured at Unife with process 2 on CZ material, under 1 sun.

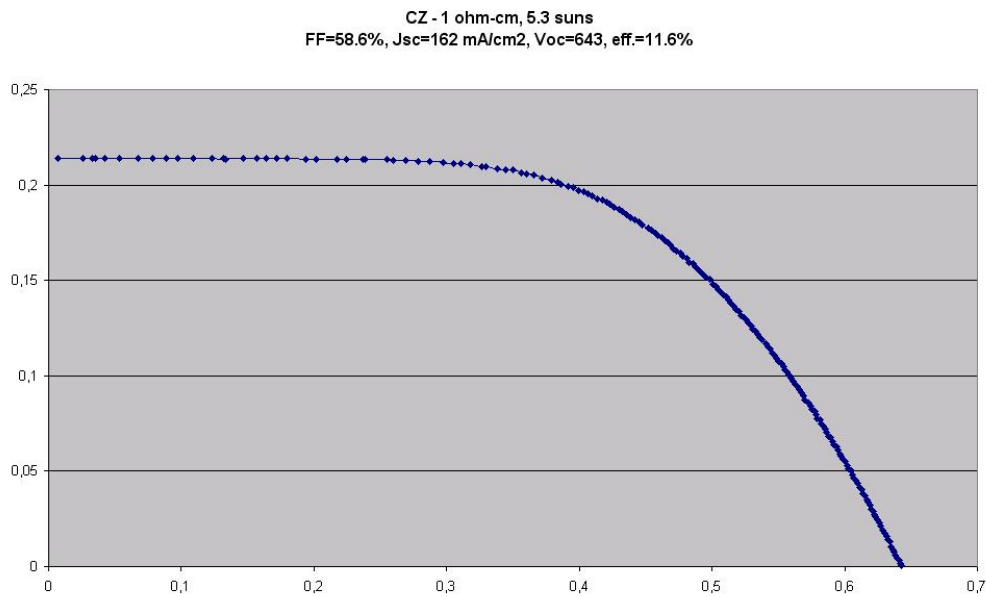


Figure 6-30 - I-V characteristics of a cell with contact layout and size for concentration manufactured at Unife with process 2 on FZ material, under 5.3 suns.

Again, the QSS photo-voltage decay analysis has been carried out on the cells; the results for the device of the I-V curves of fig.(6-29, 6-30) is in fig.(6-31)

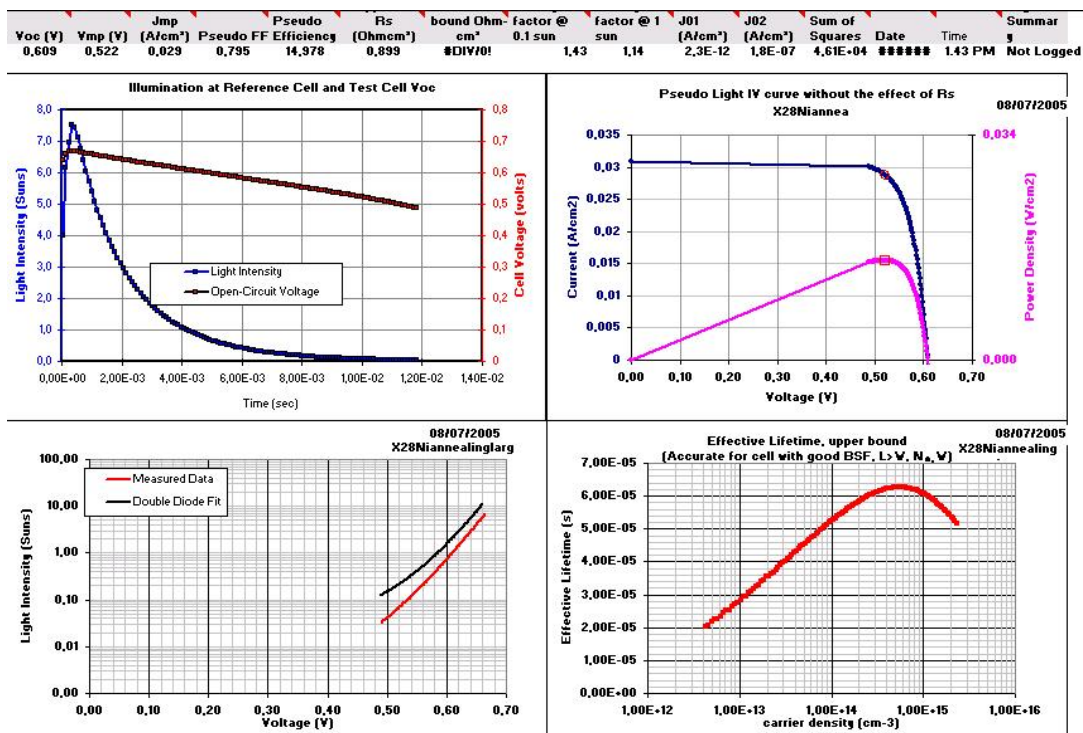


Figure 6-31 - OCVD analysis of the material properties on the ultimate cell with the results of fig.(6-29)

A contactless photoconductance decay (PCD) measurement [101,102,103] has been done on CZ wafers from the same batch used for the cells fabrication. The results of the lifetime test, and a consequent implied open circuit voltage, for a wafer at the process step just before the contacts deposition, are in fig.(6-32).

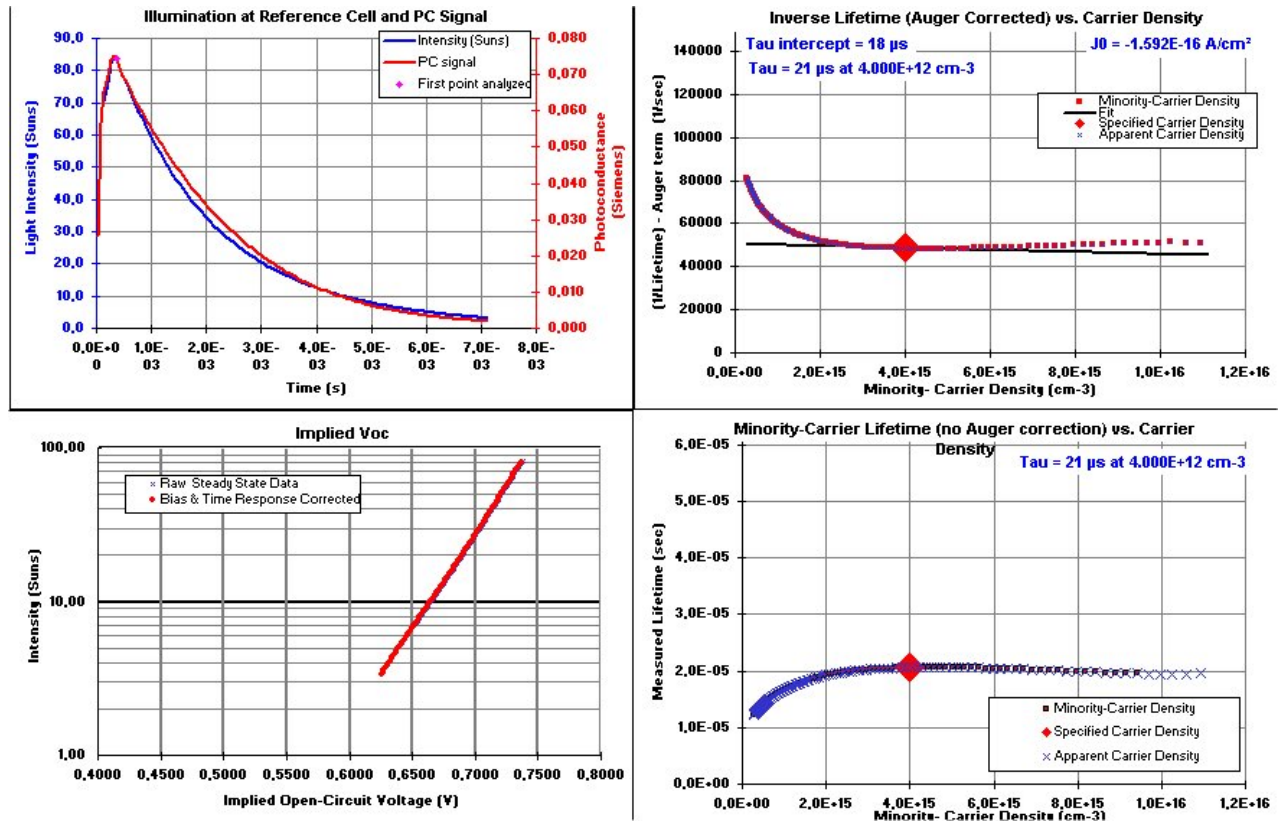


Figure 6-32 Contactless generalized PCD analysis of the material properties on a CZ wafer from the same batch as that used for the cell with the I-V characteristic of fig.(6-29)

As evidenced from the current-voltage characteristics, the series resistance of the device is too high for concentration purposes. Because this effect appears quite independent on the metal contact layout, the reason of this effect has been attributed at the resistance at the interface silicon-metal.

Process 3

Unfortunately, this process, even if it shows improvements at the previous problem, hasn't given yet good cell efficiencies, because of a probable contamination of the process line and some imperfection in the fabrication procedure. The contamination is supposed because of the very low material lifetime for the devices measured with the OCVD

technique and the consequent very low open circuit voltage obtained. In particular, fig.(6-33) shows the results for a cell fabricated on a CZ 0.3 ohm-cm wafer.

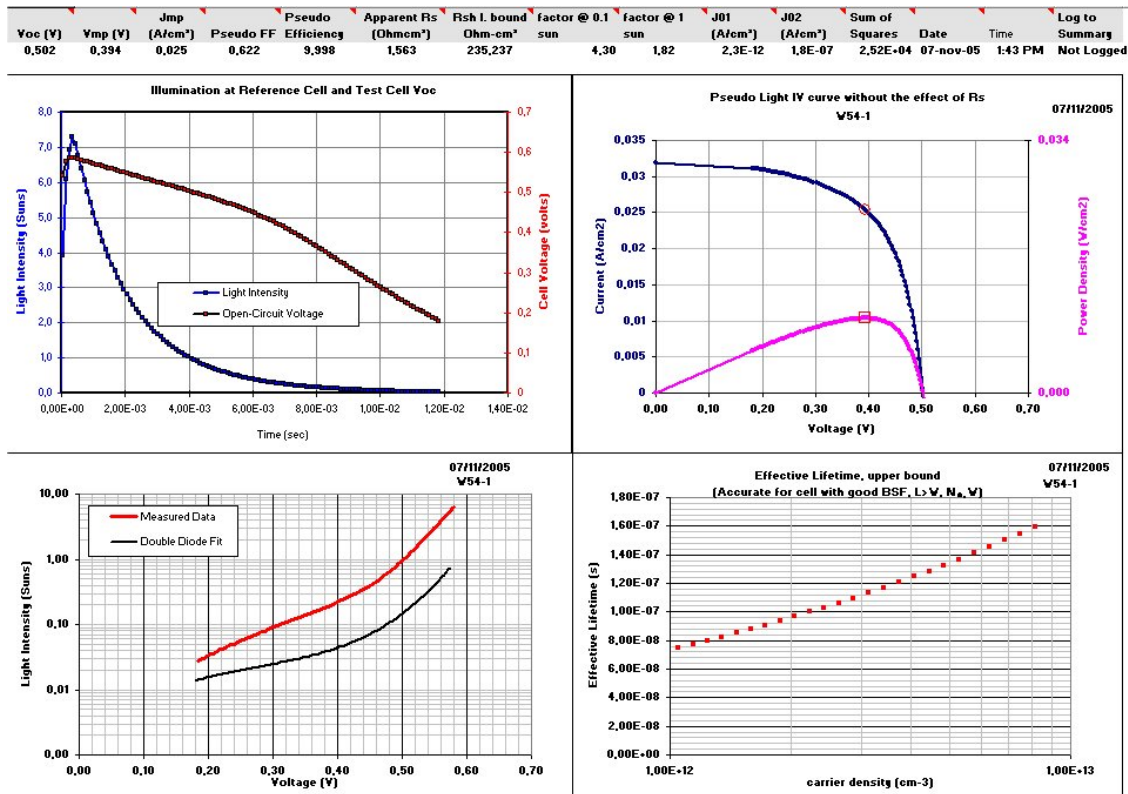


Figure 6-33 - OCVD analysis of the material properties on an ultimate cell on CZ material following process 3; the degradation of the lifetime respect to the previous results suggests a contamination of the material during the process

Slightly better results have been obtained with FZ 0.1 ohm-cm, but not comparable with that obtained with the previous processes, as in fig.(6-34). The more interesting results have been obtained with an FZ 0.3 ohm-cm wafer, under a concentrated flux of about 16 \times , as the fig.(6-35) shows; the supported flux is fairly higher than in the previous case; the series resistance here present, which lows the performances at higher concentration as in fig.(6-36), can be attributed again at a non uniformity in the metal-semiconductor interface, due to the process step of etching of the back diffused layer, as described in cap.5, and can be attributed also at the too thin metal layer deposited. However, discriminating the reasons of these not optimal results, this last process appears to be the more reliable and cost effective for the concentration silicon solar cell production, among those evaluated.

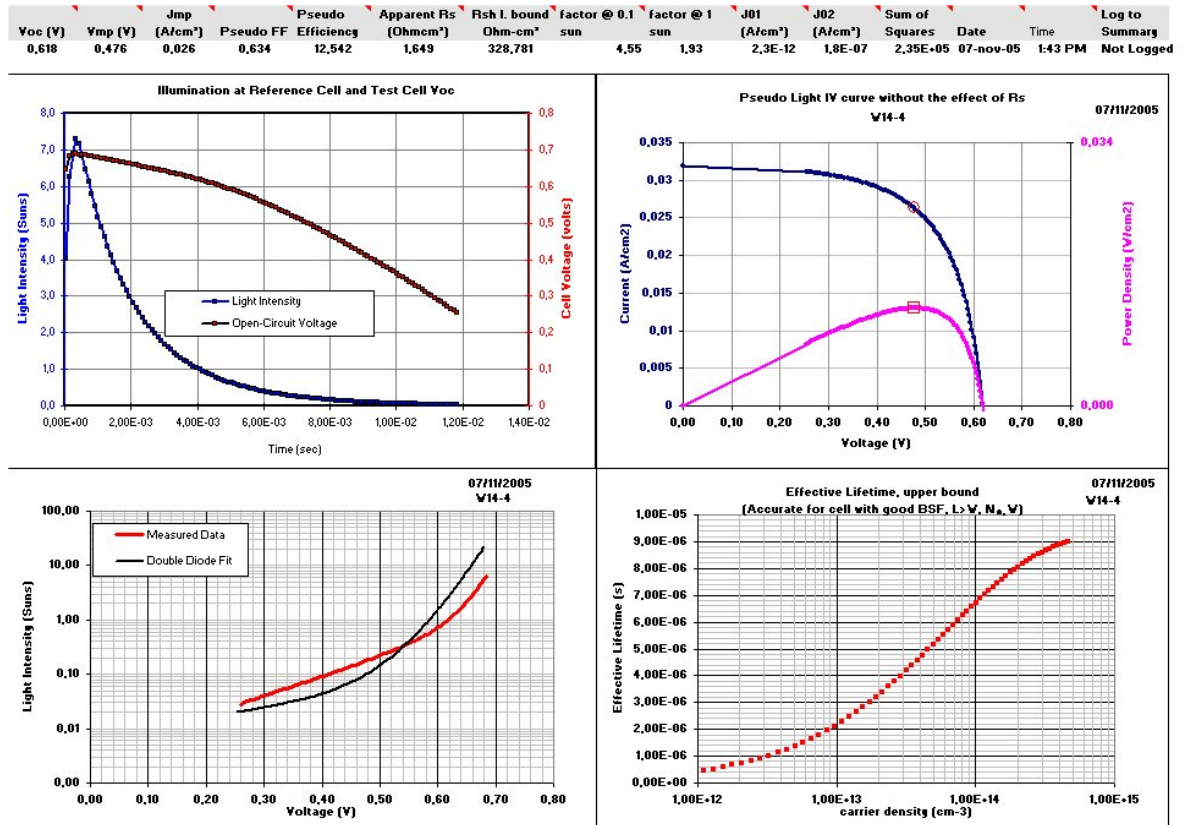


Figure 6-34 - OCVD analysis of the material properties on an ultimate cell on FZ material following process

3

FZ - 0.3 ohm-cm, 1.3cm² 16 suns
 Jsc=460mA/cm², Voc=0.68V, FF=72.5%, eff.=14.3%

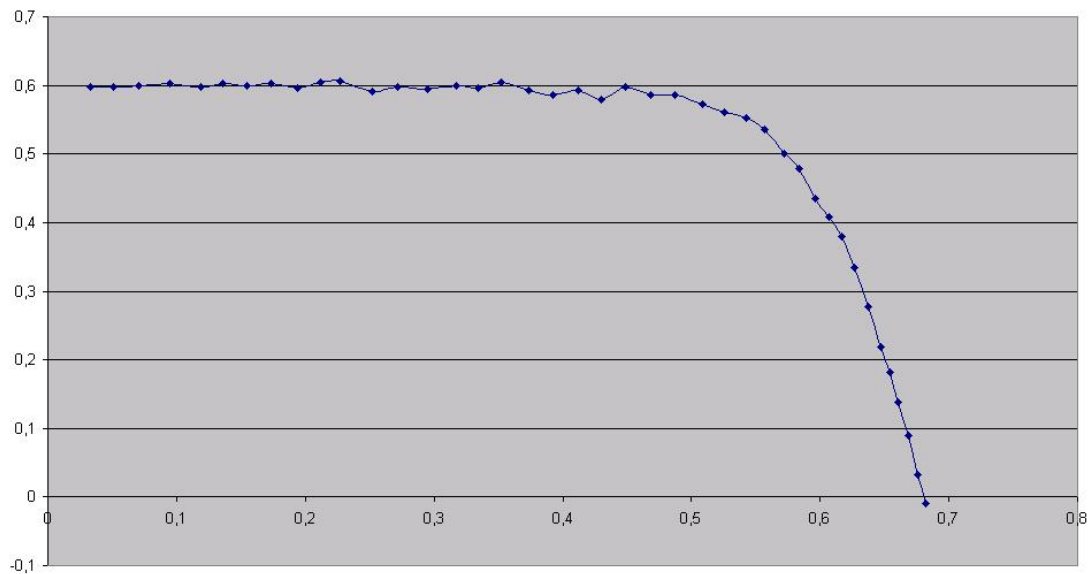


Figure 6-35 - I-V characteristics of a cell with contact layout and size for concentration manufactured at Unife with process 3 on FZ material, under 16 suns.

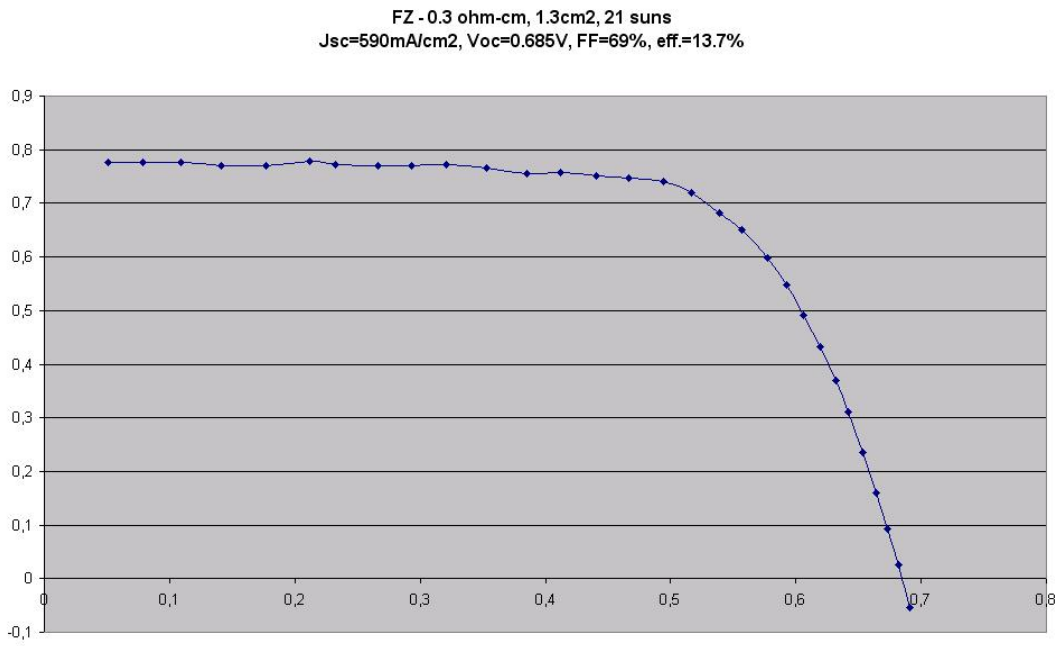


Figure 6-36 I-V characteristics of a cell with contact layout and size for concentration manufactured at Unife with process 3 on FZ material, under 21 suns.

Conclusions and Future Developments

The concentrated PV appears one of the most promising solution for the photovoltaic solar energy production. The complexity of the concentrator systems is due to the several components employed and to the necessity to get their good cooperation in a stable configuration. The strong correlation among all these parts requires a parallel development of them, in order to understand the potentiality of the followed directions and to give the possibility to select the best solution, step by step. The here proposed systems seem to have the potentialities to compete effectively with the other systems currently under development in the world. The simplicity of these flat faceted systems and their low-cost approach allow a fairly high confidence in their next development. In particular, the way to improve the overall efficiency of energy conversion using dichroic filters, combined with the concentration, seems to be a very interesting route for the next future. Doesn't appear insurmountable, conceptual obstacles or requirement of edge technology but only the necessity to optimise the already present prototypes.

Diversely from the approach followed from large part of the PV community which aims at high concentration levels, systems working in the range of 100-200 suns are here developed; this fact allow us weaker constrains for the structure in operative conditions and permits the implementation of low cost solar cells. Regarding the silicon solar cells for the Si panel in the receiver, both for the concentrators with single reflector as well as for the dichroic dish, an original, cost effective process for the cells fabrication has been developed; first results give confidence for the next device productions. The panel of InGaP cells fabricated at CESI with MOCVD technique on Ge substrate gives assurance of the possibility to find these products with a quite low price and good efficiency. The chance to further reduce the price of these device is give by the possibility to use virtual substrate for the grown of efficient single junction III-V solar cells. Moreover, the two concentrating shells of the concentrator dish can be designed differently, to give two different concentration factors for using in the better way both the modules.

In the next future will be complete the assessment of the two kind of concentrators, the flat faceted with single concentrating collector and the dichroic dish, with two concentrating shells. Apposite modules already projected with opportune secondary optical elements will be mounted, in order to have a continued and monitored energy production.

Aside, other runs for the silicon solar cells fabrication with the developed process will be done to achieve the optimised receipt for up to 150× solar cells and so, to gather all the fundamental issues for the developed concentrated PV systems.

Bibliography

- [1] Hermann Scheer, "A solar manifesto", James & James, July 2001
- [2] Karl E. Knapp, Theresa L. Jester, "An empirical perspective on the energy pay back time for photovoltaic modules, Proceedings of Solar 2000 Conference, June 16-21, 2000, Madison, Wisconsin
- [3] Richard M. Swanson, "The Promise of Concentrators", Prog. Photovolt. Res. Appl. 8, 93-111 (2000)
- [4] Charles Kittel, Introduction to Solid State Physics, W.H. Freeman and Company, New York
- [5] Standard ISO 9845-2: 1992, ASTM E892-87: 1992
- [6] C. Kittel, H. Kroemer, Thermal Physics, second edition 1995, W.H. Freeman and Company, New York
- [7] Martin A. Green, "Solar Cells: Operating Principles, Technology and System Applications", Prentice-Hall, New Jersey, (1982)
- [8] Dieter K. Schroder, "Carrier Lifetimes in Silicon", IEEE Transactions on electron devices, Vol. 44, No 1, January 1997
- [9] Martin A. Green, "High Efficiency Solar Cells", Trans Tech Publications, 1987
- [10] Micheal G. Mauk, Silicon Solar Cells: Physical Metallurgy Principles, JOM, Vol.55, Issue 5, May 2003
- [11] A.A.Istratov et al., Impact of metal impurities on solar cell performance, Proceedings of NCPV and Solar Program Review Meeting 2003, page 228-231
- [12] Stewart, K. and Cuevas, A. and Macdonald, D. and Williams, J. (2001) Influence of copper on the carrier lifetime of n-type and p-type silicon. In Proceedings 11th Workshop on Crystalline Silicon Solar Cell Materials and Processes, Estes Park, Colorado
- [13] L. J. Geerligs, D. Macdonald, Base Doping and Recombination Activity of Impurities in Crystalline Silicon Solar Cells, Prog. Photovolt: Res. Appl. 2004, J. Schmidt, A.G. Aberle, R. Hezel, Proceedings of the 26th IEEE Photovoltaic Specialists Conference, Anaheim, California, USA, IEEE, New York, NY, USA, 1997
- [14] B. Pivac, A. Sassella, A.Borghesi, Non-doping light impurities in silicon for solar cells, Materials Science and Engineering, B36, (1996) 55-62
- [15] Tang, Y.H., Dai, X.M., Zhao, Z., Wang, A., Wenham, S.R., and Honsberg, C.B., "Rear Surface Passivation in Buried Contact Solar Cells", 26th IEEE Photovoltaic Specialists Conference, Anaheim, CA, 29 September - 3 October, 1997

- [16] Lifetime measurements in solar cells of various thickness and the related silicon wafers, R. Van Steenwinkel, M.C. Carotta, G. Martinelli, M. Merli, L. Passari, D. Palmieri, *Solar Cell*, 28 (1990) 287-292
- [17] Mark J. Kerr, “, Emitter and Bulk Recombination in Silicon and Development of Silicon Nitride Passivated Solar Cells”, Phd Thesis ANU, June 2002
- [18] <http://www.pv.unsw.edu.au/links/products/pc1d.asp>
- [19] G. Siefer, P. Abbott, C. Baur¹, T. Schleg, A.W. Bett, DETERMINATION OF THE TEMPERATURE COEFFICIENTS OF VARIOUS III-V SOLAR CELLS, Proceedings of 20th European Photovoltaic Solar Energy Conference, 6 – 10 June 2005, Barcelona, Spain
- [20] S. Yoon and V. Garboushian, "Reduced Temperature Dependence of High-Concentration Photovoltaic Solar Cell Open Circuit Voltage (Voc) at high Concentration Levels", 1st World Conference on Photovoltaic Energy Conversion, (1994), 1500-1504
- [21] V. M. Andreev, V. A. Grilikhes, V. D. Romyantev, “Photovoltaic Conversion of Concentrated Sunlight”, Hardcover, June 1997
- [22] M. Hermle, E. Schneiderlocher, G. Grupp, S.W. Glunz, "Comprehensive comparison of different rear side contacting methods for high-efficiency solar cells”, 20th European Photovoltaic Solar Energy Conference, 6 – 10 June 2005, Barcelona, Spain
- [23] A. Antonini et al., Contact grid optimization methodology for front contact concentration solar cells, *Solar Energy Materials & Solar Cells* 80 (2003) 155–166
- [24] S. Bowden, and A. Rohatgi, "Rapid and Accurate Determination of Series Resistance and Fill Factor Losses in Industrial Silicon Solar Cells," 17th European Photovoltaic Solar Energy Conference, pp. 1802-1806, Oct 2001
- [25] J.P. Gambino, E.G. Colgan, “Silicides and ohmic contacts”, *Materials Chemistry and Physics*, Vol.52, (1998) 99-146
- [26] Wenham, S.R., Chan, B.O., Ghozati, S., Ebong, A.U., Tang, Y.H., Koschier, L., McIntosh, K., Slade, A., Honsberg, C.B., and Green, M.A., “Unusual Behaviour in Laser Grooved Solar Cells”, 14th European PVSEC, Barcelona, Spain, 30 June, 1997
- [27] Armin G Aberle, “Surface passivation of crystalline silicon solar cells: a review”, *Progress in Photovoltaics: Research and Applications*, Volume 8, Issue 5 , Pages 473 – 487
- [28] M. Hermle, E. Snhneiderlochner, G. Grupp, S.W. Glunz, “Comprehensive comparison of different rear side contacting methods for high-efficiency solar cells”, Proceedings of the 20th European Photovoltaic Solar Energy Conference and Exhibition, 6-10 June 2005, Barcellona

- [29] , B. Vogl et al., The use of silicon nitride in buried contact solar cells, *Solar Energy Materials & Solar Cells* 66 (2001) 17-25
- [30] Ebong, A. U. and Lee, S. H. (1997) overcoming the fill factor limit of double sided buried contact silicon solar cells. *Solid State Electronics*, Vol 41, No 11, pp. 1745-1747, 1997
- [31] Hermann, Wiesner, Modelling of PV modules – the effects of non-uniform irradiance on performance measurements with solar simulators, *Proceedings of 16th European Photovoltaic Solar Energy Conference*, 1-5 May 2000, Glasgow, UK
- [32] M.A.M.Shaltout, M.El-Nicklawy, A.F.Hassan, U.A.Rahoma, M.Sabry, "The Temperature dependence of the spectral and efficiency behaviour of Si solar cell under low concentrator solar cell", *Renewable Energy*, 445-448, 2000
- [33] V.Andreev, V.Grilikhes, V.Rumyantsev, N.Timoshina, M.Shvarts, *Proceedings of WCPEC-3*, Osaka, Japan, 2003
- [34] A.W. Blakers, Efficient 20-50 sun concentrator cells, *16th European Photovoltaic Solar Energy Conference*, 1-5 May 2000, Glasgow, UK
- [35] Ting L. Chu, Shirley S. Chu, "Thin film II-VI photovoltaic", *Solid-State Electronics*, Vol.38, No.3, pp.533-549, 1995
- [36] Jeffrey M. Gordon et al, Experimental Study of Multi-Junction Solar Cells at Ultra-High Concentration, *Proceedings of "International Conference on Solar Concentrators for the Generation of Electricity or Hydrogen"* May 1-5 2005 Scottsdale, Arizona (USA)
- [37] Masafumi Yamaguchi, Multi-junction solar cells and novel structures for solar cell applications, *Physica E* 14 (2002) 84 – 90
- [38] R. McConnell and M. Symko-Davies, DOE High Performance Concentrator PV Project, *Proceedings of "International Conference on Solar Concentrators for the Generation of Electricity or Hydrogen"* May 1-5 2005 Scottsdale, Arizona (USA)
- [39] R.R. King et al, Bandgap engineering in high-efficiency multijunction concentrator cells, *Proceedings of "International Conference on Solar Concentrators for the Generation of Electricity or Hydrogen"* May 1-5 2005 Scottsdale, Arizona (USA)
- [40] C. Rosenblad, HR Deller, M. Döbeli, E. Müller, H. von Känel, "Low-Temperature Heteroepitaxy by LEPECVD", *Thin Solid Films* 318 p. 11-14 (1998)
- [41] C. Flores, G. Timò, G. Gavetta, R.Campesato, G. Smekens & J. Vanbegin, "GaAs Solar Cells on Si Substrates for Concentrator Systems", *20th European Photovoltaic Solar Energy Conference*, 6-10 June 2005, Barcelona, Spain
- [42] G. Gabetta, C. Flores, R. Campesato, C. Casale, G. Timo, G. Smekens, J. Vanbegin, H. von Kanel, G. Isella, "SJ and TJ GaAs concentrator solar cells on Si virtual wafers", *Photovoltaic Specialists Conference*, 2005. *Conference Record of the Thirty-first IEEE*, pp. 850- 853 (2005)

- [43] A.W. Bett, G. Siefer, C. Baur, S. v. Riesen, G. Peharz, H. Lerchenmüller & F. Dimroth, “FLATCON[®] Concentrator PV-Technology Ready for the Market”, 20th European Photovoltaic Solar Energy Conference, 6-10 June 2005, Barcelona
- [44] V.Díaz, J.Alonso, J.L. Alvarez, C. Mateos, The Path for Industrial Scale Production of Very High Concentration PV Systems, Proceedings of “International Conference on Solar Concentrators for the Generation of Electricity or Hydrogen” May 1-5 2005 Scottsdale, Arizona (USA)
- [45] K. Araki et al., “Development of A New 550X Concentrator Module with 3J Cells - Performance and Reliability-”, Proc. 31st IEEE Photovoltaic Specialists Conference, January 3-7, 2005, Lake Buena Vista, USA (IEEE, 2005) pp.631- 634
- [46] Lewis Fraas, James Avery, David Scheiman, “AM0 CALIBRATION OF 34% EFFICIENT MECHANICALLY STACKED GaInP/GaAs-GaSb CIRCUITS”, 29th PVSC Conference, 2002
- [47] Matsubara H.; Tanabe T.; Moto A.; Takagishi S.; Mine Y., “Over 27% efficiency GaAs/InGaAs mechanically stacked solar cell”, Solar Energy Materials and Solar Cells, Volume 50, Number 1, January 1998, pp. 177-184(8)
- [48] D.J.Farrell, A.J.Chatten, C.M.Jermyn, P.A.Thomas, A.Büchtemann and K.W.J.Barnham, “THE LUMINESCENT CONCENTRATOR: LARGE AREA MODELLING AND RESULTS WITH DYE BASED STACK CONCENTRATORS AND THIN-FILM COMPOSITE PLATES”, 20th European Photovoltaic Solar Energy Conference, 6 – 10 June 2005, Barcelona, Spain
- [49] W. Welford and R. Winston, “High Collection Nonimaging Optics”, Academic Press, New York, 1989
- [50] DANIEL FEUERMANN and JEFFREY M. GORDON, HIGH-CONCENTRATION PHOTOVOLTAIC DESIGNS BASED ON MINIATURE PARABOLIC DISHES, Solar Energy Vol. 70, No. 5, pp. 423–430, 2001
- [51] Solar Systems, Flux Uniformity and Spectral Reproduction in Solar Concentrators Using Secondary Optics (2001) R. Leutz, A. Suzuki, A. Akisawa, T. Kashiwagi; Proceedings ISES Solar World Congress, 25-30 November, Adelaide, Australia, Harald Ries, J.M. Gordon, M. Lasken, High-flux photovoltaic solar concentrators with kaleidoscope-based optical designs, Solar Energy, Vol.60, No.1, pp.11-16,1997
- [52] C. Bingham et al., Concentrating Photovoltaic Module Testing at NREL's Concentrating Solar Radiation Users Facility, NCPV and Solar Program Review Meeting Proceedings 2003

- [53] M. Stefancich, A. Antonini, A. Ronzoni, M. Armani & G. Martinelli, Flat Faceted Photovoltaic Concentrator, the Prometeo Approach, Presented at 20th European Photovoltaic Solar Energy Conference, 6 – 10 June 2005, Barcelona, Spain
- [54] L. Pancotti, M. Stefancich, A. Antonini, A. Ronzoni, M. Armani & G. Martinelli, Optimized Profile of a Flat Faceted Reflective Concentrator for Optimal Light Transfer, Presented at 20th European Photovoltaic Solar Energy Conference, 6 – 10 June 2005, Barcelona, Spain
- [55] Thomas Keck and Wolfgang Schiel, ENVIRODISH AND EURODISH - SYSTEM AND STATUS, Proceedings of ISES Solar Energy Conference 2003, June 14-19 2003, Goteborg, Sweden
- [56] E. Lorenzo and A.Luque, Comparison of Fresnel lenses and parabolic mirrors as solar energy concentrators, Vol.21, 10, Applied Optics, (1982)
- [57] V.Díaz, J.Alonso, J.L. Alvarez, C. Mateos, The Path for Industrial Scale Production of Very High Concentration PV Systems, Proceedings of the 20th European PV Conference, Barcellona 2005
- [58] Shaped nonimaging Fresnel lenses (2000) R. Leutz, A. Suzuki, A. Akisawa, T. Kashiwagi; Journal of Optics A: Pure and Applied Optics 2, 112-116, K. Araki et al., “Development of a new 550X concentrator module with 3J cells-Performance and Reliability-”, Proc. 31st IEEE PVSC Orlando, 2005
- [59] Bazilian M., Leenders F., Van der Ree B., Prasad D. (2000) Photovoltaic cogeneration in the built environment, Solar Energy Journal, Volume 71, Issue 1, 2001
- [60] Coventry, J. S. and Lovegrove, K., “Development of an approach to compare the 'value' of electrical and thermal output from a domestic PV/thermal system”, Solar Energy, 75, 63-72 (2003)
- [61] S.R. Kurtz et al., Outdoor rating conditions for photovoltaic modules and systems Solar Energy Materials & Solar Cells 62 (2000) 379-391
- [62] M.A. Green, K. Emery, D.L. King, S. Igari and W. Warta, “Solar Cell efficiency Tables”, Progress in Photovoltaics, Vol. 9-1, 2001, pp. 49-56
- [63] P.J. Verlinden, A. Terao, S. Daroczi, R.A. Crane, W.P. Mulligan, M.J. Cudzinovic and R.M. Swanson, "One-Year Comparison of a Concentrator Module with Silicon Point-Contact Solar Cell to a Fixed Flat Plate Module in Northern California", Proceedings of the 16th European Photovoltaic Solar Energy Conference, May 1-5, 2000, Glasgow, UK
- [64] A.Parretta, G.Nenna, A.Antonini, M.Stefancich, “Monitoring of Concentrated Solar Radiation by Scattering from a Lambertian Surface and CCD Recording”, presented at OpDiMon’04, “Optical Diagnostics and Monitoring: from Advanced Components to Novel Devices”,Capo Miseno, Bacoli (NA), Italy, 21-26 March 2004

- [65] G. Johnston, Focal Region Modelling and Characterisation of Paraboloidal Dish Solar Concentrators, Australian National University, Canberra (1998), PhD Thesis
- [66] J.S.Coventry, M. Stefancich, A. Antonini, A. Ronzoni, M. Armani, P. Zurru and G. Martinelli, Analysis of the radiation flux profile of the 100 sun Prometeo faceted dish concentrator, Proceedings of 20th European Photovoltaic Solar Energy Conference, Pag. 2399-2402
- [67] John Harrison “Investigation of Reflectivity Materials for the Solar Cooker” Florida Solar Energy Center, 24-12-2001
- [68] Per Nostell, Arne Roos, Bjorn Karlsson, Ageing of solar booster reflector materials, Solar Energy Materials and Solar Cells 54 (1998) 235–246
- [69] B.M. Clive, “Very low cost PV concentrators”, DTI/Pub URN 01/1120
- [70] Fraas L M, Avery J E and Huang H X., “Thermophotovoltaics: heat and electric power from lowbandgap ‘solar’ cells around gas fired ladiant tube burners”, Proc. 29th IEEE PVSC (New Orleans) pp 1553–6, 2002
- [71] A.G. Imenes, D.R. Mills, Spectral beam splitting technology for increased conversion efficiency in solar concentrating systems: a review, Solar Energy Materials & Solar Cells 84 (2004) 19–69
- [72] G. Martinelli et al, “Dichroic flat faceted concentrator for PV use”, Proceedings of “International Conference on Solar Concentrators for the Generation of Electricity or Hydrogen” May 1-5 2005 Scottsdale, Arizona (USA)
- [73] G.Martinelli, M.Stefancich, A.Antonini, Italian Patent Pending : MI2005A000590
- [74] F.C. Marques, J. Urdanivia, I. Chambouleyron, A simple technology to improve crystalline-silicon solar cell efficiency, Solar Energy Materials and Solar Cells 52 (1998) 285–292, A.Hubner, C.Hampe, and A.G. Aberle, “A simple fabrication process for 20% efficient silicon solar cells”, Solar Energy Materials and Solar Cells 46, 67-77 (1997)
- [75] A. Rohatgi & S. Narasimha, Design, fabrication, and analysis of greater than 18% efficiency multicrystalline silicon solar cells, Solar Energy Materials and Solar Cells, 48, 1997, 187–197
- [76] www.sunpower.com
- [77] M. Castro, G. Sala, I. Antón, M. Martínez, MEDIUM PRODUCTION OF CONCENTRATOR SILICON SOLAR CELLS: APPROACHING THE INDUSTRIALISATION, 20th European Photovoltaic Solar Energy Conference, 6 – 10 June 2005, Barcelona, Spain
- [78] P. S. Plekhakov, R. Gafiteanu, U. M. Gösele and T. Y. Tan., “Modeling of gettering of precipitated impurities from Si for carrier lifetime improvement in solar cell applications” Applied Physics Letters 86, No. 5 (1999), 2453

- [79] S. Schwartzman, A. Mayer and W. Kern. " Megasonic Particle Removal from Solid–State Wafers". RCA review 46 , 81 (1985)
- [80] A. Goetzenberger, J. Knobloch and B. Voss, "Crystalline Silicon Solar Cells", John Wiley & Sons, 1998, page 95
- [81] Osamu Tabata et. Al., Anisotropic etching of silicon in TMAH solutions, Sensors and Actuators A, 34 (1992) 51-57
- [82] A. Parretta, A. Sarno, P. Tortora, H. Yakubu, P. Maddalena, J. Zhao, A. Wang, "Angle-dependent Reflectance and Transmittance Measurements on Photovoltaic Materials and Solar Cells", Opt. Comm., 172 (1999) 139-151
- [83] Sze, S.M., Physics of Semiconductor Device 2nd ed. New York, Wiley, 1981
- [84] M.L. Joshi, S. Dash, Dislocation-Induced deviation of phosphorus- diffusion profiles in silicon, IBM Journal of Research and Development, Vol.10, number 6, pag.446 (1966)
- [85] Christensen J.S., Dopant diffusion in Si and SiGe, Doctoral Thesis at ISRN KTH/FTE/FR-2004/2-SE, ISSN 0284-0545 KTH, Royal Institute of Technology, Department of Microelectronics and Information Technology, Stockholm, 2004
- [86] M. Sasani, The simple approach to determination of active diffused phosphorus density in silicon, Semiconductor Physics, Quantum Electronics & Optoelectronics. 2004. V. 7, N 1. P. 22-25
- [87] S.R. Wenham, J. Zhao, X. Dai, A. Wang, M.A. Green, "Surface passivation in high efficiency silicon solar cells", Solar Energy Materials & Solar Cells 65 (2001) 377-384
- [88] A. Kaminski, B. Vandelle, A. Fave, J.P. Boyeaux, Le Quan Nam, R. Monna, D. Sarti, A. Laugier, Aluminium BSF in silicon solar cells, Solar Energy Materials & Solar Cells 72 (2002) 373–379
- [89] Z. Makaró , G. Battistig,, Z. E. Horvath, J. Likonen and I. Barsony, Backside aluminisation effects on solar cell performance, Vacuum /volume 50/number 3–4/pages 481 to 485/1998
- [90] I. Perichaud, Gettering of impurities in solar silicon, Solar Energy Materials & Solar Cells, 72, (2002) 315-326
- [91] D. Bouhafs, A. Moussi, A. Chikouche, J.M. Ruiz, Design and simulation of antireflection coating systems for optoelectronic devices: Application to silicon solar cells, Solar Energy Materials & Solar Cells, 52, (1998) 79-93
- [92] J. Baumann et. Al., Investigation of copper metalization induced failure of diode structures with and without a barrier layer, Microelectronic Engineering 33 (1997) 283–291

- [93] Xin-Ping Qua,, Yu-Long Jiang, Guo-Ping Ru, Fang Lu, Bing-Zong Li, C. Detavernier, R.L. Van Meirhaeghe, Thermal stability, phase and interface uniformity of Ni-silicide formed by Ni–Si solid-state reaction, *Thin Solid Films* 462–463 (2004) 146– 150
- [94] Lee, E.J.; Kim, D.S.; Lee, S.H., “Ni/Cu metallization for low-cost high-efficiency PERC cells”, *Solar Energy Materials and Solar Cells* Volume: 74, Issue: 1-4, October, 2002, pp. 65-70
- [95] Bernhard Vogl*, Alexander M. Slade, Stephen C. Pritchard, Mark Gross, Christiana B. Honsberg, Jeffrey E. Cotter, Stuart R. Wenham, The use of silicon nitride in buried contact solar cells, *Solar Energy Materials & Solar Cells* 66 (2001) 17-25
- [96] C. Lavoie , F.M. d’Heurle, C. Detavernier, C. Cabral Jr., Towards implementation of a nickel silicide process for CMOS Technologies, *Microelectronic Engineering* 70 (2003) 144–157
- [97] Franklin, E. and Coventry, J., Effects of highly non-uniform illumination distribution on electrical performance of solar cells. In *Proceedings 40th Annual Conference for the Australian New Zealand Solar Energy Society*, Newcastle, New South Wales, (2002)
- [98] M. Pellegrino, S. Bolognesi, G.Flamínio, C. Privato, A. Romano and A. Sarno, A Global Approach for Measuring the Concentrating PV Cells, *20th European Photovoltaic Solar Energy Conference*, 6 – 10 June 2005, Barcelona, Spain
- [99] Sala, G., et al, (2000), "The 480 kWp Euclides-Thermie Power Plant; Installation, set up and first results,", *16th European Photovoltaic Solar Energy Conference*, 1-5 May, Glasgow, UK
- [100] R.A. Sinton and A. Cuevas, “A quasi-steady-state open-circuit voltage method for solar cell characterisation”, *16th European Photovoltaic Solar Energy Conference*, 1–5 May, Glasgow, UK, 1152–1155 (2000)
- [101] R.A. Sinton and A. Cuevas, “Contactless determination of current-voltage characteristics and minority-carrier lifetimes in semiconductors from quasi-steady-state photoconductance data”, *Appl. Phys. Lett.* 69
- [102] R.A. Sinton, A. Cuevas, and M. Stuckings, "Quasi-Steady-State Photoconductance, A New Method for Solar Cell Material and Device Characterization," *Proc of the 25th IEEE Photovoltaic Specialists Conference*, pp. 457-460, 1996, 2510–2512 (1996)
- [103] T. PISARKIEWIC, Photodecay method in investigation of materials and photovoltaic structures, *OPTO-ELECTRONICS REVIEW* 12(1), 33–40 (2004)

Acknowledgments

I really want to thank all my colleagues for their fundamental contributions in the development of the project; my contribution has been only a piece of the efforts required for the growth of the PV concentrator systems here described. The work is still continuing and each member of the group is fundamental. First, I want to thank all the colleagues and friends of the Department of Physics at the University of Ferrara; each one has participated at the development of the project as well as at the growth of the group skills. So I want to name the colleagues and friends who have directly contributed at this work: Marco Stefancich, scientific leader of the project, Alessandro Ronzoni, Maurizio Armani, Mariangela Butturi, Paolo Zurru, Lorenzo Pancotti and Emiliano Milan. Moreover, I want to greatly thank Prof. G. Martinelli, my scientific tutor and supervisor of the group, who has efficiently directed the project; in particular, I'm very grateful for the trust and autonomy he has given to me.

Besides, I cannot forget the important contribution given from Donato Vincenzi when he has worked with us; during the period of the doctorate I have found significant help from external colleagues; in particular from Antonio Parretta, researcher at the research centre ENEA in Bologna, but often working personally with us at the Unife, and from Joe Coventry of the Australian National University, who has spent some months working in our group. I thank also the two referees of my thesis work, dott. C. Flores and Prof. A. d'Amico for the comments and suggestions they have given to me.

Out of the scientific world, I want to thank a lot my family for the great support given to me and Federica, who has been able to stand by me all this time...

Thanks to All

Andrea